Hydrodynamic loading on the shaft of a gravity based offshore wind turbine

Final Report Master Thesis
Henno Smaling
Delft, 26 May 2014

Final report Master Thesis
Delft, 26 May 2014

Written by Henno Smaling
Student number: 1504924

The research is performed to fulfil the requirements of the Master of Science degree in Civil Engineering as set forth by Delft University of Technology, Faculty of Civil Engineering and Geosciences, Section of Hydraulic Engineering, Chair of Hydraulic Structures and Flood Risk.

Graduation Committee

Prof.dr.ir. S.N. Jonkman	TU Delft, section Hydraulic Engineering
Ir. W.F. Molenaar	TU Delft, section Hydraulic Engineering
Dr.ir. R.J. Labeur	TU Delft, section Environmental Fluid Mechanics
Ir. M.L.A. Segeren	TU Delft, section Offshore Engineering
Ir. E. ten Oever	BAM Infraconsult

PREFACE

After a period of hard work I am pleased to present this report, where I investigated the hydrodynamic load on a gravity based offshore wind turbine. This thesis was written as final step of the Master Civil Engineering at Delft University of Technology. At the start of my Msc thesis I was looking for a subject where both hydrodynamic and structural behaviour would be part of. The gravity based offshore wind turbine fascinated me, also because of its link with the field of offshore engineering. It took me a while to come up with a 'new' research question. But finally, the deepening was sought in the field of hydrodynamic loading. Working with a CFD program like FinLab was not easy in the beginning, mainly because of working with Linux. The first results made me question whether the output was correct, but also gave rise to deepen myself in the background of both FinLab and the Morison equation. Looking back, I've been able to gain lots of knowledge on hydrodynamic loading and all its processes involved. I'm proud that by means of this thesis a new application field of FinLab could be added.

Also, I've been able to learn about the structural behaviour of an offshore wind turbine, mainly with respect to fatigue. All the processes involved (an effort to be done) leading to that one single fatigue load fascinated me. Unfortunately performing a full fatigue analysis was too much work and not the focus of this thesis. But luckily I've been able to gain insight in the methods available.

This work could not be completed without the help of lots of other people. At first, I'd like to thank BAM Infraconsult for initiating this research, and giving me the opportunity and support to perform my Msc thesis. I thank my mentor at BAM Infraconsult, Erik ten Oever, for all the time he invested in me and especially for helping me to keep making progress. Gratitude goes to my colleagues for their discussions. Special gratitude goes to Markus Muttray and Nhut Nguyen for sharing their knowledge with me. I thank Robert Jan Labeur for the many hours he took to help me to turn my CFD calculations with FinLab into a succes. Also I'd like to thank him for his patience in explaining me the physics behind FinLab and for reviewing my report. I'd like to thank Wilfred Molenaar for helping me to maintain the headline of this thesis. Wilfred, also thank you for your support at the moments I needed this most. Further I'd like to thank Maxim Segeren for helping me to understand a little more about the field of offshore wind energy when I got stuck. I thank Prof. S.N. Jonkman for his time and his reflection on my work.

Lastly I'd like to thank my friends and family. The last time I may have been a bit absent. But I thank them for their interest in my work and their trust in me. Finally I'd like to thank God, my Father in heaven, for giving me the strength and wisdom I needed. All glory to Him.

Henno Smaling
Gouda, may 2014

SUMMARY

Over the last decades the offshore wind sector has grown rapidly. Based on targets it is expected that the sector will grow even faster in the future. Trends in offshore wind energy engineering are an increase in wind turbine size and water depth. Next to targets for the amount of wind turbines to be installed, also targets for a strong cost reduction of 30% by 2030 are set.

With 30% of the construction costs the support structure is an important aspect for cost reduction. By a joint venture of BAM and Van Oord an innovative type of Gravity Based Structure (GBS) was developed. The GBS consist of a concrete caisson and a steel shaft. The developed GBS fulfils in the demand of support structures for deeper waters (>20m). For water depths between 35 and 60m it leads to a cost reduction compared to a jacket when industrial production of the caisson is possible.

In order to optimize the support structure, the hydrodynamic loading on the steel shaft was investigated. In practise the wave forces on a steel shaft are calculated with the so called 'Morison equation'. Due to the presence of the caisson (probably influencing the flow around the steel shaft) it was unclear whether the standard design rules based on the Morison equation could be applied. Therefore the (numerical) CFD model FinLab was used to investigate the influence of the caisson on the wave forces on the steel shaft. The model was validated for a nearly linear wave on a monopile. The results seemed to agree very well with theory.

The steel shaft of the GBS has to be strong enough to resist an extreme wave. Together with the extreme wind load, this is the so called Ultimate Limit State (ULS). Next to this extreme event, in the Fatigue Limit State (FLS) all individual wind and wave loads during the lifetime of the structure are taken into account. These loads lead to deterioration of the material with possible breaking as result, named fatigue. The influence of the caisson was investigated within FinLab for the extreme wave (ULS) and for two relative moderate waves (FLS). The presence of the caisson led to an increase of the maximal horizontal force on the shaft of about 20%. The bending moment cycle (important for fatigue) did not change significantly.

This gave answer to the first research question. But, while investigating the influence of the caisson, for the shaft a comparison with the Morison equation was made. It was found that FinLab gave much higher forces for the ULS wave (a 75% higher maximal horizontal force on the shaft) than the Morison equation. By also interpreting the results of the FLS waves there seemed to be a relation with the degree of non-linearity of the wave. Different possible causes for the difference were discussed. Those causes gave a possible explanation why the Morison equation would be less accurate for a highly non-linear wave. It is however recommended to calibrate the outcomes of FinLab with experimental data.

The influence of the wave forces obtained with FinLab on the design of the shaft (the second research question) was investigated by means of a case study. A location near the U.K. with a water depth of 34m was used for this purpose. By performing a FLS and ULS analysis the required dimensions of the shaft could be determined. The FLS analysis was based on a simplified method to be used for pre-design only.

With respect to fatigue (FLS analysis), the higher loads found by FinLab for highly non-linear waves did not result in a higher fatigue load. This had to do with the small probability of occurrence of highly non-linear waves. Also the presence of the caisson did not change the fatigue load, due to the bending moment cycle being unchanged. With respect to the extreme event (ULS analysis) the strong increase in bending moment due to waves found by FinLab (+120%) resulted in a 26% higher total bending moment, because also wind loads play a role. However, for this water depth the dimensions of the shaft didn't have to be increased, because the FLS was governing the design.

The most important conclusions of this research are that 1) The caisson does not significantly influence the ULS and FLS analysis 2) The Morsion equation gives lower wave forces than an analysis with FinLab. For further design these conclusions have the implication that the caisson does not have to be part of the structural schematisation when the wave loads are determined. For the FLS waves most likely the Morison equation can be used, which has large benefits for the calculation time. For the ULS wave another method than the Morison equation is suggested.

TABLE OF CONTENTS

1

1 INTRODUCTION

1.1 GENERAL INTRODUCTION

The last decades the development of wind energy has grown rapidly. An increasing number of wind turbines are installed offshore, mainly at the North-Sea. Where now only about 5 GW [1] of offshore wind power is installed this amount is expected to increase to about 250 GW in 2030 [2].

Trends in offshore wind energy engineering are an increase in the size of a wind turbine and an increase in water depth. Combination BAM/ Van Oord has developed a new type of Gravity Based Structure (GBS) for water depths varying between 35 and 60 m. The GBS consists of a concrete caisson and a steel shaft. See Chapter 2 for more background on this general introduction.

In order to make offshore wind energy viable for application at large scale a strong reduction of the costs per megawatt will have to be achieved.
For an offshore wind turbine the support structure contributes to about 30% of the total construction costs. For deeper water (>20m) the contribution will probably be even more. The support structure has a high potential for cost reduction. The GBS concept developed for deeper waters on itself already results in a cost reduction when applied at large scale. This has to do with industrial production and an innovative installation method.

But the GBS can be optimized further. An important contributor to the total costs of the support structure are the material costs of the steel shaft. This part of the support structure is chosen as optimization subject for this thesis.

1.2 PROBLEM DESCRIPTION

The hydrodynamic loading on a support structure has an important influence on its design. For a monopile structure the hydrodynamic forces (waves, currents) are in practice calculated by application of the Morison equation. This equation is based on a coupling between an incident wave and the force on a cylinder.
For a GBS the presence of the caisson may lead to a distortion of the flow around the steel shaft. Therefore it cannot be stated on forehand that the Morison equation (theory) is still valid for the steel shaft.

Desired is a situation where the wave forces on the shaft of this specific GBS are determined in a more accurate way. The influence of the resulting forces on the design of the steel shaft (the resulting cross-sectional dimensions) is also desired to be known. This leads to the following problem definition:

1. What is the influence of the caisson on the hydrodynamic loading of the steel shaft?
2. What is the influence of a detailed hydrodynamic loading on the design of the steel shaft?

1.3 APPROACH

1.3.1 Objective

In order to answer both research questions, first more has to be investigated about the design process of the steel shaft. By doing so, the place of the hydrodynamic loading in the total design of the support structure becomes clear. Also insight is obtained in the underlying assumptions and the hydrodynamic loading analysis itself.

To find an answer on the first question one can investigate the hydrodynamic load by 1) performing laboratory tests 2) performing a numerical simulation. The second approach is used within this thesis. The numerical CFD (Computational Fluid Dynamics) model FinLab was used for this purpose.

With the output of FinLab the influence on the design of the design of the steel shaft can be investigated. This gives insight in the influence of performing a more detailed hydrodynamic analysis on the design.

1.3.2 Thesis outline

In this thesis the outline of Figure 1.1 is used. Chapters 2-4 are introducing and a result of a literature study: Chapter 2 as general introduction to offshore wind, Chapters 3-4 describe the design of the steel shaft and all aspects playing a role. If one is already familiar with the design of the support structure of an offshore wind turbine, the advice is to read at least the introductory and concluding sections of each chapter.

The main of this thesis is presented in Chapter 5 and aims to answer the first research question. Within this chapter the influence of the caisson on the hydrodynamic force of the shaft is investigated.
The second question is answered by means of implementing the results from FinLab in a case study in Chapter 6. By doing so the influence of the detailed hydrodynamic analysis with FinLab becomes clear.

Finally in Chapter 7 conclusions are drawn and recommendations are given.

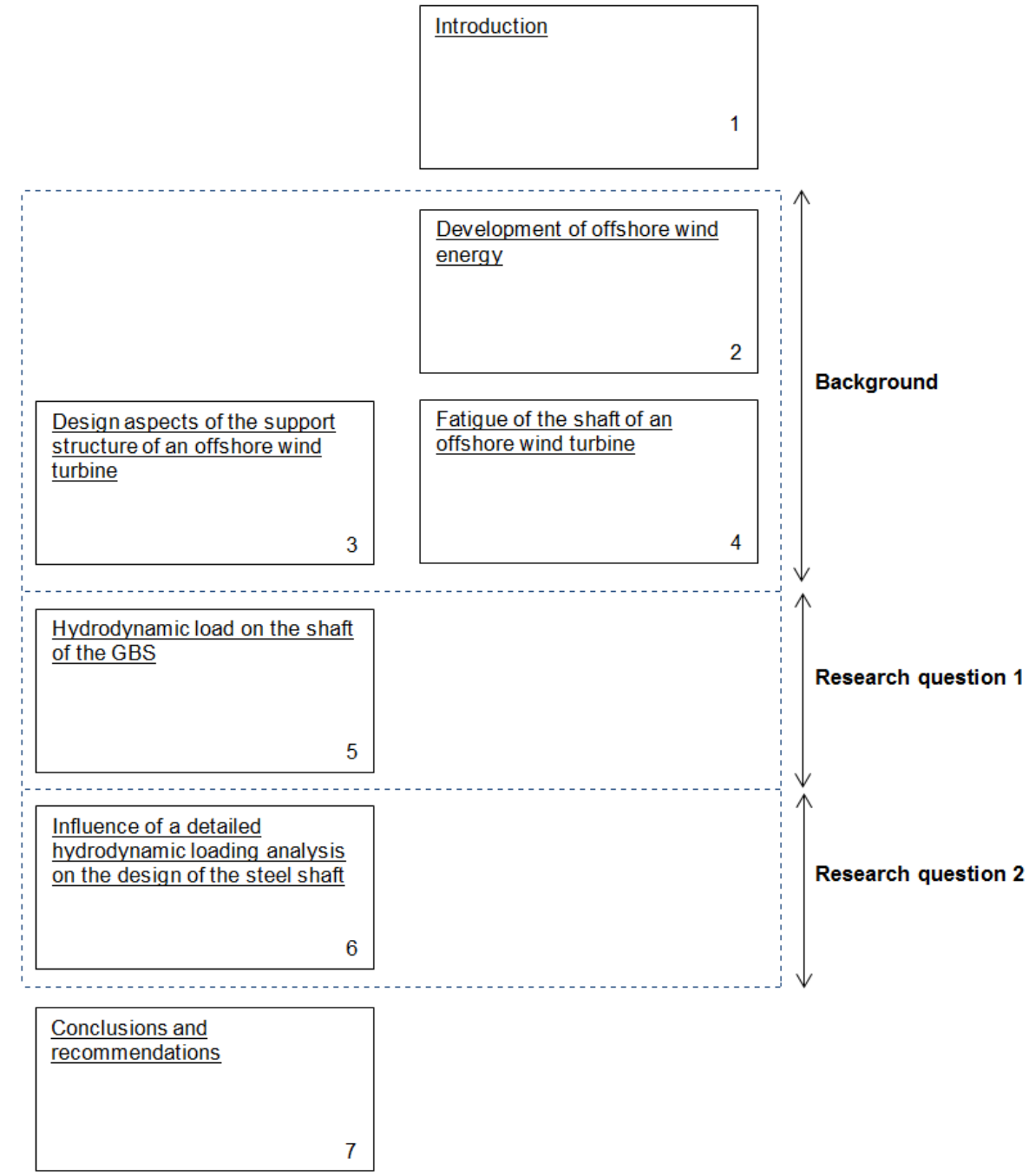

Figure 1.1 – Thesis outline

2

2 DEVELOPMENT OF OFFSHORE WIND ENERGY

2.1 INTRODUCTION

This chapter aims to give insight in the question why optimising an offshore wind turbine is necessary. This is performed by showing expected future developments and economic aspects of offshore wind farms.

Over the past decennia the wind energy sector has grown rapidly. Although offshore wind is only a small fraction of the total wind energy sector, it is becoming more and more important. In order to gain insight in the future growth, section 2.2 gives an overview of the targets and trends.

Section 2.3 gives an overview of the economic aspects of an offshore wind turbine. Although the rise of wind energy is mainly driven by sustainability reasons, economical aspects are very important as well. The rate of development of (offshore) wind energy is strongly related to economics. At this moment offshore wind energy is still quite expensive compared to onshore wind energy. Different countries strive after cost reduction of offshore wind energy of about 30% by 2020. Optimisation of an offshore wind turbine is one of the fields where a cost reduction could be achieved.

With respect to costs, an important element of an offshore wind turbine is the support structure. Trends in offshore wind engineering are an increase in water depth and turbine size. The turbine size is increased in order to reduce the costs per MW. The increase in water depth results in a higher contribution of the support structure to the total costs and makes it even more important to optimize the support structure.
Section 2.4 gives an overview of the type of support structures available. The focus is laid on the optimisation of a new type of Gravity Based support Structure (GBS) developed by a joint venture of the companies BAM and Van Oord, which is suitable for relative large water depths (>35m).

This type of support structure is the subject of this thesis. Characteristics of the support structure are given in section 2.4.4. Due to an innovative installation method, a hybrid structure, and possibilities for industrial production a cost reduction compared to other support structures may be achieved.

2.2 FUTURE DEVELOPMENTS

2.2.1 Targets

The industry of wind energy is mainly driven by the following two motives:

- A decrease of available fossil fuels, the search for alternative energy sources
- Targets to diminish the amount of CO2 pollution

Offshore wind energy has grown over the past years. At the end of 2012 about 283 GW of wind power (of which 5.4 GW offshore) was installed globally [1]. Half of the installed offshore wind capacity is installed in the United Kingdom. Most of it in relatively shallow water (<20 m) and not too far from the shore (<20 km).
The market for offshore wind is expected to increase [2]. For example the European Wind Energy Association has identified a target for the EU members of 40 GW offshore wind power to be installed by 2020 [3]. By 2030 the target is 150 GW. See Appendix A.1 for predicted scenario.
Also targets with respect to costs reduction are set. In the UK a cost reduction of 30% by 2020 is targeted for.

2.2.2 Trends

At most potential shallow locations near the coast already wind farms have been installed. Therefore a trend to deeper water is expected, see Figure 2.1. Also the turbine size is expected to increase, in order to reduce the costs per MW.

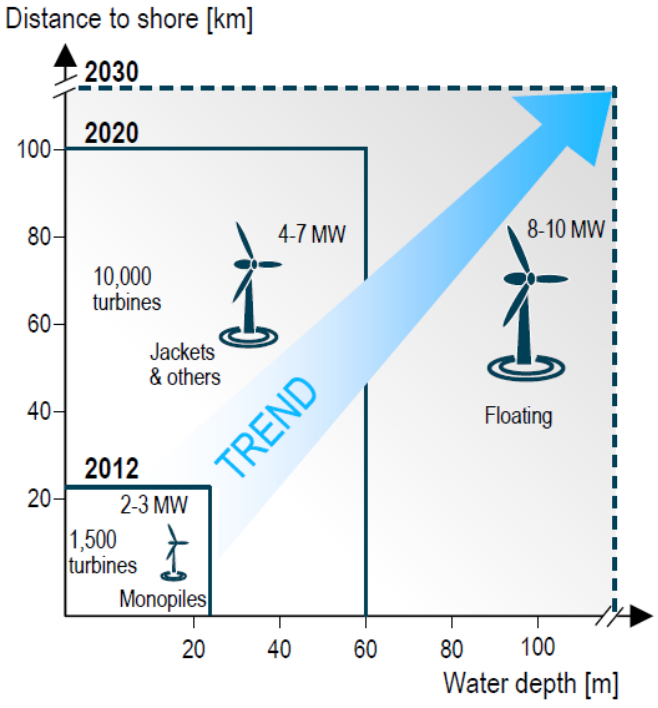

Figure 2.1 – Expected trends in the field of offshore wind energy [4]

2.3 ECONOMICAL ASPECTS

2.3.1 Wind energy economics

Comparison of different energy generating concepts is often done by determination of the Levelized Costs Of Energy (LCOE). This term calculates all the costs over the lifetime for a certain quantity of energy (often 1 kWh). For an offshore wind turbine the LCOE is determined by the following costs:

- Construction costs (75%) [4]
  - Costs of design
  - Material costs
  - Fabrication costs
  - Installation
- Operation & maintenance (25%)
- Balancing of power production
- Demolition

The German institute ISE Fraunhofer has calculated the LCOE for on- and offshore wind farms. In Figure 2.2 a forecast is given for the LCOE for on-and offshore wind and the expected rise in energy prices. It can be concluded that there is still a long way to go for offshore wind to become competitive with other technologies. For onshore wind the case seems more beneficial, as this technology is expected to become competitive in an economic sense from 2017 if the price of the electricity mix keeps rising. See Appendix A.1 for more studies on wind energy economics.

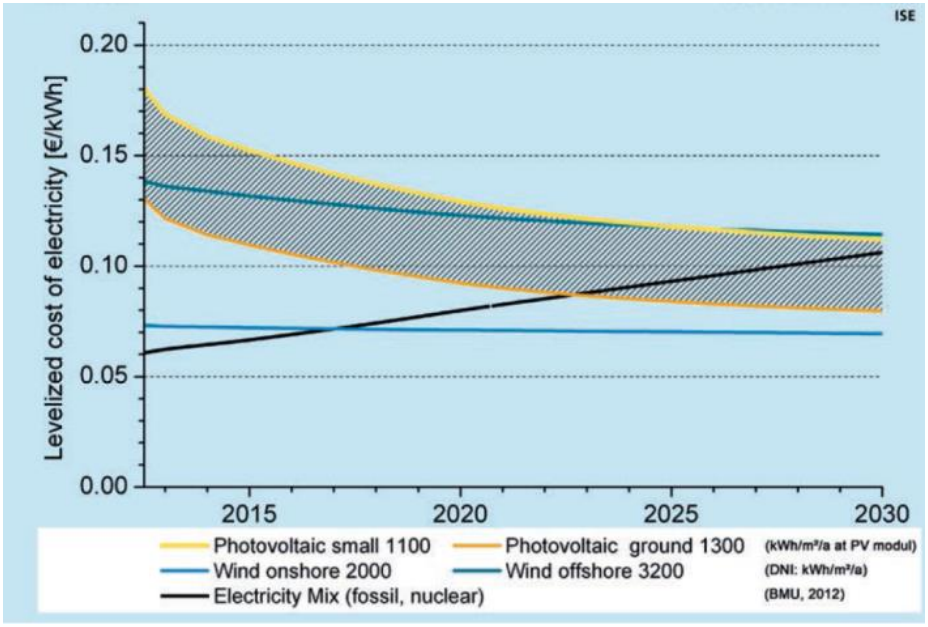

Figure 2.2 - LCOE forecast of renewable energies in Germany to 2030, based on learning curves [5]. Numbers in the legend are full load hours per year. Offshore wind has more full-load hours than onshore.

2.3.2 Cost distribution

The cost distribution of the construction costs for an offshore wind turbine is given in Figure 2.3. More information can be found in Appendix A.1. Some remarks:

- Material costs of the steel shaft are about 3% of the total costs. The other part of the support structure cost exist mainly on assembly of the substructure onshore.
- All the costs, except for the turbine, are to a large extent influenced by the location (distance to the shore and water depth).

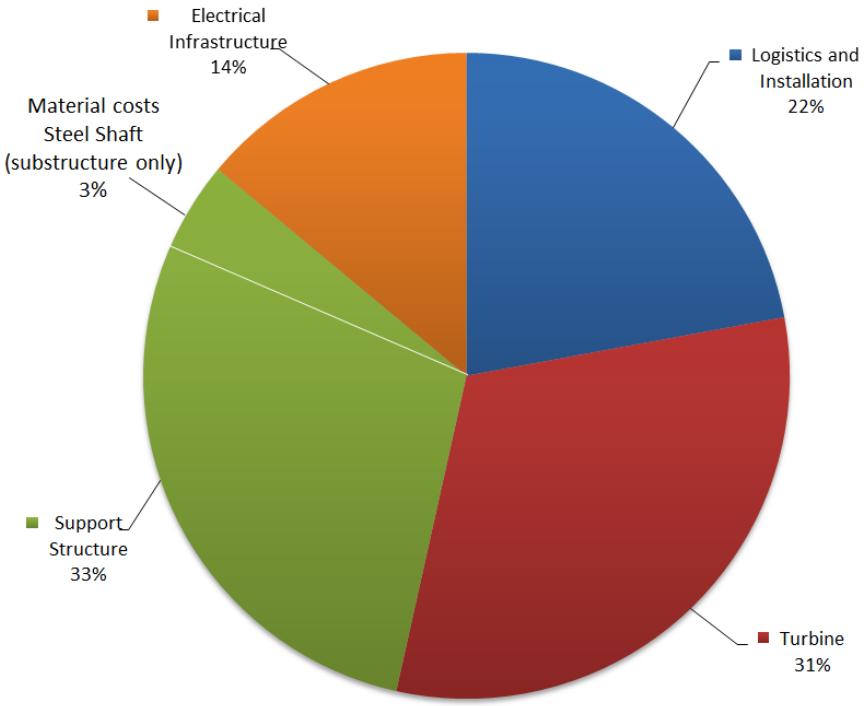

Figure 2.3 - Cost distribution of construction costs for a hypothetical 5MW offshore wind turbine in a water depth of 20-30 m; partly based on [6]. Construction costs are 3.65 m€/MW [4], steel shaft has a weight of about 600t (€1000/t). The definition of support structure in this figure consists of the foundation and substructure of Figure 2.4 only.

2.3.3 Support structure optimisation

A reduction of the LCOE for offshore wind energy can be achieved by reducing the costs of all the individual components. The most important fields of cost reduction as mentioned in [4] are:

- Increasing the size of the wind turbine, resulting in a higher power output per support structure.
- Improving support structures and enabling serial production.
- Increasing experience with O&M, and developing innovative O&M concepts.

This thesis is focussing on the construction costs of the support structures.

For an offshore wind turbine the support structure contributes to about 30% of the total construction costs for water depths up to 30 m, and probably even more in deeper water. Therefore optimisation of the support structure is an important subject to bring the overall costs for offshore wind down.

2.4 SUPPORT STRUCTURES

2.4.1 Terminology

An offshore wind turbine consists of two parts: the support structure and the turbine. The turbine consist of a rotor and a nacelle. With the support structure is meant: the structure supporting the turbine. The representation of Figure 2.4 is followed in this report. The Gravity Base Structure (GBS) is a type of support structure and consists of a substructure and foundation.

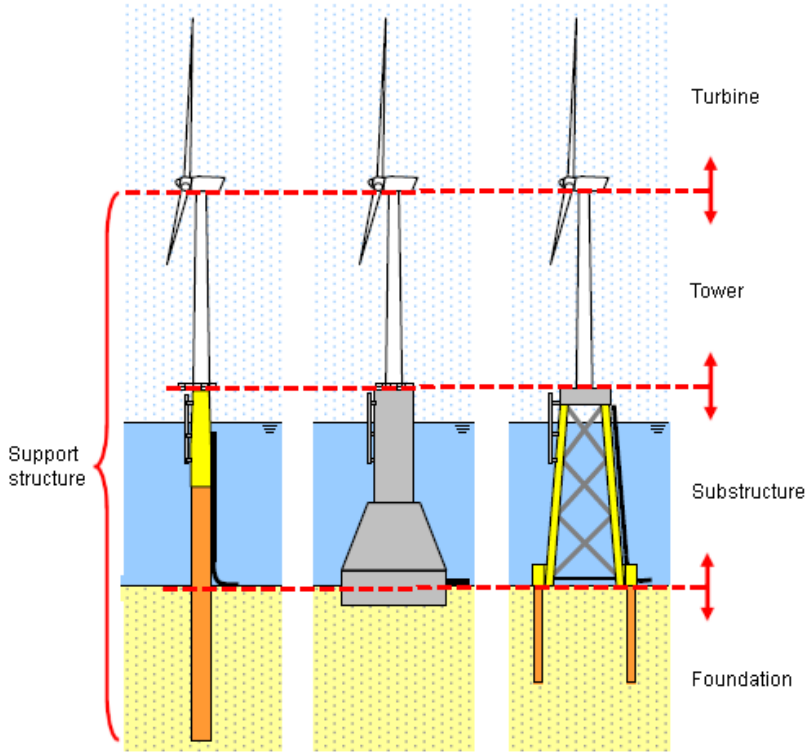

Figure 2.4 - Offshore wind turbine terminology [7]

2.4.2 Support structure concepts

In general one can distinguish three types of support structures: piled, gravity based and floating. In fact all the support structure concepts are based on concepts applied in the oil and gas sector. There is a lot of experience with various support structure concepts in this sector. However the loads resulting from a wind turbine are very different from the loads on a platform. The concepts can be divided in the next categories:

- Monopile
- GBS
- Suction pile
- Tripod
- Jacket
- Floating

More information about each concept can be found in Appendix A.2.
For each support structure the strengths and weaknesses are listed in Table 2.1.

Concept	Economical water depth range	Advantages	Disadvantages
Monopile	3 - 25 m	– Minimal construction site investment – Easy transportation to site – No seabed preparations	– Relative sensitive to scour – Not suitable for weak and rocky soil – Cost sensitive to large wall thickness and diameter – Relative expensive drilling equipment – Environmental impact from drilling – Protection against corrosion required
GBS (original)	3 – 30 m	– Performance insensitive to soil parameters – Whole installation as a single unit – No driving/drilling – Relative insensitive to corrosion	– Large scour protection required – Stiff dynamic response – Poorly suitable in weak soil – Heave forces during wave passage – Large construction site investment – Seabed preparation required – Barge with large lifting capacity
Suction pile	<30 m	– Self-installing – No seabed preparation – No driving/drilling	– Scouring protection necessary – No proven technology yet for offshore wind turbines – Time consuming installation – Not suitable for rocky soil and dense sand
Tripod	8 – 30 m	– Relative insensitive to scour – Small displacements and rotations at jack top – No seabed preparation	– Needs protection against corrosion – Piling equipment required – Difficult transport – Unsuitable for rocky soil
Jacket	8 – 40 m	– Relative insensitive to scour – Small displacements and rotations at jack top – No seabed preparation	– Needs protection against corrosion – Piling equipment required – Difficult transport – Unsuitable for rocky soil
Floating	> 50 m	– No seabed preparation – No scour protection – Relative insensitive to subsoil conditions	– Rather expensive mooring system – No proven technology yet for offshore wind turbines

Table 2.1 - Strengths and weaknesses for different support structures (as applied up to now), the 'original' GBS regarded here consist of concrete only. Table is based on [2]

It has to be noted that the concepts are technical not restricted to the indicated water depths of Table 2.1, but probably the concept is most economical in the given water depth ranges. Off course this will also depend on other boundary conditions. New developments may change the picture and may make a concept competitive with another for a certain water depth. An example is the BAM Van Oord GBS concept (section 2.4.4) which can be applied up to water depths of 60 m. In contrary to the 'original' GBS concept (concrete only) this concept (concrete + steel) is suitable for larger water depths.
With respect to deeper waters (>30 m) only the jacket, floating support structure and the new type of GBS are options.

In the offshore wind engineering field a lot of research is and was done on support structures. Although each type of support structure is still subjected to research, this thesis focusses on the GBS.

2.4.3 Development of the GBS concept

The last decennia multiple gravity based offshore wind turbines were installed. Most of them in relatively shallow water (~10m). See Appendix A.2. for an overview. Worth mentioning is the Thornton Bank project, where 6 wind turbines were installed on a GBS. The water depth was varying between 12 and 28 m. The 'erlenmeyer' shaped GBS consisted of concrete completely. They were constructed on a quay onshore and transported offshore by a heavy lifting vessel.

For the second (a batch of 30 turbines) and third phase (a batch of 18 turbines) the GBS concept was exchanged for a jacket with pre-piling. Arguments were a decrease in steel price compared to the first phase, less time required, simpler logistics, less weather sensitiveness, less harbour space needed, less marine preparation works and less design issues. More information about the projects can be found in Appendix A.2.

2.4.4 The BAM Van Oord GBS concept

A new GBS concept has been developed by a joint venture of the companies BAM and Van Oord. This GBS should be suitable for water depths varying between 35 and 60 m.
The concept was developed to supply in the demand for installation of wind turbines in deeper waters (Figure 2.1). With this development the GBS is not only suitable for shallow water anymore (see Table 2.1). Because the GBS concept has a number of advantages with respect to other concepts a new market is opened for the application of the GBS.
The concept was developed about 5 years ago. Part of the development took place in the FLOW (Far and Large Offshore Wind) program, an innovation programme for the Dutch wind energy industry. The program aims to accelerate development and to reduce costs and risk by 20% in 2015 (with respect to 2010).

The developed concept (see Figure 2.5) exists of a concrete caisson and a steel shaft and is a so called 'hybrid structure'. In fact it is a combination between the concrete foot of a GBS and a monopile tube.

The specifications are:

- Concrete caisson
  - A diameter of about 30 m and a base slab.
  - Vertical walls with a roof on top of it.
  - Total caisson height of about 20 m.
  - Six shear walls, to improve the behaviour during the immersion process [8].
  - Sloping roof in order to support the shaft and to resist the bending moment and shear forces of the shaft
  - Empty weight: 6000t
- Steel shaft
  - Diameter varying between 6 and 7 m.
  - Weight: ~500t

The caisson will be fabricated on a yard using an industrial production method. After construction the steel shaft is installed. Next the GBS is lifted into the water. The GBS is self-floating and is transported to its final location by tug-boats. At location it is immersed on a prepared seabed. After immersion the GBS is ballasted with sand (8000t). Finally, around the GBS a scour protection layer is placed.

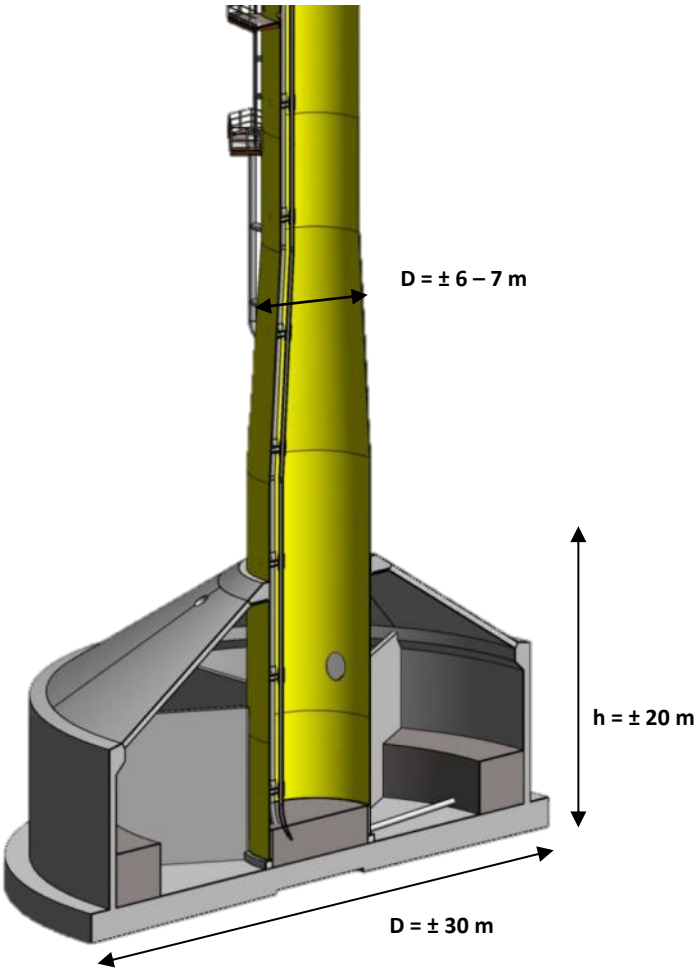

Figure 2.5 – GBS concept [8]

Compared to a traditional GBS (concrete only) the BAM Van Oord concept has the following advantages:

- The smaller diameter of the steel shaft (with respect to a concrete one), results in a strong reduction of the wave loads.
- No heavy lifting vessel is required for transport and installation
- By making the shaft from steel, it weighs less than similar structures with a concrete shaft. This results in a lower centre of gravity and improves the metacentric height during marine operations [8].

In addition, with respect to a jacket, the BAM Van Oord GBS concept has the following advantages:

- A limited construction time, with minimal offshore activities.
- No drilling of piles, this is beneficial for environmental impact, risks and fatigue damage.
- Economically attractive from 35 m water depth (for more than 200 wind turbines due to mass production) [9].

2.4.5 Optimisation of the BAM Van Oord GBS

In this chapter was seen that the price of offshore wind energy should go down.
The support structure concept developed by BAM and Van Oord aims to come up with a cost effective design by introducing a new type of GBS concept and installation method. By means of this concept the construction and installation costs are aimed to decrease with respect to the standard type of support structure (a jacket) for water depths between 30-60m.

In addition the GBS concept can be optimised. Optimisation can be achieved by:

- Adapting the shape of the GBS in order to reduce the loads (while not reducing the strength)
- Reducing uncertainties in the magnitudes of loads, leading to a reduction of safety factors
- Applying a less conservative design method by increasing knowledge

The first optimisation technique will probably cost more money with respect to the original case. The second and third method will require more computational and man-hour expensive calculations. It depends on the amount of savings whether these optimisation steps are attractive. The second optimisation technique is applied within this thesis.

3

3 DESIGN ASPECTS OF THE SUPPORT STRUCTURE OF AN OFFSHORE WIND TURBINE

3.1 INTRODUCTION

In order to be able to optimize the support structure of an offshore wind turbine, all aspects playing a role in the design have to be known. Therefore section 3.2 describes the design process of an offshore wind turbine.

The operational phase is often governing for the (cross-sectional) dimensions of the support structure. Designing the support structure of an offshore wind turbine is a complex process, because a lot of design aspects play a role. In section 3.3, as an overview, a component breakdown has been performed.
Most aspects in this chapter are in general valid for all types of support structures, but are in principle described for a GBS.

For all components of a gravity based offshore wind turbine the most important loads and design aspects for the support structure are mentioned. For most aspects, based on a first estimation or small calculation, the relative importance is mentioned. This is done by applying the theory to a small case study for a GBS at the North-Sea near the U.K.
The same location is also used for the case study of Chapter 6.

For the design all loads and design aspects are combined in so called load combinations. The support structure has to be strong enough to resist all the loads during its lifetime. Section 3.4 gives an overview of the load combinations.

The chapter ends with a summary of the theoretical background of the most important loads influencing the design of the support structure. These theories are used in further chapters.

3.2 DESIGN PROCESS

The design of an offshore wind turbine consists in general on the design of the next components:

- Turbine
- Support structure
- Scour protection
- Electrical grid connection

The design process consists on different steps. In general a pre-design and a detailed design can be distinguished. For the design of an offshore wind turbine the following phases are considered:

- Fabrication on-shore
- Transport and installation off-shore
- Operation: stability and structural strength
- Decommissioning

The final goal of the design process is a cost effective design that fulfils all the requirements in every phase. Design in general is an iterative process.

An offshore wind turbine is often designed by a consortium of participants from different fields. An offshore contractor installs and sometimes designs the support structure, while a wind turbine manufacturer produces a design of the wind turbine. Due to the strong influence on each other, optimisation of the support structure is an iterative process between all parties.

3.3 SYSTEM OVERVIEW

A gravity based offshore wind turbine (see Figure 3.1) can be subdivided in the following components:

1. Turbine (rotor and nacelle)
2. Support structure
    - Tower
    - Transition piece tower-shaft
    - Steel shaft
    - Transition shaft-caisson
    - Concrete caisson
    - Foundation

Below per component a description of the most important design aspects is given. Also the structural schematisation and some assumptions (marked by [A]) for the rest of the thesis are given. Most assumptions are based on application of the theory to a case study in Appendix B. The effect of the assumptions on the outcome of this thesis is discussed in Chapter 7.1.

3.3.1 Rotor and nacelle

Wind passing through the rotor disk causes a force on the rotor blades, acting on the nacelle as an axial force. Within the nacelle the rotation axis drives a power generating system. Due to turbulence the wind force is not constant in time, leading to the following effects:

- The axial force can be seen as a static force accompanied by a dynamic component. These dynamic components are mostly caused by eddy-slicing of the rotor, leading to load peaks at the 1P and 3P frequencies (load peaks in time due to turbulence, see section 3.5.1).
- Due to the varying wind load the wind turbine starts to deflect. By this displacement the wind load increases or decreases, leading to a damping force. This effect (called aerodynamic damping) is treated in section 3.5.6.

Both the 1P and 3P frequency and aerodynamic damping are characteristics of the wind turbine and are often specified by the wind turbine manufacturer.
[A]: For calculations within this thesis it is assumed that the wind forces, both extreme and during lifetime, as provided by the wind turbine manufacturer can be used. It is assumed that all dynamic effects of the turbine and tower are included in these values.

3.3.2 Tower

The tower has the function to transfer the loads from the turbine to the substructure. In addition it is loaded with a drag force due to wind. Due to its large length the shaft has an important influence on the natural frequency of the offshore wind turbine. Damping consist of structural damping only, the magnitude of aerodynamic damping of the shaft is negligible.

3.3.3 Transition piece tower-shaft

The transition piece between tower and shaft is in this case a bolted connection (see Appendix A.2.2). Due to the use of pre-stressed bolts this type of connection can be seen as rigid. The bolted ring leads to an increase of the structural damping.

3.3.4 Steel shaft

The steel shaft fulfils the same function as the tower. But instead of being surrounded by air it is surrounded by water. The next aspects are of influence for this section:

- Wave breaking/slamming: this may lead to high forces on the shaft.
  [A]: For the goal of this thesis, loads due to wave breaking are no part of the design procedure of the steel shaft. This is mainly based on their assumed low probability of occurrence.
- Wave loads: forces due to waves and currents acting at the shaft. Wave run-up also has to be taken into account. Due to the periodic character of the wave loads and elasticity of the shaft it will move. This effect should be accounted for in determining the wave loads.
- Waves and currents lead to the following forces: drag, inertia and lift forces.
  [A]: Due to the often lower force magnitude compared to the drag and inertia forces, lift forces are assumed not to be governing for the design of the steel shaft.
- [A]: For simplicity loads due to currents not taken into account within this thesis.
- Tides and storm surges influence the local water depth.
  [A]: Local water elevations due to tides and storm surges are not taken into account.
- Displacement of the shaft (due to varying wind and wave loads) leads to fatigue.
  [A]: For the dynamic behaviour it is assumed that the shaft can be schematised as a clamped beam at the level of the top of the cone.
- Added water mass: while determining the structural mass, for a moving structure also a part of the surrounding water mass has to be taken into account.

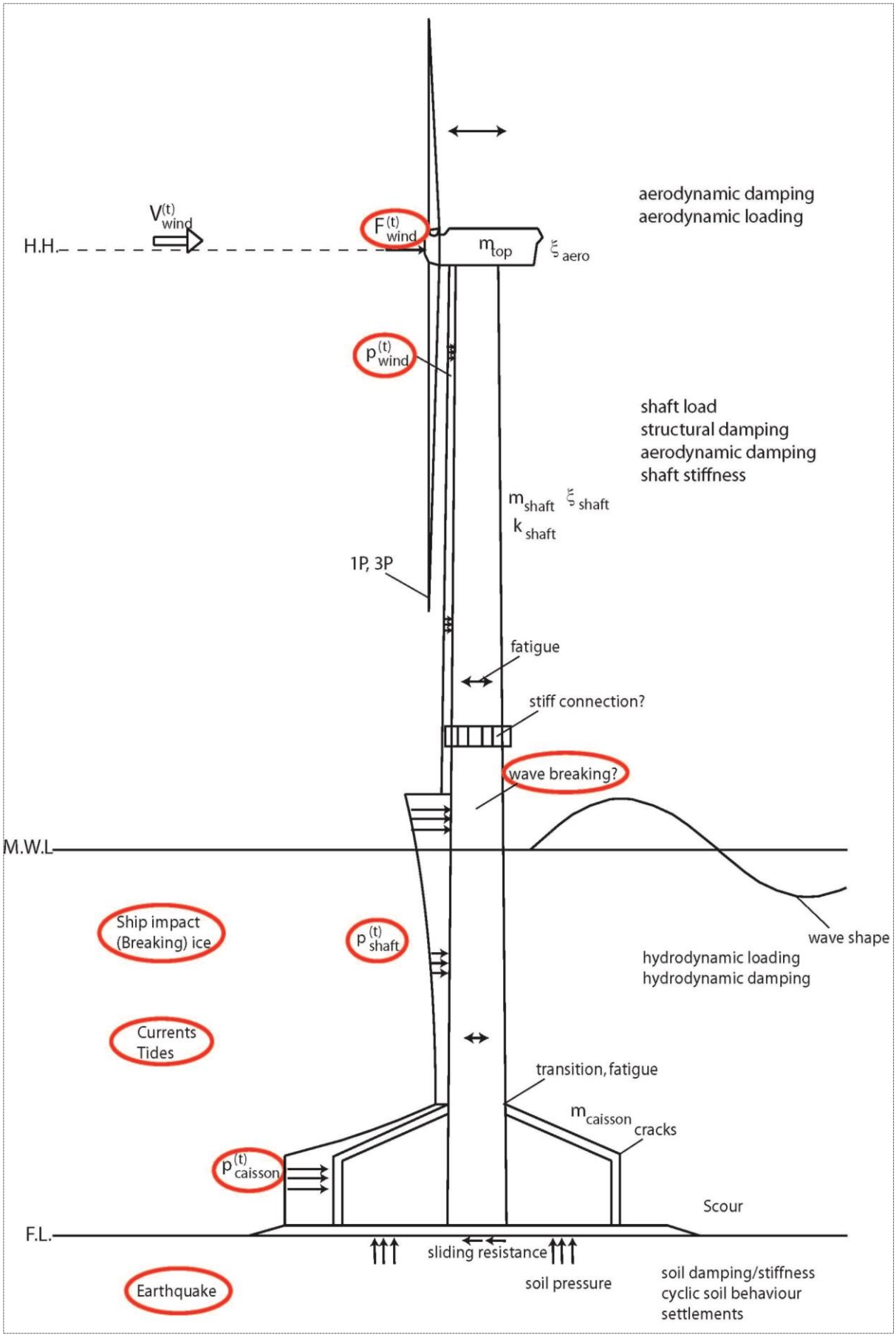

Figure 3.1 - Component breakdown of the gravity based offshore wind turbine. Environmental loads are encircled. m=mass, ξ=damping, k=spring stiffness, V=wind speed, F=force, p=distributed force

- Hydrodynamic damping: a moving structure in water is damped via hydrodynamic forces. The amount of hydrodynamic damping is very small compared to other damping sources (see section 3.5.6).
- [A]: The impact load due to ship collision is assumed to be non-governing for the design of the steel shaft. Ice loads are not assumed to occur at the North-Sea.
- [A]: It is assumed that no corrosion occurs. Marine growth is only partly accounted for by incorporating a relative high roughness.

3.3.5 Transition shaft – caisson

The transition between shaft and caisson roof is made by a concrete ring. This ring doesn't allow for displacements and can be seen as a rigid connection. The bending moment in the shaft is acting as a horizontal force at the connection. The periodic character of the bending moment leads to a varying load in the concrete ring, and will introduce fatigue loads in the ring.

3.3.6 Concrete caisson

Due to varying loads at the shaft-caisson connection, and due to varying wave loads at the caisson, the forces in the roof and walls will vary in time. This leads to fatigue of the reinforced concrete. In addition the crack width of the concrete has to be checked.

The only environmental load acting on the caisson is the wave load. For the caisson diffraction is an important aspect. For an extreme wave the force on the caisson is much higher than on the shaft (although no topic of this thesis, see Appendix A.4.2 for a first estimate). The structural motions within the caisson are not dealt with in this study.

3.3.7 Foundation

With respect to the foundation the next aspects are of influence:

- For relative small loads the soil behaviour can be assumed to be linear-elastic. For resulting stresses close to the limit state the assumption of linear-elastic material is not valid any more (see Appendix A.4.3.2).
  [A]: Assumed is that the bearing capacity is not exceeded. This assumption is based on a pre-design report.
- Cyclic behaviour leads to strength reduction and settlements.
  [A]: It is assumed that settlements stay within acceptable limits. This assumption is based on a pre-design report [10].
- Internal soil friction leads to damping. A value from literature is used within this thesis.
- The influence of the soil stiffness on the behaviour (natural frequency) is not investigated. A design study showed that the influence is very small.
- [A]: An earthquake is not taken into account due to the low probability of occurrence at the North-Sea.

3.4 LOAD COMBINATIONS

3.4.1 Standards

With respect to an offshore wind turbine the next type of load analysis can be distinguished [7]:

- Serviceability Limit State (SLS) — maximum acceptable deformations of the structure and crack width
- Ultimate Limit State (ULS) — structural strength and stability of elements and joints and the strength of the foundation
- Fatigue Limit State (FLS) — structural strength due to fatigue loads
- Accidental Limit State (ALS) — strength and stability due to accidental loads like ship collision or earthquakes

The load cases to be taken into account are prescribes in design codes.
Design rules for the support structure of offshore wind turbines are described in the DNV-OS-J101 code published in 2007 by 'Det Norske Veritas' [11]. The DNV code leads to 31 load cases, subdivided by:

- State of wind turbine (8 states like parked/operational/etc.)
    - Environmental conditions (wind/waves/current/water level etc)

3.4.2 Fatigue Limit State (FLS) loads

With respect to fatigue six load cases have to be considered, see Table 3.1. The table gives an overview of which environmental loads have to be taken into account for a certain state.
Some remarks with respect to the turbine states:

- The power production state (1.2) will be the most usual state to take into account. A probability distribution of wind and wave conditions is used to determine the loads.
- Start-up, shutdown and parked conditions also contribute to the fatigue load.
- During parking there is no aerodynamic damping to reduce the movement of the wind turbine.
- Fault conditions (for example the absence of aerodynamic damping or grid loss) may lead to an increase of fatigue load.

M/c state	Load case no.	Equiv LC on land	Wind condi-tions	Wind speed	Wave conditions	Water level	Grid, yaw and fault status
Power pro-duction	1.2	1.2	NTM	Cut-in – Cut-out	NSS Joint prob. distribution of $H_s, T_p, \overline{U}$	NWLR or ≥MSL	None
Power pro-duction with fault	2.4	2.4	NTM	Cut-in – Cut-out	Normal sea state i.e. $H_s = E[H_s\|\overline{U}]$	NWLR or ≥MSL	Fault con-dition
Start-up	3.1	3.1	NWP	Cut-in – Cut-out	Normal Sea State i.e. $H_s = E[H_s\|\overline{U}]$	NWLR or ≥MSL	None
Normal shut down	4.1	4.1	NWP	Cut-in – Cut-out	Normal sea state i.e. $H_s = E[H_s\|\overline{U}]$	NWLR or ≥MSL	None
Parked	6.4	6.4	NTM	$< 0.7U_{ref}$	NSS joint prob. distribution of $H_s, T_p, \overline{U}$	NWLR or ≥MSL	None
Parked with fault condition	7.2	None	NTM	$< 0.56U_{ref}$	NSS joint prob. distribution of $H_s, T_p, \overline{U}$	NWLR or ≥MSL	Fault con-dition

Table 3.1 – FLS load combinations. NTM=Normal turbulence model, NWP=Normal wind profile without turbulence, NSS=Normal sea state, NWLR=Normal water level range, MSL=Mean Sea Level [12]

3.4.3 Ultimate Limit State (ULS) loads

For the ultimate limit state the extreme wave, current and turbine load have to be combined. For the case regarded in Table 3.2 the wind contributes 'only' about 25% to the total horizontal force, but due to its higher point of action it contributes about 75% to the total overturning moment.

	Wind (%)	Wave (%)
Horizontal force	25	75
Overturning moment	75	25

Table 3.2 - Contribution to horizontal force and moment to be taken by the support structure for a 3.5 MW turbine on a monopile in shallow water [13]

For the ULS the DNV prescribes 25 load cases like for the FLS in Table 3.1. When no detailed information for each state is available yet the combinations of Table 3.3 can be used.

Limit state	*Load combination*	*Wind*	*Waves*	*Current*	*Ice*	*Water level*
ULS	1	50 years	5 years	5 years		50 years
	2	5 years	50 years	5 years		50 years
	3	5 years	5 years	50 years		50 years
	4	5 years		5 years	50 years	Mean water level
	5	50 years		5 years	50 years	Mean water level

Table 3.3 - ULS load combinations (when detailed information per state of the wind turbine is absent) [27]

3.4.4 Load combinations for the design of the steel shaft

For the design of the steel shaft in this thesis only the FLS and ULS are looked at. The steel has to be strong enough to resist the loads of all load combinations described above. Because of an increasing wall thickness and diameter of the shaft every section has to be checked in a final analysis. The next checks have to be performed:

- FLS: Resistance against fatigue load (Chapter 4)
- ULS: Local buckling and yielding of steel (Chapter 5)

In Chapter 6 the influence of both load cases on the design of the shaft is investigated.

3.5 THEORETICAL BACKGROUND OF LOADS AND DESIGN ASPECTS

A summary of the theoretical background of the loads on an offshore wind turbine is given below. See Appendix A.4 for a detailed description. The magnitude of the loads is estimated by means of a case study in Appendix B.
Please keep in mind that this section gives the theoretical background for the design of the whole support structure, and not for the steel shaft only. Although not directly used further in this thesis, a description of the wind loads has been added in order to gain insight in the background of this load as an important contributor to the design of the steel shaft.

3.5.1 Wind loads

Wind description

The wind velocity measured in the field shows variations in space and time. The wind speed increases with height above sea level (Figure 3.2). Wind is often schematized in terms of a mean wind speed with a standard deviation caused by turbulence. The Von Karman spectrum describes the wind signal (distribution of wind energy as a function of frequency).

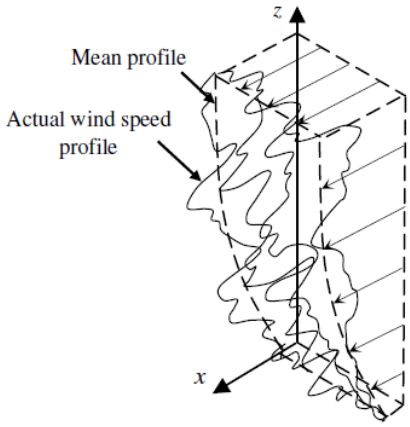

Figure 3.2 - Wind speed profile [14]

Wind loads

The wind will result in the following loads on the substructure:

- Wind turbine:
  - Axial force due to wind loading of the rotor,
  - Bending moment due to self-weight
  - Bending moment due to mass imbalance
  - Torsional moment due to misalignment between wind and nacelle direction
- Shaft loading due to drag

See Appendix A3 for more information about wind turbine characteristics.

Turbulence effects

Due to turbulence effects (in the shape of eddies) the turbine structure will experience a load peak at the rotation frequency of the rotor, called 1P. Often an eddy is seen multiple times by the blades, which will result in a load peak at the frequency of all the blades passing at 3P (and it's multiples) for a three-bladed turbine [2], see Figure 3.3 and Figure 3.4.

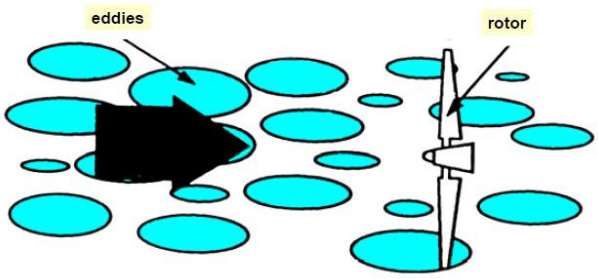

Figure 3.3 - Rotational sampling of turbulence [15]

The 1P and 3P ranges can be calculated with [16]:

$$f_{NP} = N\frac{\lambda V}{2\pi R} \tag{3.1}$$

with:

N	number of blades	[-]
λ	tip speed ratio	[-]
V	wind speed	[m/s]
R	rotor radius	[m]

Variable speed turbines (Appendix A.3.2) are gaining market share from fixed speed turbines. Compared to the fixed speed turbine, the frequency interval of a variable speed turbine is wider as it has multiple rotation speeds.

Tower top load

When the wind spectrum is shoved through the wind turbine the tower top load is found. An example of such a response spectrum can be found in Figure 3.4. This spectrum shows the relation between a certain wind speed and the tower top load. It results from time domain simulations with a wind turbine.

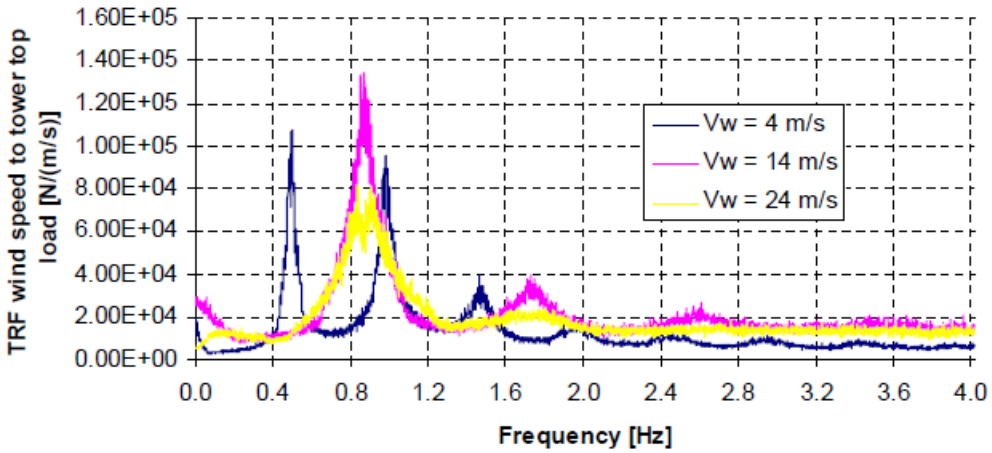

Figure 3.4 – Example of a relation between wind speed and tower top load. Load peaks are1P and 3P frequencies. [17]

3.5.2 Hydrodynamic loads

Wave description

Waves can be categorised by their frequency. According to [16] waves containing a lot of energy (wind-generated waves) have periods between 2 and 20s (0.5-0.05 Hz), where the extremes have a period between 7 and 13s (0.14-0.076 Hz).

The wave field can be described by wave-spectra:

- Pierson-Moskowitz spectrum: fully developed sea with infinite fetch.
- JONSWAP spectrum: non fully developed sea.

Wave fields can be categorized in:

- Regular waves: harmonic waves, narrow banded wave spectrum (swell waves).
- Irregular waves: broad banded wave spectrum. These waves can be composed in regular waves.

For an individual wave the particle velocities can be described by wave theories. Airy's wave theory is most convenient, but it is only valid for linear waves and up to still water level. Non-linear waves have to be described by Stokes wave theory or with Dean's Stream function. The applicability of the wave theories depends on the wave steepness and relative water depth. Based on these parameters one can select an appropriate wave theory, see Figure 3.5.

Depending on the d/L ratio (waterdepth/wavelength), waves can be categorized according to the definitions of Table 3.4.

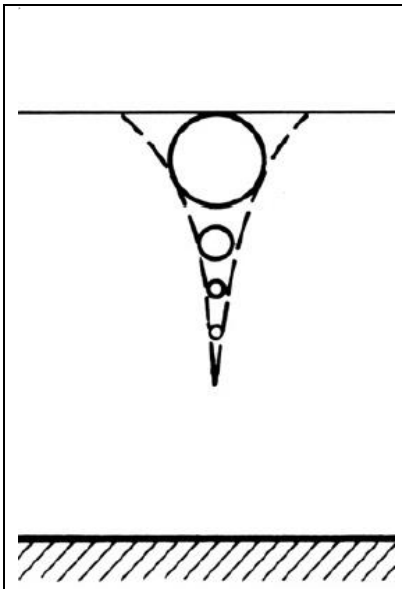	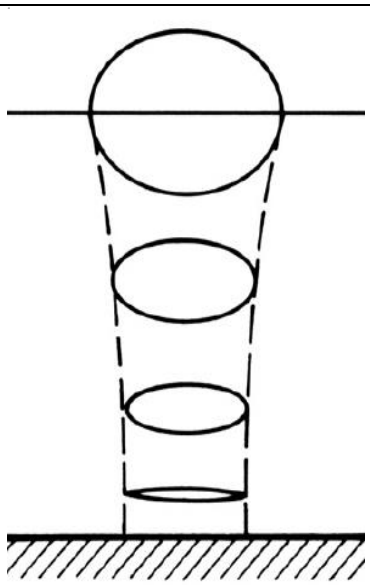	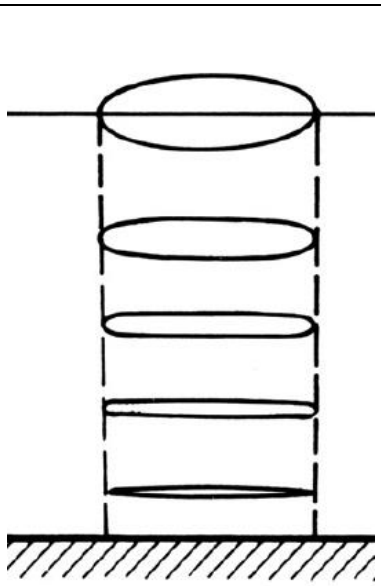
$d/L > 0.05$ Deep water Short waves	$0.05 < d/L < 0.5$ Intermediate depth -	$d/L < 0.05$ Shallow water Long waves

Table 3.4 – Classification of waves and the corresponding orbital motion [18]

Wave loads

For wave loads a distinction has to be made with regard to the shape of the structure [19]:

- For slender structures (D/L<0.2) the presence of the structure on the wave induced flow can be ignored when calculating the force on the structure. In this case Morison's theory is often used. See Chapter 5.4 for more information.
- Compact structures on the other hand will influence the movement of the water significantly. For these structures the drag force can be neglected, as inertia dominates. However, in this case the influence of diffraction has to be taken into

account. An adaption of the inertia coefficient in the Morison equation gives acceptable results.

In general the wave loads can be subdivided in:

- Drag forces
- Inertia forces
- Lift forces

More information about the drag-and inertia forces can be found in Chapter 5.3.
With respect to the lift forces in Appendix A.4 that possibly resonance may occur.

Currents

Sea currents, driven by tides and ocean circulations, may cause extra local currents. These currents influence the drag and lift force due to waves. Currents can simply be added in the wave load analysis by linear superposition with the horizontal particle kinematics. For the situation of combined waves and flow other Morison coefficients have to be used as for waves or currents only [20].

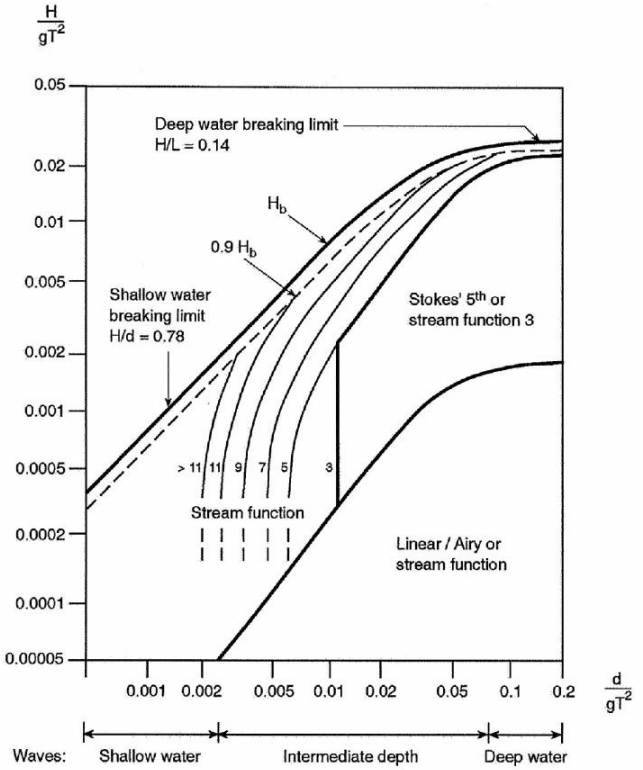

Figure 3.5 - Ranges of suitability of regular wave theories (d= water depth, g= gravity acceleration, H = wave height, L = wave length, T = wave period) [11].

3.5.3 Accidental loads

The next loads can be considered as accidental loads:

- Earthquake loads: it depends on the probability of occurrence whether these loads are taken into account.
- Ship collisions: often taken into account by determining the impact load for a given type of ship with a certain navigation speed.

3.5.4 Geotechnical aspects

The subsoil must be able to resist all the loads acting on the offshore wind turbine. The following aspects are of importance:

- Vertical bearing capacity & overturning: the vertical bearing capacity can be calculated according to the theory developed by Prandtl, Terzaghi and Brinch Hansen.
- Sliding resistance.
- Behaviour under cyclic loading:
  - Strength reduction due to excess pore pressure (reduction due to effective stresses and a decrease in the shear strength).
  - Settlements due to densification/ liquefaction.
  - Removal of material due to pumping motion.
- Relative settlements: due to consolidation. There is a strict maximum rotation prescribed due to wind turbine operations.

Scour

A structure at the bottom of the sea influences the local flow pattern, causing local scour. For a GBS scour is expected to be unacceptable, due to their high reliance on near-surface soil [19]. Scour can be prevented by a scour protection.
In addition to scour natural sediment displacement may result in rise or drop of the entire seabed around the structure. When the magnitude is in the order of 1m the foundation level can be chosen at the lowest expected seabed level during the lifetime of the structure.

3.5.5 Other

Other aspects to be taken into account are:

- Corrosion: corrosion leads to a reduction of the strength, but can be prevented by protection.
- Marine growth: marine growth may have influence on the hydrodynamic loads, dynamic response (due to added weight) and corrosion rate.
- Ice load: accumulation, collision (horizontal loads) and ice attachment (vertical load).

3.5.6 Dynamic behaviour

3.5.6.1 Dynamic system

The dynamic behaviour of a system can be distinguished in three kinds of responses [2]:

1. Quasi-static: $f_{ex} < f_{nat}$: displacement of mass follows time varying force almost instantaneously
2. Resonance: $f_{ex} = f_{nat}$: response is number of times larger than it would be statically
3. Inertia dominated: $f_{ex} > f_{nat}$: response is small and almost counter-phase

Here f_{ex} is the excitation frequency of the load, and f_{nat} the first natural frequency of the offshore wind turbine. For linear systems the magnitude of the response can be expressed with the Dynamic Amplification Factor (DAF): the ratio between the dynamic response magnitude and the static response magnitude (Figure 3.6). The phase lag can be related to this factor. The peak in Figure 3.6 corresponds to the system's natural frequency and the height is determined by damping.

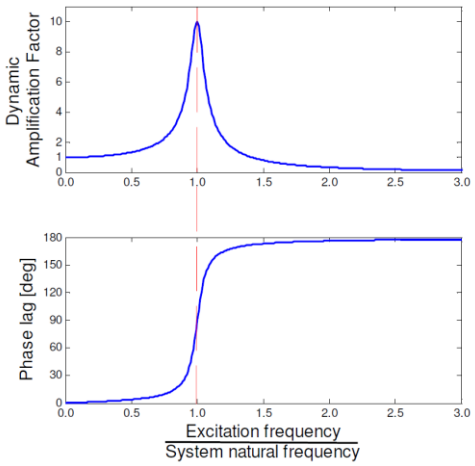

Figure 3.6 - Example of a DAF graph [14]

Resonant behaviour can cause severe load damage and even failure, but it is most feared because of possible fatigue damage. Therefore these excitation frequencies should be avoided as much as possible. As such, the structure should be designed so that its first natural frequency does not coincide with either 1P (the rotor frequency f_R), or 3P (the blade passing frequency f_B). In order to reduce resonance behaviour the rotation speed can be tuned in order to skip the first natural frequency. This is not the case with the waves: they can be (and often are) in the range of the natural frequency of the offshore wind turbine (see for example Figure 3.7).

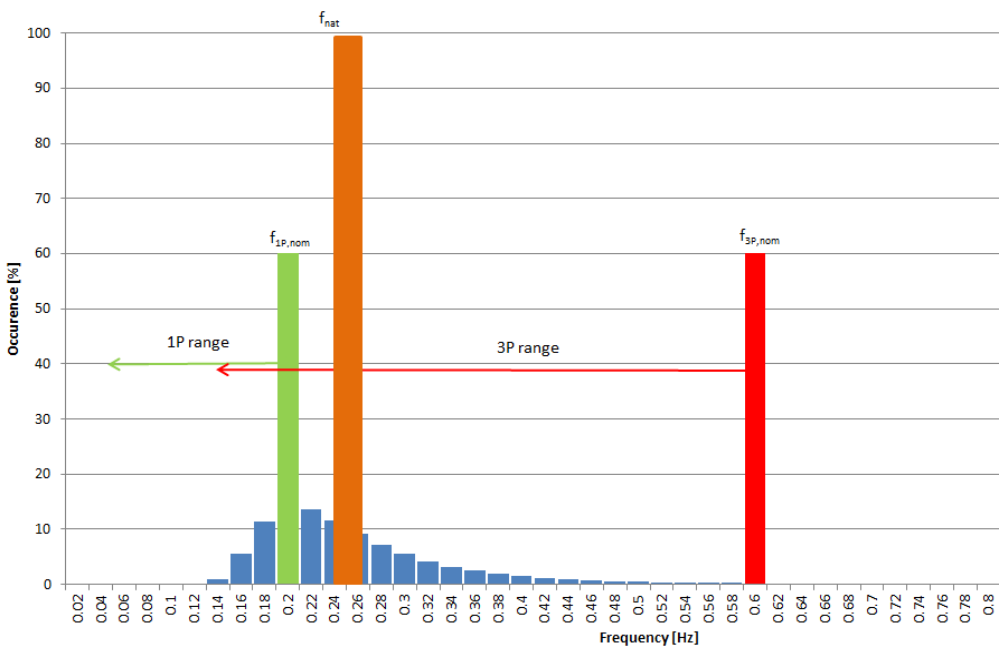

Figure 3.7 - Wave, 1P, 3P and prescribed natural frequencies for a variable speed Siemens SWT 6.0-154 turbine. Waves: PM spectrum with Hs=2m and Tp=5s

3.5.6.2 Damping sources

Damping will determine the height of the resonance peak. Damping is often expressed as percentage of critical damping ($\zeta = 1$), see Appendix A.4.5. The types of damping to be taken into account, based on literature, are (see Appendix A.4.5.4):

1. Structural damping: internal material friction and the effect of a bolted connection: 0.5%
2. Aerodynamic damping: damping source introduced by operating turbine. The amount of damping is strongly dependent on the type of offshore wind turbine, its behaviour and the wind speed. A conservative engineering estimate is 4% for all wind speeds.
3. Hydrodynamic damping: next to radiation of wave energy the viscosity of water leads, via the drag force, to hydrodynamic damping when the support structure moves with respect to the wave: 0.1%
4. Soil damping: internal soil friction and radiation of vibration energy: 1%

Ad 2. When the turbine moves forward (against the wind), the blades experience an increase in total wind speed. As a result the wind load on the blades increases. This load acts against the tower top motion (Figure 3.8), so it introduces a kind of a damping effect. For backward motion, the situation is analogous, now resulting in a reduced tower top load, also reducing the tower top motion [14].

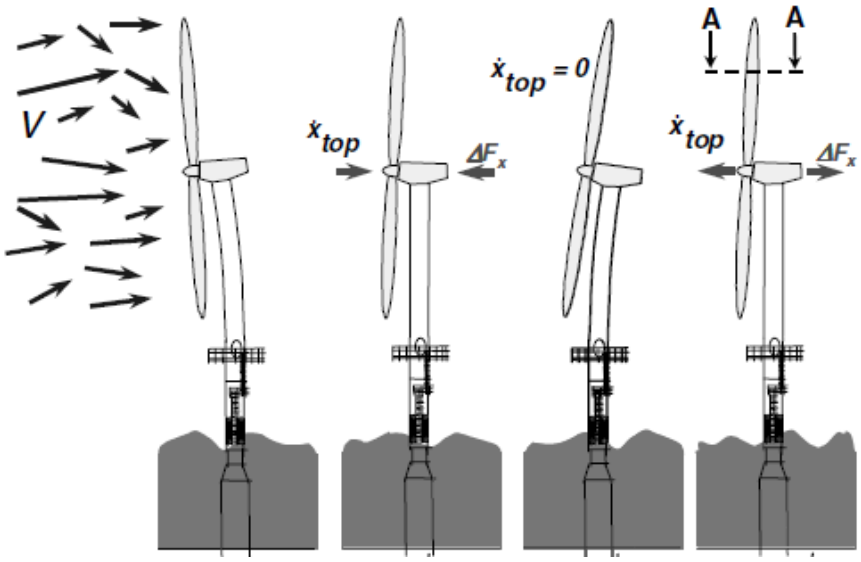

Figure 3.8 – Illustration of aerodynamic damping effect [21]

Taking all the individual damping sources into account a conservative damping estimate is:

- Non-operating: 0.5% (structural) + 0.1% (hydrodynamic) + 1% (soil) = 1.6%
- Operating: 1.6% + 4% (aerodynamic) = 5.6%

3.6 CLOSING REMARKS

Within this chapter an overview of the design of an offshore wind turbine was presented. Designing the support structure is only a part of the whole design process of an offshore wind turbine.

In order to design the support structure, one has to know all the forces and design aspects. Therefore a component breakdown was performed. It followed that the main function of the support structure is to transfer the loads from the turbine to the foundation. In addition the support structure itself is also loaded by wind and wave loads.

For the design of the support structure two important load cases play a role: the ULS and FLS. The ULS was found to be characterized by, amongst all, extreme wind and wave loads. The magnitude follows from different load cases as prescribed by design codes. Within such a load case a certain wind load is combined with a wave load. The maximum wind load is strongly related to the wind turbine behaviour, and does not necessarily have to occur at highest wind velocity.

Also for the FLS different load cases are prescribed. For the FLS not only the magnitude of the force is important, but also its frequency. The (non)operational behaviour of the wind turbine has a strong influence on the fatigue load. Damping becomes an important aspect now. Also for the waves both the magnitude and frequency play a role.

Except from the design of the steel shaft, the design of the caisson and foundation are important aspects of designing a GBS as well. Important questions are whether the caisson is able to resist the forces from the shaft, and whether the foundation is able to resist the loads from the support structure (both during ULS and FLS). For the rest of this thesis these questions are however left outside the scope.

4

4 FATIGUE OF THE SHAFT OF AN OFFSHORE WIND TURBINE

4.1 INTRODUCTION

This section gives an overview of the fatigue analysis for an offshore wind turbine. This is an important aspect for the design of the steel shaft of the support structure. The chapter gives a general overview based on literature. In Chapter 6 the theory described here is applied in order to answer the second research question.

First in section 4.2 the theoretical background of fatigue is given. In order to take all the load cycles for the lifetime of the offshore wind turbine into account, one can choose between two types of analysis:

- a Time Domain analysis (based on numerical simulation)
- a Frequency Domain analysis (based on analytics)

Both types of analysis lead to different methods to calculate the combined fatigue load due to wind and waves. An important aspect is the combination of wind and wave loads when they would be calculated separately.

Section 4.3 gives an overview of the four methods available to calculate the fatigue load for an offshore wind turbine. The section ends with the description of a practical method for pre-design. This method is applied in Chapter 6 to calculate the fatigue load.

4.2 THEORETICAL BACKGROUND OF THE FATIGUE ANALYSIS

4.2.1 Fatigue principle

Fatigue is caused by changing stresses. Due to these stress changes, the material slowly deteriorates, initiating cracks which will eventually lead to breaking of the material. Offshore wind turbines are by default subjected to loads varying in time from wind and waves. This means that the stress response will also vary continuously, making offshore wind turbines sensitive to fatigue.
An empirical design method is commonly used to consider fatigue in the design process. From laboratory tests a so called S-N curve (see Figure 4.1) is deduced, with:

- S: a certain bending stress range
- N: the number of cycles at which failure of the material occurs

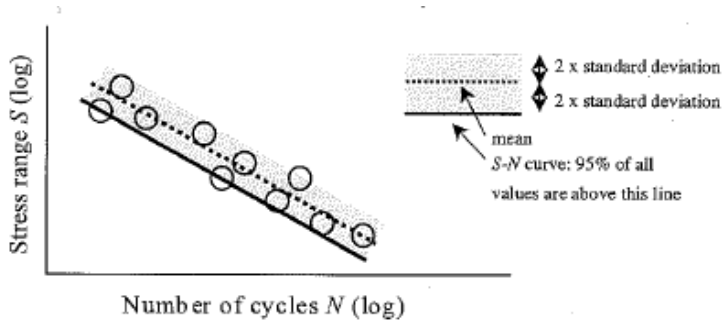

Figure 4.1 - Typical shape of an S-N curve [14]

The S-N curve is described by equation (4.1) [11]:

$$logN = loga - m \cdot log\left(\Delta\sigma\left(\frac{t}{t_{ref}}\right)^{k}\right) \qquad (4.1)$$

with:

N	number of stress cycles to failure at stress range $\Delta\sigma$	[-]
$\Delta\sigma$	stress range	[N/mm^2]
m	slope of S-N curve (3-5)	[-]
$\log a$	intercept of log *N* axis	[-]
t_{ref}	reference thickness, 32 mm for tubular joints	[mm]
t	thickness through which the potential fatigue crack will grow ($t \geq t_{ref}$)	[mm]
k	thickness exponent (0.20 – 0.25)	[-]

Figure 4.2 gives the flowchart for a fatigue calculation:

- Fatigue calculations start with determining governing details or sections.
- Next, the stresses the section will experience during its lifetime should be predicted.
- When all stress variations in the time domain are known they can be binned in a number of variations n_i per stress range class S_i. The result is a stress histogram that can be obtained by the so called RainFlow Counting (RFC) method [2].
- The next step is to determine the maximum allowable number of stress variations N_i for each stress range class S_i from the S-N curve.
- Finally the Miner Rule can be applied:

$$D_{fat} = \sum_i \frac{n_i}{N_i} < 1 \qquad (4.2)$$

with:

D_{fat}	fatigue load (fatigue damage)	[-]
n_i	number of stress range variations S_i	[-]
N_i	allowable number of variations for stress range S_i	[-]

According to this rule no failure due to fatigue will occur as long as the above criterion is met.

Often the fatigue influence is expressed by the damage equivalent stress $\Delta\sigma_{eq}$. This is a certain stress range applied N_R (often $1 \cdot 10^7$) times, leading to the same amount of damage as all the individual stress cycles over the life period. The load causing the damage equivalent stress $\Delta\sigma_{eq}$ is defined as the Damage Equivalent Load (DEL).

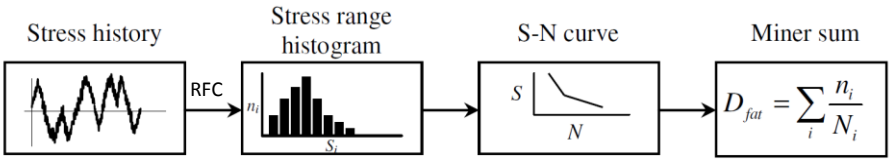

Figure 4.2 - Flowchart of a fatigue load calculation in time domain [3]

4.2.2 Time vs. Frequency Domain

The main contributors to the fatigue load are wind and wave loads. These loads result in bending stresses in the steel shaft of the wind turbine. Due to their periodic character they will lead to a continuously varying stress response.
To obtain the stress history of Figure 4.2 there should be a method that couples the loads over time with the response within the structure. In general two types of analysis exist to determine this bending stress response:

1. A Time Domain (TD) analysis: time series of wind and wave distributions are entered in a computer program. The program simulates in fact for the whole lifetime the behaviour of the wind turbine and produces time series of stress responses.
2. A Frequency Domain (FD) analysis: in frequency domain load spectra are directly transferred to stress response spectra. The link between the two is laid by a so called transfer function. The transfer function lays the relation between a load and the structural response and can be determined analytical or with the aid of a software package.

Table 4.1 gives an overview of some characteristics of both methods. In short:

- The FD analysis is common practise in offshore engineering. This mainly has to do with the fact that the restriction to linear loads is not a problem for this field, enabling fast FD calculations.
- Within the field of (offshore) wind energy the non-linear behaviour of the wind turbine often leads to the application of the TD analysis for the whole structure.
- A disadvantage of the TD analysis is the high computational effort. On the other hand the FD analysis is characterized by fast calculations which makes optimisation possible. It gives good insight in the behaviour of the system and is therefore suitable in early stages of the design.

	Time domain	Frequency domain
Area	(Offshore) wind industry	Offshore engineering
(Non) linearity	(Non)-linear	Linear only
Computational time	Several hours	2 minutes (parameter variation possible)

Table 4.1 - Time versus Frequency domain analysis [14]

Although the two types of analysis are different the results are interchangeable. This coupling is achieved by the Fourier Transformation (Figure 4.3).

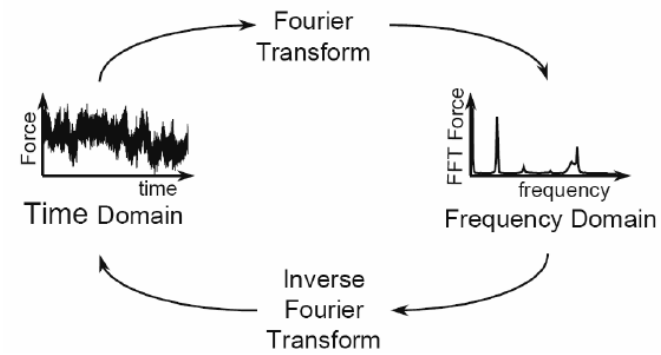

Figure 4.3 – Coupling between Time and Frequency domain [14]

4.2.3 Superposition of wind and wave loads

For an offshore wind turbine both wind and wave loads lead to fatigue. Within the TD analysis both influences are calculated at the same time and taken into account. Within the FD analysis however wind and wave loads are regarded via a separate loading spectrum. The responses can be combined in the following manner (see Figure 4.4):

1. A separate analysis of wind and waves. This method determines the response signals from both loads (wind and waves) separately. Afterwards both signals are combined. This approach is often used in an early design stage, as it gives rather fast results. This method leads to an overestimation of the response as wind and wave responses cannot be treated as being independent. In fact they influence each other through aerodynamic damping (section 3.5.6.2).
2. An Integrated Approach. In the integrated approach, contributions from wind and waves are considered simultaneously. Due to this combination a reduction in response occurs due to cancellation from phasing and the effect of aerodynamic damping. These effects are taken into account by applying the quadratic superposition method as presented in section 4.3.2 and used in Chapter 6.

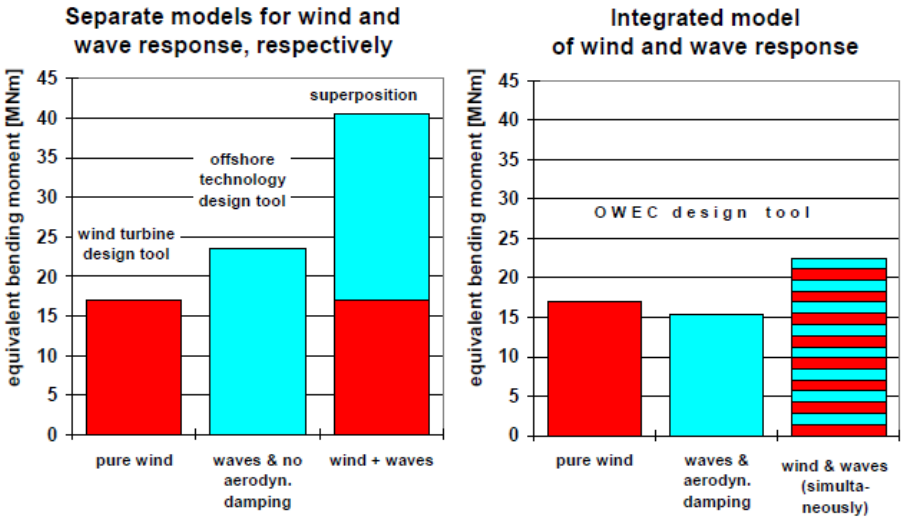

Figure 4.4 - An example of the response for the Separate Analysis versus the Integrated Approach [22]

4.3 METHODS TO DETERMINE THE FATIGUE LOAD

4.3.1 Fatigue analysis for an offshore wind turbine

In general a full fatigue analysis for an offshore wind turbine consists of the following steps:

- The first step is to determine the sections of the tower and steel shaft where the fatigue load will be governing (transitions where the wall diameter changes; important is the bottom of the shaft due to the highest bending moment).
- Next, environmental data has to be collected. Based on measured wave data for the lifetime of the structure a prediction can be made of the wave spectrum. Also for the wind load spectra are predicted, which can be determined based on measured wind data. The environmental conditions (a combination of wave height, period and wind speed) are lumped until about 30 environmental states with their probability of occurrence remain. Each environmental state has its own wind and wave spectrum.
- For a time domain analysis the spectra have to be transformed to a time series by Inverse Fourier Transform. For a frequency domain analysis the loading spectra are used directly.
- Next a TD or a combination of a TD and FD analysis is performed in order to determine the stress responses over the lifetime of the structure. See section 4.3.2 for the methods available.
- The resulting stress responses can be transformed to fatigue loads by different counting methods. For a FD analysis a different method has to be used than for a TD analysis, due to the different output (a response spectrum instead of time series).
- The fatigue load D_{fat} is transformed to a DEL (Damage Equivalent Load) in order to be able to include safety factors and perform a unity check. If the fatigue load is higher than the resistance, the structure has to be strengthened. If not, it can do with less material.

4.3.2 Overview of methods

One can distinguish different methods to determine the fatigue load, because:

- For the support structure one can apply both TD and FD analysis.
- At different points in the process one can add the responses due to wind and wave loads.

The most common methods are described below [23]:

1. The wind response is found by a TD analysis and transferred to a spectrum. The wave response is found with a FD analysis. Both spectra are combined.
2. The wind response is found by a TD analysis. The wave response is found with a FD analysis and transferred to a time series. Both time series are added (see [21]).
3. The wind response is found by a TD analysis and calculated towards a damage equivalent stress. For the wave response the same is done in a TD or FD analysis. Next, the method of weighted quadratic superposition is applied.
4. Full TD analysis, by simulating both wind and wave field in a TD model.

Ad. 1:
This approach is based on the so called superposition of response spectra: under the assumption of independent wind and wave excitations on the long term both responses can

be simply added. In fact these responses are coupled through aerodynamic and hydrodynamic damping. These effects should be taken into account in the analysis.
The advantage of the method is that it is a useful tool in pre-design. The FD analysis enables optimisation due to small computational effort and provides valuable insight in the behaviour of the offshore wind turbine. The disadvantage is however that, as known to the author, the amount of aerodynamic damping can only be based on an engineering model (a rough estimate being constant for every wind class). Another disadvantage is that the wind turbine manufacturer should cooperate in providing the wind turbine responses by means of a TD analysis. The method is extensively described in [14] and applied in [17].

Ad. 3:
The quadratic superposition of wind and wave loads is based on the next equation:

$$\Delta\sigma_{eq,ah} \approx \sqrt{\Delta\sigma_{eq,a}^2 + \Delta\sigma_{eq,h}^2} \text{ for } T_{z,a} \approx T_{z,h} \quad (4.3)$$

with:

$\Delta\sigma_{eq,ah}$	total damage equivalent stress range	[MPa]
$\Delta\sigma_{eq,a}$	damage equivalent stress range due to wind	[MPa]
$\Delta\sigma_{eq,h}$	damage equivalent stress range due to waves	[MPa]
$T_{z,a}$	zero crossing period of wind response	[s]
$T_{z,h}$	zero crossing period of wave response	[s]

The above equation, which is only valid if the aerodynamic response has the same zero-crossing period as the hydrodynamic response, is a simplification of a more sophisticated formula of the so-called weighted quadratic superposition (also called the Kuhn-Hannock expression).
With respect to the long term it was found that the quadratic superposition also can be used as an approximation for the pre-design phase [24]. The method was investigated in [21] where it gave errors in the order of 10%. This is relative low compared to the errors resulting from approximations of the aerodynamic damping in this phase [21].

4.3.3 Method for pre-design

For pre-design a method based on quadratic superposition can be used to determine the fatigue load. See Figure 4.5 for a schematic overview of the method. The method is applied to a case study in Chapter 6. The method was used for the Ultgrunden wind farm [14], and for a pre-design study at BAM [10]. The following steps have to be performed:

- First the level where the fatigue load is calculated has to be determined. Often the lowest section of the shaft is governing due to the highest bending moment.

Wave loads

- Now, first the stress ranges from the wave loads are determined. Input for the calculation is a wave scatter diagram. The wave scatter diagram is lumped to about 20 wave classes in order to reduce the amount of required wave force calculations. This is done so, by weighing the quasi-static damage of all the original sea states. For each lumped wave class the amount of waves n is given. Wave directionality should be taken into account. See Table 5.1 for the lumped wave-scatter diagram used within this thesis.

- For each of the wave classes the resulting force on the structure and stress range in the structure at the governing location for fatigue is calculated. A (dynamic) structural model is used for this purpose. The wind turbine can be schematized as a tower with a certain mass on top.
- Now, per wave class the stress cycle is known. Per combination of wave class and direction the number of stress cycles n_i is known from the lumped wave scatter diagram.
- The stress cycles are transformed to the governing fatigue direction (the governing wind or wave direction) by simple mathematics. For each stress cycle the influence on the total allowable fatigue (n_i/N_i) is calculated. These influences are summed up according to the Miner Rule, see equation (4.2). This leads to a fatigue load due to waves $D_{fat;h}$
- In order to add the fatigue load of the waves to the wind the same amount of cycles N_R has to be regarded. Therefore the fatigue load is transformed to a damage equivalent stress $\Delta\sigma_{eq,h}$ for N_R cycles (fixed amount, see section 4.2.1).

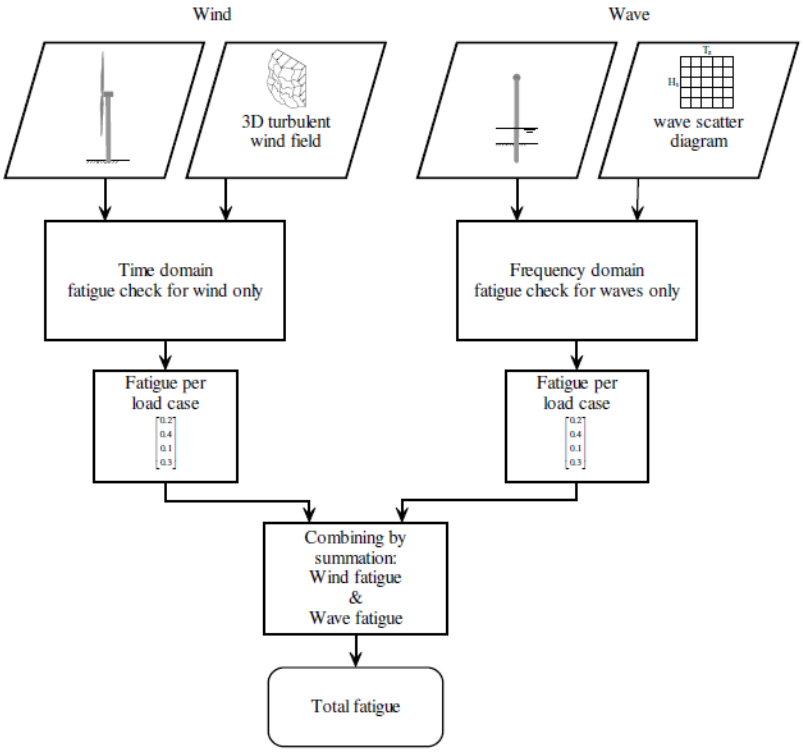

Figure 4.5 - Quadratic superposition method for pre-design [14].

Wind loads

- The stress ranges from wind loads are provided by the wind turbine manufacturer, who has performed a TD analysis of the fatigue loads. It is recalled that for the wind loads this is the only option due to the non-linear behaviour of the wind turbine. For the lifetime of the structure the resulting bending moment at tower base accompanied by a certain number of cycles is prescribed. These forces can be converted to stress cycles.
- The wind turbine manufacturer also gives a damage equivalent load for N_R cycles. This leads to a damage equivalent stress for wind $\Delta\sigma_{eq,a}$.

Quadratic superposition

- Finally, the quadratic superposition method (section 4.3.2) is used to combine the wind and wave stress cycles, leading to $\Delta\sigma_{eq,ah}$. This value should be compared with the maximum allowable damage equivalent stress $\Delta\sigma_{eq,max}$ for a certain cross section. This value follows from a S-N curve, as described by equation (4.1).
  In [11] a safety factor DFF (the so-called Design Fatigue Factor) of 3 is prescribed for seawater environments. From equation (4.1) the value of $\Delta\sigma_{eq,max}$ can be determined as function of $N = 3 \cdot N_R$ cycles, $D_{fat} = 1$ and the wall thickness t.
- Now, by performing the unity check $UC._{FLS} = \Delta\sigma_{eq,ah}/\Delta\sigma_{eq,max} \leq 1$ the required wall thickness can be determined.

4.4 CONCLUDING REMARKS

Within this chapter the theoretical background of the fatigue analysis was given. For the wind loads only a TD analysis has to be applied due to the non-linear behaviour of the wind turbine. For the response due to wave loads both a TD and FD analysis can be performed. This combination leads to several different methods. An overview of four different methods available was given.

The most sophisticated method is to perform a full TD analysis to determine the fatigue load (method 2 and 4 of section 4.3.2), but this requires high computational effort. Therefore it is only applied in detailed design. For pre-design a method based on superposition of response spectra was found (method 1). But this method still required output data (response spectra) of a TD analysis by the wind turbine manufacturer. This data was not available, so another method was chosen. The method of quadratic superposition was used for this purpose (method 3). This method only requires a damage equivalent load, which was given by the wind turbine manufacturer as a result of a TD analysis of the wind turbine. The method is applied to the design of the shaft in Chapter 6.

5

5 HYDRODYNAMIC LOAD ON THE SHAFT OF THE GBS

5.1 INTRODUCTION

The hydrodynamic load on the shaft of the GBS has an important influence on the design. For a monopile structure the hydrodynamic forces (waves, currents) are in practice calculated by application of the Morison equation (section 5.3 and 5.4). This equation is based on a coupling between incident wave kinematics and the force on a cylinder. For a GBS the application of the Morison equation is not so straightforward anymore, because the caisson may influence the flow pattern around the shaft. In this chapter it is investigated what the influence of the caisson is for both ULS and FLS waves (first research question). At the end of this chapter it is recommended whether the Morison equation can be used to determine the hydrodynamic load on the shaft of the GBS or not.

Next to a model or full scale test, the influence of the caisson can be investigated by using a numerical model. For this purpose the numerical finite element model FinLab was used. The background of the model is described in section 5.5.
For this application the model is extended with a force module (based on already existing output: the hydrostatic pressure and velocities around the shaft). The resulting wave kinematics and force module are validated for a monopile structure, see section 5.6.
The results seem to match very well with theory.

In order to reduce calculation time a selection of the FLS cases is made. Section 5.7 gives an overview of the performed simulations. The influence of the caisson is investigated in section 5.8 by modelling two different structures with exactly the same environmental and numerical conditions by FinLab:

- a monopile
- a GBS

A sensitivity check is performed in section 5.9. The influence of the caisson is investigated by comparing the wave kinematics around the upper part of the monopile, and the shaft of the GBS. By comparing the wave forces on the shaft of the GBS and exactly the same section of the monopile, the influence of the caisson on the force is determined. See section 5.10 for an analysis of the results.

The chapter starts with an introduction to the case study, being used throughout Chapter 5 and 6.

5.2 INTRODUCTION TO THE CASE STUDY

In order to determine the hydrodynamic loads with FinLab and the influence on the design of the steel shaft, a certain case has to be selected. Based on this case the water depth, structural dimensions and wave climate can be selected. Please note that the case study given here is different from the case study corresponding to Appendix B, this appendix is used as a rough estimate of the magnitude of the loads presented in Chapter 3. The case study presented here is used in Chapters 5 and 6, and the corresponding Appendix C and Appendix D .

5.2.1 Location and environmental loads

5.2.1.1 Location

A hypothetical wind farm near the coast of the U.K. has been selected for this purpose. The influence of the caisson on the hydrodynamic load on the steel shaft is expected to be strongest for a small water depth (see section 5.7.1). Therefore a water depth of d=34m has been selected, the minimum of the applicable water depth range of the GBS (35-60m).

5.2.1.2 Wave climate

For the FLS a wave scatter diagram has to be selected, based on the wave climate of the hypothetical location. The wave scatter diagram used is based on a lumped wave scatter diagram for the Beatrice wind farm near the U.K, see Table 5.1.
Assumed is that this wave scatter diagram can be used for our hypothetical location.

Lumped wave scatter diagram				Annual Wave Conditions: Sea & Swell							
Class	Sign. wave height		Period	Wave direction (coming from) [deg]							
	Range	Average	T02	N	NE	E	SE	S	SW	W	NW
(-)	[m]	[m]	(s)	0	45	90	135	180	225	270	315
1	0 - 1	0.5	3.8	117249	1224952	449588	222917	307944	366480	384716	200702
2	0 - 1	0.5	5.1	84457	365254	241443	111423	164237	564644	357057	178436
3	0 - 1	0.5	7	2100	4677	5693	774	6784	34799	22097	10127
4	1-2	1.5	4.8	38972	215350	125899	60129	78761	102070	123895	65399
5	1-2	1.5	5.9	29411	58180	62718	25954	16525	26960	42608	16119
6	1-2	1.5	7	7348	17158	20796	2799	6219	27737	21741	8985
7	2-3	2.5	5.4	16314	41336	37595	16084	12894	19304	28055	11828
8	2-3	2.5	7.2	2039	4854	5871	801	692	2326	2810	972
9	3-4	3.5	5.9	2176	3713	4457	1810	979	1711	2864	1004
10	3-4	3.5	7.2	2674	6410	7731	1192	603	1518	2739	847
11	4-5	4.5	5.9	375	640	768	312	169	295	494	173
12	4-5	4.5	7.3	777	1709	2052	457	230	485	862	280
13	5-6	5.5	7.4	229	840	1023	76	15	78	205	63
14	6-7	6.5	7.5	48	219	272	12		13	46	13
15	7-8	7.5	7.9	5	57	77				7	
16	8-9	8.5	7.9		14	24					
17	9-10	9.5	8.5			6					
18	10-11	10.5	8.5			1					
		Total		304173	1945362	966014	444739	596052	1148419	990194	494949

Table 5.1 – Lumped annual wave scatter diagram used. Based on wave data measured at the Beatrice Wind farm (UK) [10]

For the ULS an extreme wave has to be defined. This wave has a return period of 50 years, see Table 3.3. In fact the characteristics of this wave should have to follow from a probabilistic calculation, with the measured wave climate as input.
In another research of the wave load on a GBS by BAM the following wave was selected as ULS wave for a water depth of about 35m:

Maximum wave height ($H_{max,50}$): 16.9 m
Wave period (T): 12.7 s
This wave is selected for our hypothetical location.

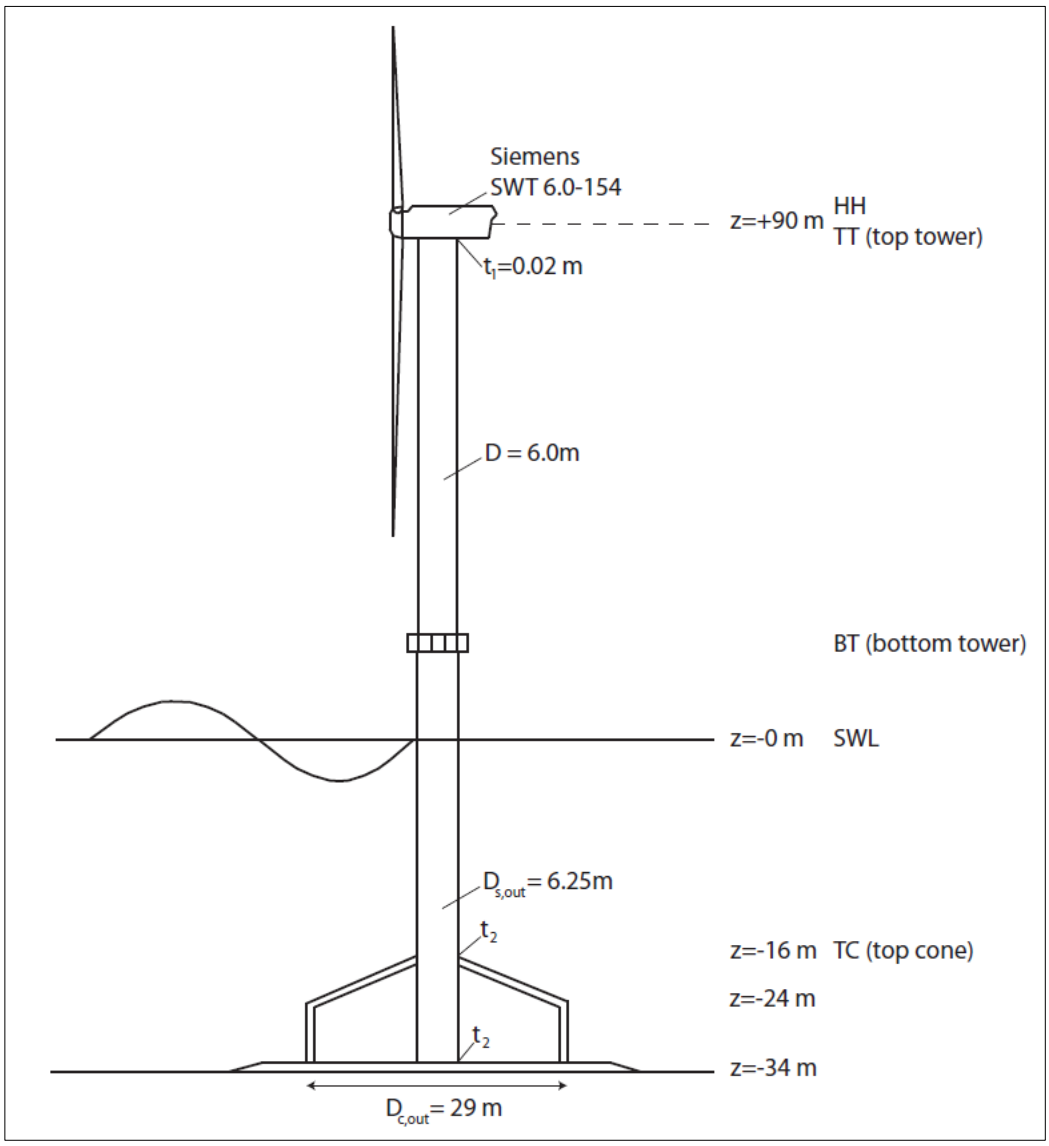

Figure 5.1 – Schematisation of the offshore wind turbine for Chapter 5 and 6. D=diameter, t=wall thickness, HH=Hub Height, SWL=Still Water Level

5.2.2 Structural schematisation

The dimensions of the structure are assumed to be (see Figure 5.1):
Seabed level: -34 m SWL

Diameter caisson: 29 m
Height walls: 10 m
Height cone: 8 m
Diameter shaft (-34<z<BT): 6.25 m
Diameter turbine tower (BT<z<TT): 6.00 m
Roughness according to Nikuradse ($k = kN0$): 0.02 m

Wind turbine:	Siemens SWT 6.0-154 (6MW)
Hub Height (HH)/ Tower top (TT):	+90 m SWL
Bottom Tower (BT):	+15 m SWL
Wall thickness z=TT:	0.02 m
Wall thickness TC<z<TT:	varying linearly
Wall thickness z≤TC:	constant (determined in Chapter 6)
First natural frequency as prescribed by the wind turbine manufacturer (f_{nat}):	0.25 Hz ± 5% [10]

5.2.3 Assumptions made

In section 3.3 already a list of assumptions was given as a result of the component breakdown. The most important assumptions for this chapter are summarized here:

- Loads due to wave breaking are not taken into account.
- Lift forces are not taken into account.
- Currents are not taken into account.
- Local water elevations due to tides and storm surges are not taken into account.

In addition the following assumptions are made:

- Within this chapter it is assumed that structural displacements are small and that for determination of the hydrodynamic forces the structure can be modelled as being rigid.
- For simplicity only regular wave loads are taken into account.

In addition the assumptions for Chapter 6 can be summarized by:

- The wind forces (instead of a loading spectrum) as provided by the wind turbine manufacturer can be used.
- The shaft can be schematised as a clamped beam at TC level.

5.3 PHYSICAL PROCESSES

Wave forces on structures can be calculated for different situations. One can distinct the type of waves (breaking or non-breaking), the dimensions of the structure (slender or large) and type of flow regime (separated or non-separated). In this section the physical background of flow and waves around a cylinder are given. See Appendix C.1 for more information.

5.3.1 Cylinder in steady current

The most basic principle is a cylinder in steady current. For a structure in a current the Reynolds number is related to the type of flow regime. The Reynolds number is a function of the horizontal particle velocity at water level, the cylinder diameter and the kinematic viscosity:

$$RE = \frac{uD}{\nu} \tag{5.1}$$

with:

RE	Reynolds number	[-]
u	horizontal particle velocity	[m/s]
D	diameter	[m]
ν	kinematic viscosity	[m^2/s]

For very low (Re<5) Re numbers no separation occurs. For higher numbers a wake behind the cylinder develops, first laminar and for higher numbers turbulent. Also the process of vortex shedding start, leading to lift forces perpendicular to the flow. For very high Re number (Re>$4 \cdot 10^6$, so called trans-critical flow) the both the wake and boundary layer are completely turbulent.

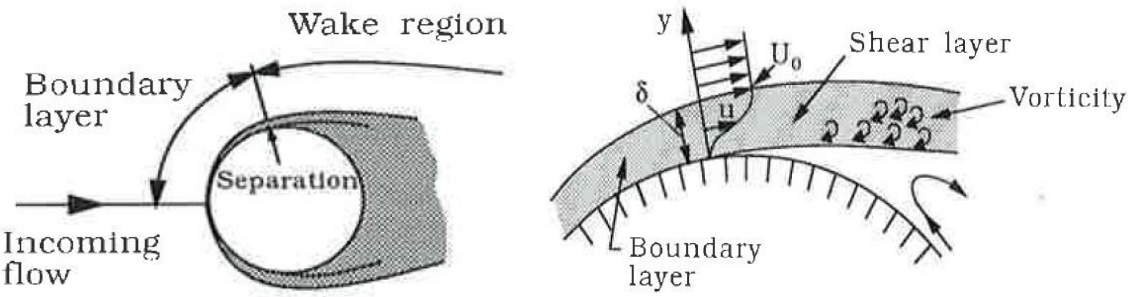

Figure 5.2 – Flow around a cylinder [25]

Based on the Re number, and associated flow regime, the force on a structure in flow can be determined. Flow around a cylinder leads to two force contributions:

1. Pressure force: due to the wake the pressure at the rear of the cylinder is lower than at the front. The pressure force is related to the separation point, see Figure 5.2. Each flow regime can be related to a certain value of the separation angle.
2. Friction force: due to wall roughness a friction force develops parallel to the wall.

Both forces lead to the so called drag force:

$$F_D = \frac{1}{2}\rho C_D D u|u| \tag{5.2}$$

with:

F_D	drag force (per unit of length)	[N/m]
ρ	density of the water	[kg/m^3]
C_D	drag coefficient	[-]
D	diameter	[m]
u	horizontal flow velocity	[m/s]

The drag force per unit length is dependent on the horizontal particle velocity. The drag coefficient, C_D, can be deduced from experiments, see section 5.4.

5.3.2 Cylinder in oscillatory flow

For an oscillatory flow the Keulegan-Carpenter number describes the flow regime. The KC number is a function of the horizontal particle velocity amplitude, the wave period and the diameter:

$$KC = \frac{u_a T}{D} \approx \frac{drag}{inertia} \tag{5.3}$$

with:

KC	Keulegan-Carpenter number	[-]
u_a	horizontal particle velocity amplitude	[m/s]
T	wave period	[s]
D	diameter	[m]

The KC number determines the drag force, relative to the inertia force.
For very small KC number no separation occurs. For increasing KC number about the same happens as for an increase in Re number for steady current.
In addition to the drag force, oscillatory flow leads to the following forces:

1. Hydrodynamic mass force: the resistance against movement of 'attached water'
2. Froude-Krylov force: the resistance against movement of the 'displaced water' by the cylinder (submerged volume of the cylinder).

Both forces lead to the so called inertia force:

$$F_M = \underbrace{\rho C_a A \dot{u}}_{\text{Hydro-dynamic mass force}} + \underbrace{\rho A \dot{u}}_{\text{Froude-Krylov force}} = \rho C_M A \dot{u} \tag{5.4}$$

with:

F_M	inertia force (per unit of length)	[N/m]
ρ	density of the water	[kg/m^3]
C_a	added mass coefficient	[-]
C_M	inertia coefficient	[-]
A	cross sectional area ($\pi D^2/4$ for a cylinder)	[m^2]
$\dot{u}$	horizontal particle acceleration	[m/s^2]

The first term is the hydrodynamic mass force, where for a slender cylinder at low KC number the added mass coefficient $C_a = 1$. The second term is the Froude-Krylov force. Both contributions can be combined in the inertia coefficient C_M, see section 5.4. For low KC number $C_M = 2$, implying that during movement an imaginary volume of twice the water volume of the cylinder is accelerated.

5.4 THE MORISON EQUATION

5.4.1 Background

When the inertia and drag force are combined, the total force as proposed by Morison in 1950, can be found by:

$$F = F_D + F_M = \frac{1}{2}\rho C_D D u|u| + \rho C_M A \dot{u} \tag{5.5}$$

with:

F	total hydrodynamic force (per unit length)	[N/m]
F_D	drag force (per unit of length)	[N/m]
F_M	inertia force (per unit of length)	[N/m]
ρ	density of the water	[kg/m^3]
C_D	drag coefficient	[-]
C_M	inertia coefficient	[-]
D	diameter	[m]
u	horizontal particle velocity	[m/s]
$\dot{u}$	horizontal particle acceleration	[m/s^2]
A	cross sectional area	[m^2]

The equation is based on the assumption that the total force exists on a linear superposition of the drag and inertia forces. In fact it is a coupling between wave kinematics and wave forces, see Figure 5.3. The Morison equation is empirical. Values of the coefficients were found experimentally from various tests. Both coefficients are functions of Re, KC and the wall roughness (k/D). Other influences that may play a role are the influence of current, angle of attack, orbital motion and proximity of a wall.

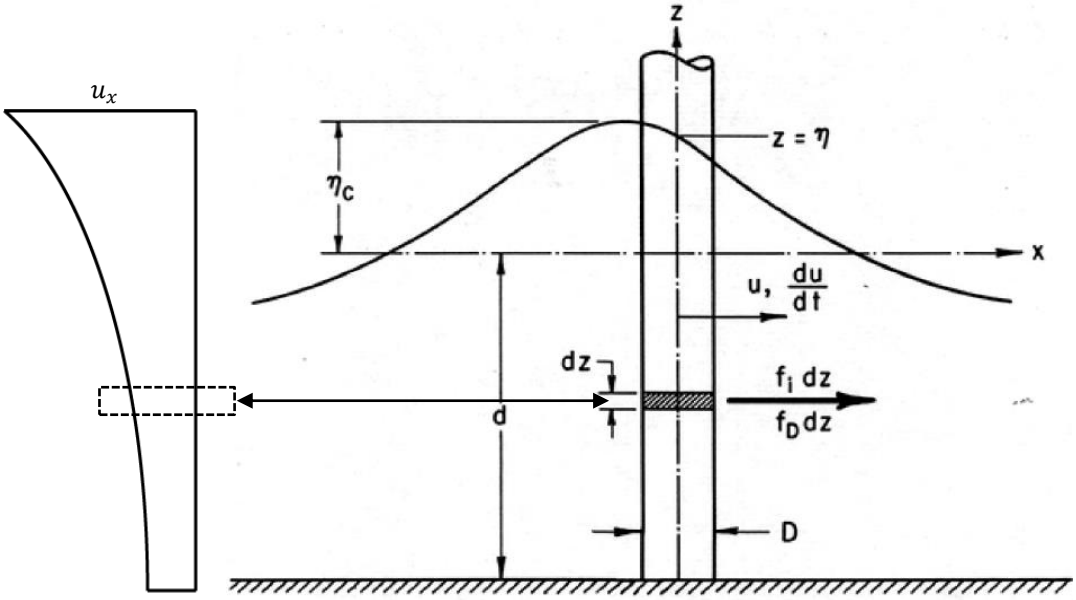

Figure 5.3 – Definition sketch of the Morison equation, being a coupling between wave kinematics and resulting force [26].

For the cases where the structural motion is also taken into account, the force can be described by the so called relative Morison equation, see equation (A.37) in Appendix A.4.

A basic assumption of the Morison equation is that the effect of the pile on the wave-induced flow is assumed negligible [26]. In other words: due to interaction of the wave with the small body, no noticeable change in the incident wave form may occur [27]. In literature the following application areas of the Morison equation are given:

- D/L<0.1-0.2 (slender structures)
- D/h<<1 (diameter/waterdepth)

5.4.2 Experiments

The values for C_D and C_M were found experimentally. Different experimental set-ups were used to determine the coefficients (see Figure 5.4).

- U-tube: in a large U-tube an oscillatory flow can be generated. An advantage is that the oscillating flow is relatively 'pure' [27], so there is hardly any orbital motion. Also the flow is relative uniform distributed over the height. There is however an ongoing discussion of the applicability of results from these kind of tests in filed situations [27]. More on this in section 5.10.
- Forced oscillations in still water: the cylinder is moved by an imposed oscillating force in still water.
- Fixed cylinder in waves: a fixed cylinder is exposed to waves. This situation looks most like field conditions. The waves can be both regular and irregular. Also all kind of different waves can be imposed (long/short, linear and non-linear). Depending on the type of wave (long/short) the wave kinematics may vary strongly as function of depth.

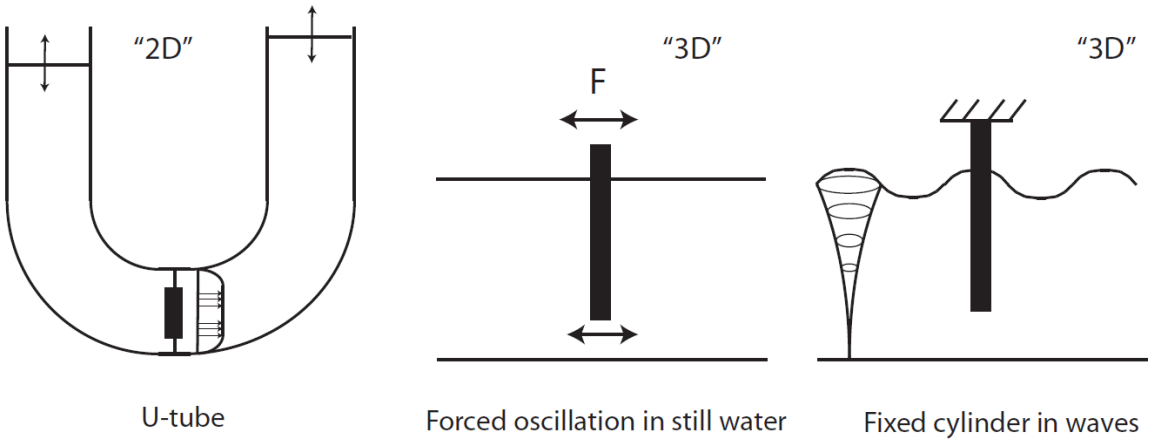

Figure 5.4 – Definition sketch of experimental set-ups

By comparing the model set-up of Figure 5.4A with Figure 5.4C one can observe the following differences (more on these effects in the discussion of section 5.10):

- Velocity-uniformity: Where in the U-tube the flow is uniform over the cylinder, for the fixed cylinder the wave kinematics may vary strongly as function of depth. This depends on the type of wave (long/short, see Table 3.4). Often a coupling between the KC or Re number and the force is made, where these parameters are based on the maximum horizontal particle velocity. For the U-tube this makes no difference due to the uniform velocity profile. But for the 3rd case the distribution of the wave kinematics as function of depth plays an important role. One could 'exclude' this effect by measuring the force on a section of the cylinder only, and assume that the velocity profile is uniform over such a small section. Also one could assume or

measure the velocity profile under a wave and make a coupling between this profile and the force measured at one section. It is unknown to the author whether this correction for non-uniformity of the velocity profile has been followed for all the experimental results found in literature.

- Orbital motion: for the U-tube the flow is pure oscillatory, so there is no orbital motion. In tests with waves there always is an orbital motion.
- Free surface: for the U-tube the cylinder is fully submerged, for other test set-ups a free surface is present. In this surface zone the circumference of the cylinder is not always equally submerged. Wave run-up at the upstream side and a drop in the water level at the downstream side lead to the so called 'free-surface effect'.

5.4.3 Coefficients

Within the experiments the force on a cylinder as function of time is measured. Also the wave kinematics were measured, either by:

- Measuring the water elevation. An appropriate wave theory was applied later in order to estimate the wave kinematics.
- Measuring velocities and accelerations at a certain distance of the cylinder.

Data processing techniques

In order to find the C_M and C_D coefficients different methods have been developed. Morison proposed a relative simple method where the C_M coefficient could be determined from the force at the time where u=0 and the C_D for $\dot{u}$=0. Although the method is simple, it lacks accuracy [27]. Also it is not recommended in a wide range of KC (8<KC<25) and Re values where both drag and inertia may be of equal importance and highly dependent on historical effects (vortex shedding) [20]. Later more sophisticated methods have been developed, like the Fourier series approach and the (weighted) least squares method, the price is higher computational effort required. The different methods lead to different C_M and C_D values. For example the weighted least square method is expected to give a more accurate prediction of the force peaks. Different data processing techniques lead to differences in the coefficients of at best in the order of several percent [27]. The C_M and C_D values resulting from experiments are constants as function of time. Whether this is true or not is discussed in section 5.10.

Experiments performed

Since the development of the Morison equation different experimental programs were started. Worth mentioning are the experiments by Sarpkaya in 1976 [28]. A lot of experiments were performed in a U-tube for a sinusoidal oscillating flow around smooth and rough cylinders. This study clearly demonstrated the dependence of the coefficients on the Re and KC number [29]. This publication gave rise to a lot of questions, like: the effect of the orbital motion, application to horizontal cylinders, application to the design of offshore structures, validity for all KC and Re values etc. Since 1976 lots of researches were performed, in order to answer those questions. Both field tests and extensions to 3D flows were performed (Figure 5.4C). See [29] and [18] for a detailed overview.
The researches performed could partially answer some of the questions and take away some of the uncertainties. However, a lot remains unclear. This mainly has to do with the large gap between laboratory experiments and field situations. There are often simply too much differences between a laboratory test in a U-tube and a field situation. Only when exactly

the same configuration (wave kinematics and structure) as in the field is modelled in a laboratory test, one would expect better agreement between the coefficients.

Design codes

Design codes like Det Norske Veritas (DNV) and the American Petroleum Institute (API) prescribe values for design (see Appendix C.1). A significant part of the prescriptions is based on tests from Sarpkaya. Comparison of the coefficients show that there is little agreement on exact values. Differences up to 40% can be found for a specific flow situation. This difference is caused by experimental inaccuracy, like different model set-up methods or data-processing techniques. For extreme wave conditions the differences are generally less [27]. This is probably caused by the high Re and KC numbers, leading to trans-critical flow. In these flow-regimes the coefficients are supposed to be constant.

5.5 DESCRIPTION OF FINLAB

Within this section the characteristics of the numerical model FinLab are given. Section 5.5.1 starts with the theoretical basis and the application area. In section 5.5.2 an overview of the most important numerical settings is provided. Section 5.5.3 describes the characteristics of the 3D grid being used within FinLab.

5.5.1 Model basics

For waves in shallow water the hydrostatic pressure assumption often is used. However, in order to model short waves or small-scale flows around hydraulic structures non-hydrostatic flows have to be included. FinLab is a fully three dimensional non-hydrostatic numerical model [30]. The model was developed at Svasek and Delft University of Technology by Robert Jan Labeur. FinLab is based on the full Navier-Stokes equations:

$$\frac{\partial \bar{u}}{\partial t} + (\bar{u} \cdot \nabla)\bar{u} - \nu \nabla^2 \bar{u} = \frac{1}{\rho}(\bar{F}_{res} - \nabla p) \tag{5.6}$$

$$\nabla \cdot \bar{u} = 0 \tag{5.7}$$

With:

- (5.6) Momentum equation: This equations expresses that the water particles are accelerated due to a pressure gradient and external forces, momentum may be dissipated by internal friction (viscosity).
- (5.7) Continuity equation, based on the incompressibility of water.

The model was developed for simulating non-hydrostatic flows in estuarine and coastal locations [31]. Unique is that it makes no approximation to the non-hydrostatic equations. In order to solve the equations the model uses the finite element approach. The model is based on a fully unstructured grid. The grid adapts itself to the position of the free water surface. The advantage of this approach is that one is able to model (complex) geometries very accurately.

5.5.2 Numerical settings

Turbulence

Turbulence leads to energy dissipation. These effects can occur at a very small scale. Modelling every little vortex would lead to high computational effort due to grid size requirements. In FinLab one can, in general, choose between the next turbulence models:

- $\kappa - \epsilon$ model: turbulent viscosity ν_t. This method is widely used, easy to implement and computationally cheap [32].
- LES (Large Eddy Simulation) model: only the large eddies (due to flow separation) are modelled, the small ones (Figure 5.2B) are left out. This method is computationally expensive, because it requires a higher resolution. It becomes interesting when turbulence is important (drag dominance).

For this application the $\kappa - \epsilon$ model was chosen, due to the presumed predominant inertia force.

Initial conditions
In FinLab all initial conditions have to meet the Navier-Stokes equations. A practical choice is to let the initial conditions be uniform and especially equal to zero: the water is not moving and the water level coincides with the zero entry of the grid. This means no wave action at t=0.

Boundary conditions
An overview of the boundary conditions used is given in Table 5.2, also see Figure 5.5. Within the upper-Riemann boundary (see Table 5.2) at t=0 a wave is imposed, based on Rienecker-Fenton theory. By application of this theory the wave is computed iteratively. The wave runs through the grid and leaves at the lower-Riemann boundary. The wave starts small, but increases with every calculated wave period. So, waves have to travel into the domain and it takes several wave periods to obtain a periodic harmonic wave. Periodic means that the wave kinematics don't change for more wave periods. In general about 10-20 wave periods (the start-up time) are necessary to reach a periodic wave, depending on the degree of non-linearity.

Boundary condition	Description	Used for
Wall	A closed, fixed, boundary, with partial slip. The amount of slip depends on the shear stress at the wall, which is dependent on the wall roughness.	Ocean bottom Support structure
Surface	A closed, moving, boundary.	Water surface
Riemann	An 'open' boundary. Outgoing waves (from the wavefront or scattered waves from the structure) are not reflected. Compared to a wall this reduces the start-up time. This boundary is only applicable for boundaries with a constant water depth [33].	Boundaries of 3D grid

Table 5.2 – Boundary conditions used in FinLab

Numerical damping
With regard to damping the next sources exist:

1. Diffusion of water (turbulence effects)
2. Numerical damping due to time integration
3. Numerical damping due to space discretization

Ad 2.
The time interval is divided into discrete time levels t_0, t_1, t_n with interval length Δt. The solution at time t_n is calculated from the previous time level [32]. One of the time integration schemes implemented in FinLab is the Θ-scheme. The properties are:

- Θ=0 (Euler Forward scheme): the solution will be first-order accurate and is not stable.
- Θ=½ (Crank-Nicolson scheme/trapezium rule): second order accurate (no damping), weakly stable only.

- Θ=1 (Euler Backward scheme): first-order accurate (strong damping) and strongly stable. Very suitable for steady state flows.

For this application first the Cranck-Nicolson scheme was chosen, due to its low damping and corresponding high accuracy. For high waves this scheme led to sharp peaks in the water elevation around the structure, so therefore the Euler Backward scheme (Θ=1) was applied.
With a numerical model the most accurate results are obtained when the physical diffusion is calculated as accurately as possible, and the numerical damping is kept as low as possible. Often it should be present in order to stabilize the simulation.
For both a low and high wave the influence on the forces by this higher damping value was found to be negligible (see section 5.6.2 and 5.9).

Coefficients
Within FinLab a number of coefficients have to be defined (see Appendix C.2 for the full list). The most important ones are:

- Time stepping parameter (dt): describes the number of time steps per wave. In order to accurately model a wave, the parameter should be: $dt \geq Tp/80$.
- Nikuradse coefficient ($kN0$): wall roughness defined by Nikuradse. For all performed simulations: $kN0$=0.02 m (relatively rough due to assumed marine growth).
- Flow velocity (U): additional flow velocity due to tides, etc. not taken into account, so U=0.

5.5.3 Description of the numerical grid

Grid characteristics
Indications for the grid characteristics are:

- The maximum cell size shall be smaller than 1/40 of the wave length
- The perimeter of the structure shall contain at least 40 grid cells
- The radius of the grid is > ½ L
- The radius of the grid is preferably > $10 \cdot D_{shaft}$

A circular grid has been chosen, amongst other due to the circular shape of the structure. Also a circular grid was already present from a previous simulation for a monopile. In addition a circular grid may be beneficial when taking cross-streams and waves from multiple directions into account.

Creating the 3D grid
In FinLab the water field is modelled by a grid. The 3D grid (see Figure 5.5) is created from a 2D grid (created with the meshgenerator of the Finite Element package SEPRAN, see Appendix C.2.1 for more information) by putting different layers on top of each other. In vertical direction about 15-20 layers are applied. The amount of layers required usually depends on the distribution of the wave kinematics over depth and the required accuracy. But here the vertical distance of the undeformed grid is mainly determined by the height of the wall and the cone of the caisson. This has to do with the fact that the height of the wall and the cone have to be a multiple of the vertical layer distance. Creating a monopile structure is relative simple: the radius of the structure is independent of its height. The GBS shape on the other hand is created by stretching the inner circle of the grid for every vertical grid layer.

Grid fixation

As described above FinLab is based on a fully unstructured grid. The vertical layer distance during simulation is determined by the distance between the free water surface and the bottom. In order to not to deform the caisson during a simulation the grid is fixed at the level of the top of the cone (TC level, see Figure 5.5), so it can only be stretched above that level. As a result the wave through cannot be larger than the length of the submerged part of the shaft of the undeformed grid.

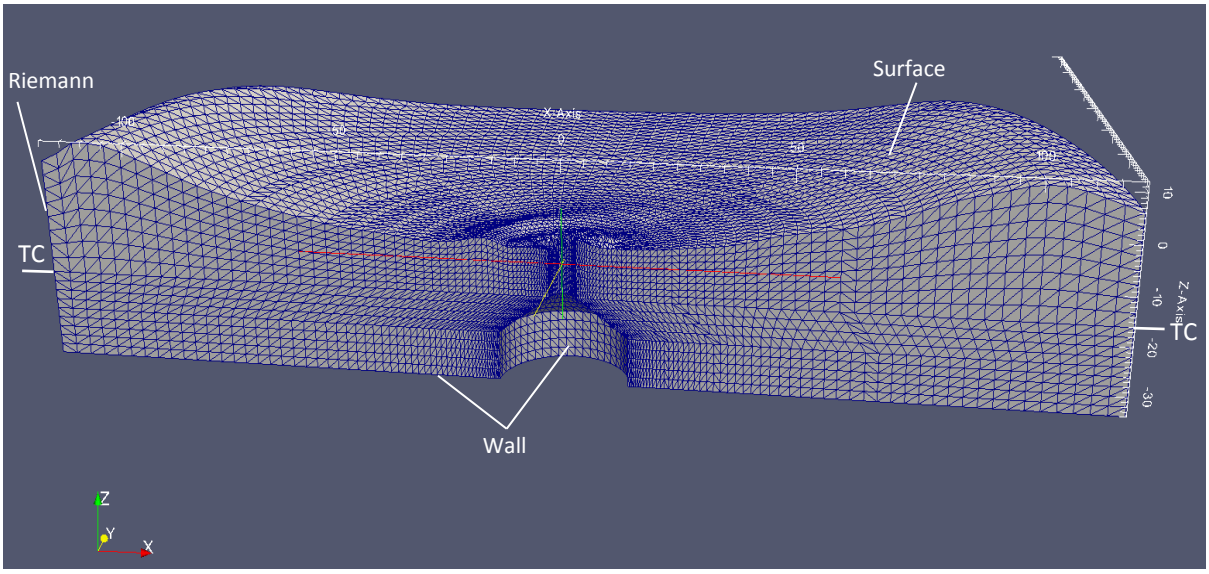

Figure 5.5 - 3D grid for a GBS (deformed) and boundaries as described in FinLab.

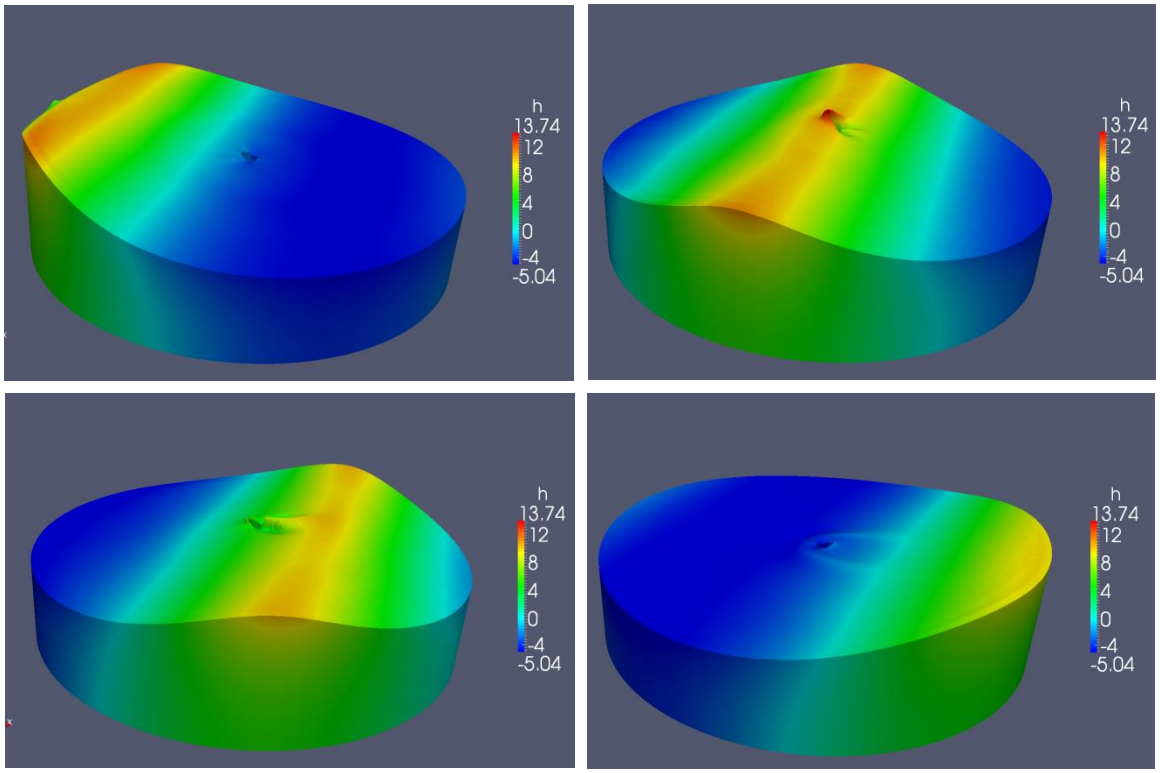

Figure 5.6 - Example of propagating wave for different wave phases

5.5.4 Output

Wave kinematics

For every grid point FinLab gives the next output:

- Velocity vector (ux,uy,uz)
- Piezometric level (h)

The output has the shape of a large data file and can be made visible with a program like Paraview, leading to images like Figure 5.6.

Wave forces

For this application the program was extended with a module to calculate the forces on a structure. The module was written by R.J. Labeur, the developer of FinLab. The force is calculated within the program by integrating the water pressures around the circumference and taking the force due to wall friction into account (see the description of the pressure and friction forces in section 5.3.1).
Originally the wave forces calculated by the program are for the whole height of the modelled structure. But the grid can also be fixed to a predefined level (see description in the previous section). Now the bending moment with respect to this predefined level and the wave force above or below this level can be calculated. So, the force module can also be used to calculate the force on a section of the structure only. The force module has not been applied before and is therefore validated in the next section.

5.6 VALIDATION FOR A MONOPILE

5.6.1 Validation procedure

In order to determine whether the output of FinLab is reliable, the results have been validated. See Appendix C.3 for the entire validation.

Structure used

The chosen structure is a full monopile, meaning that the force is calculated from the seabed till the water level (see Figure 5.7).

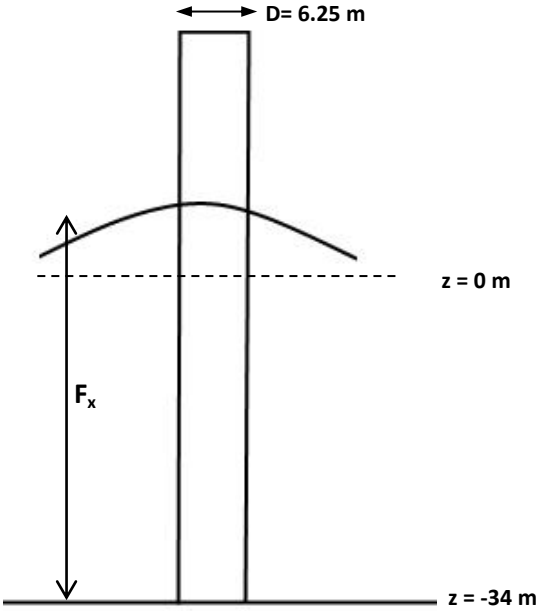

Figure 5.7 – Monopile structure used for the validation

Wave used

For the wave described below the expectation is that FinLab gives a reliable output for sure:

- A sufficiently large wavelength in order to let the Morison equation be valid (D/L<<0.2).
- A relatively long wave, because stable results were found for these waves with FinLab before. Also this type of wave is computationally less expensive due to resolution demands
- A wave with a small H/d ratio, in order to stay as close as possible to the basis of the Morison equation (coupling between a uniform velocity and the force).

Chosen was for a wave with H=2.5m and T=10.0s.

Validation is performed by:

A. Comparison of the undisturbed velocity profile resulting from FinLab and wave theory.
B. Comparison of the total force resulting from FinLab and the Morison equation.

Ad. A: Comparison of wave kinematics

The undisturbed velocity profile is extracted from FinLab at a location far 'upstream' of the structure, so near the starting boundary of the wave. Within the software package WaveLab Stream function 18 was used to obtain the theoretical non-linear wave kinematics. Stream

function 18 is an analytical expression to describe the wave kinematics, just like Airy's linear wave theory. When applied, it covers the description of the wave kinematics of all underlying wave theories (Stokes/Airy). Because the theory can describe every wave (see Figure 3.5) it was chosen within this thesis. Note that, in contrary to Airy's linear wave theory which is only valid till still water level (SWL), non-linear wave theories are valid up to the water level (WL).

Ad. B: Comparison of wave forces (Morison equation)
The theoretical force by the Morison equation as determined in this thesis is based on the following steps:

- WaveLab was used to determine the (non-)linear wave kinematics (theoretical particle velocities and accelerations as function of depth). Within WaveLab the analytical Stream function 18 was applied to all waves, in order to be sure to cover the whole range of waves (linear till highly non-linear).
- For each wave the maximum velocity (at the wave crest) was determined. Based on this value the Re_{max} and KC_{max} values were calculated.
- C_M and C_D coefficients as prescribed by the DNV code [11] were used, based on the values of the previous step. Note that only one set of C_M and C_D coefficients was used for the whole height, so C_M and C_D are assumed to be independent of depth and time (the influence of this is discussed in section 5.10.1) .
- Finally the structure is divided in small sections (~0.1m). For every section the drag and inertia forces are calculated according to the Morison equation. This is done by determining the wave kinematics for the corresponding depth. Summing up of the drag and inertia forces leads to the total horizontal force on the structure.
- The resulting maximum drag and inertia forces were compared with results from design graphs of the Coastal Engineering Manual (based on the relative depth d/gT^2 and wave steepness H/gT^2 only). Both outcomes seemed to match very well, see Appendix C.3.4

5.6.2 Validation for H=2.5m an T=10.0s

For this case a comparison of the velocities is performed in Figure 5.8. Left the velocities are compared for wave crest and wave trough and around zero crossing. Right the relative error is plotted. As can be seen, the undisturbed velocity profile resulting from FinLab matches very well with theory. Differences are in the order of 2% at the extremes. At the zero crossing the relative error is higher, but this is only locally.

In order to validate the outcome of WaveLab as well, a comparison with Stokes 3th order wave theory was made. The outcomes are based on analytical expressions. Also a comparison with Airy's linear wave theory was made, although this theory is not valid for this case (Figure 3.5). The full comparison can be found in Appendix C.3.2. It followed that Stokes 3th order gave the same outcome as WaveLab. Even Airy's linear wave theory gave a very good estimation, as can be expected from the fact that the wave is only slightly non-linear (see Figure 5.8).

In Figure 5.9 the forces on the monopile resulting from FinLab are compared with theory. The force and bending moment also seem to match very well (differences in the order of 3% at the extremes). Only the distribution as a function of time is a bit different.

The influence of the damping parameter was investigated by comparing the force for high ($\Theta = 1.0$) and low ($\Theta = 0.5$) damping. Differences in force were small: in the order of 5% (see Appendix C.3).

Concluding, it can be stated that FinLab is able to model the wave kinematics and forces on a monopile very well (at least for this specific case). The newly implemented force module seems to perform very good as well.

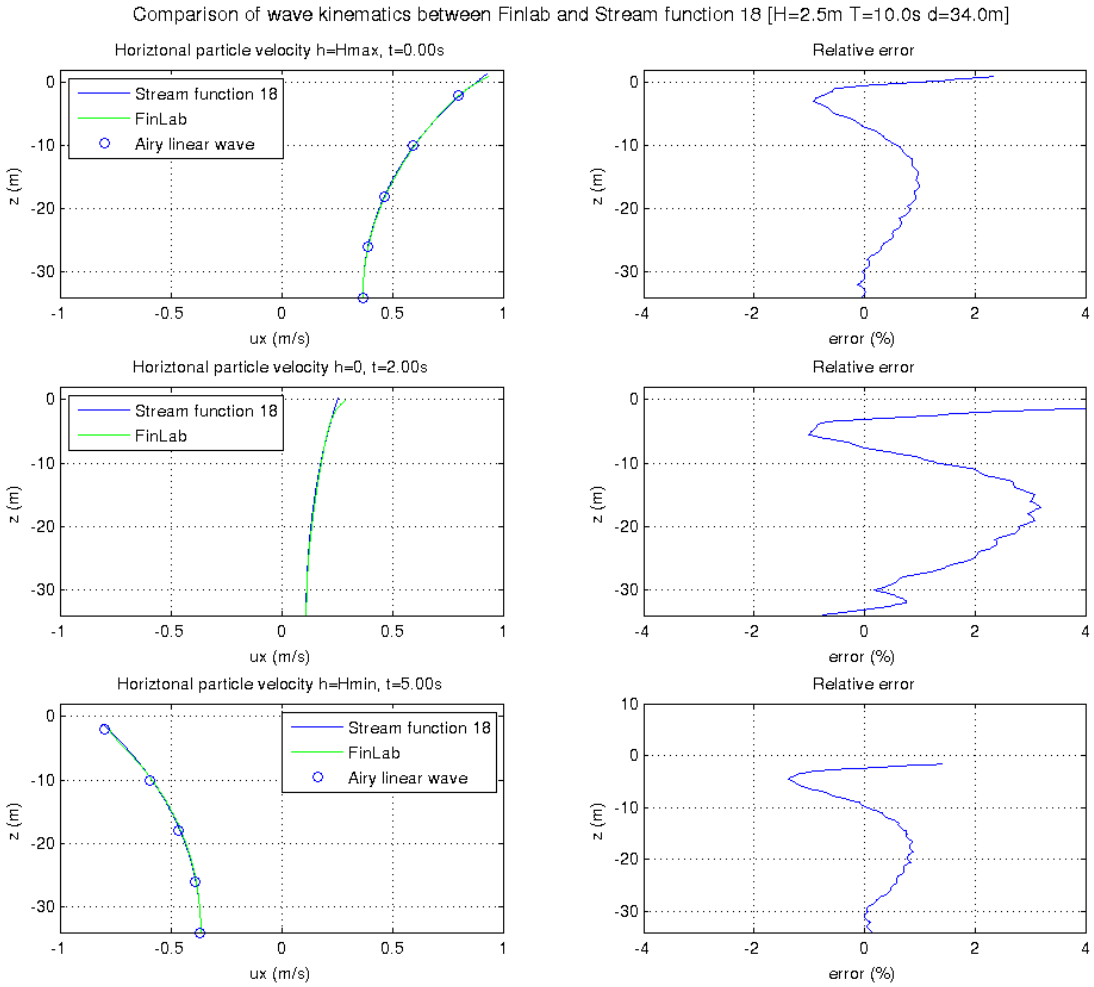

Figure 5.8 - Comparison of horizontal particle velocity profile between FinLab (extracted velocity profile at [-50;0;z]) and theory (Stream function 18 and Airy's linear wave theory) [Full monopile; H=2.5m T=10.0s d=34.0m]. Note that the relative error leads to relative high values for h≈0, because the velocity is relatively low , while the match is fairly good.

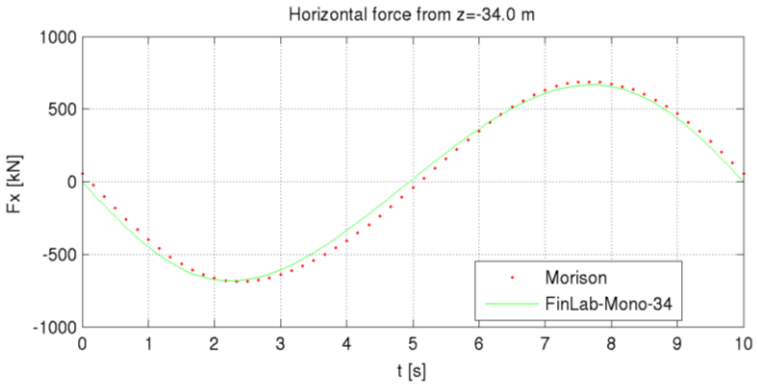

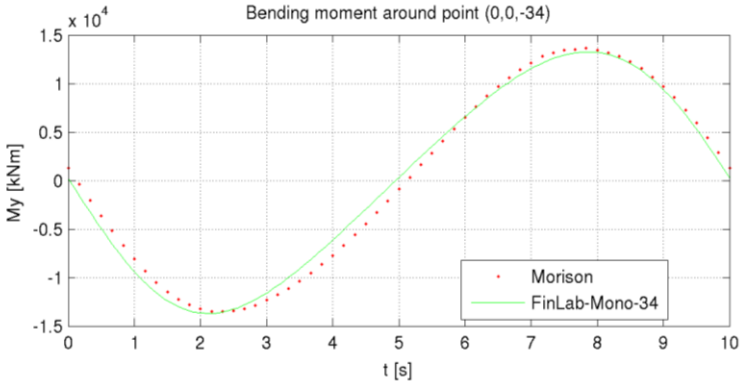

Parameter	Value	
$u_{z=WL;max}$	0.93	m/s
KC_{max}	1.40	-
Re_{max}	$5.8 \cdot 10^6$	-
k/D	0.0032	-
C_M	1.97	-
C_D	1.50	-

$F_{x;max}$ [MN]			$M_{y;\max\|z-34}$ [MNm]		
Morison	FinLab	Diff [%]	Morison	FinLab	Diff [%]
0.69	0.67	-2.9	13.61	13.26	-2.6

Figure 5.9 - Comparison of forces between FinLab and theory. Forces from z=WL..-34m, bending moment around z=-34m. [Full monopile; D=6.25m; H=2.5m T=10.0s d=34.0m].

5.6.3 Validation for H=16.9m and T=12.7s

For this wave it was investigated whether FinLab gave the same velocity pattern as theory, see Figure 5.10. It was found that the differences were little larger, but still small (maximal in the order of 5%). In Figure 5.11 the forces on the monopile resulting from FinLab are compared with theory. Here, the force and bending moment don't match any more (differences in horizontal forces in the order of 50% at the extremes). This observed effect will be discussed extensively in section 5.10.

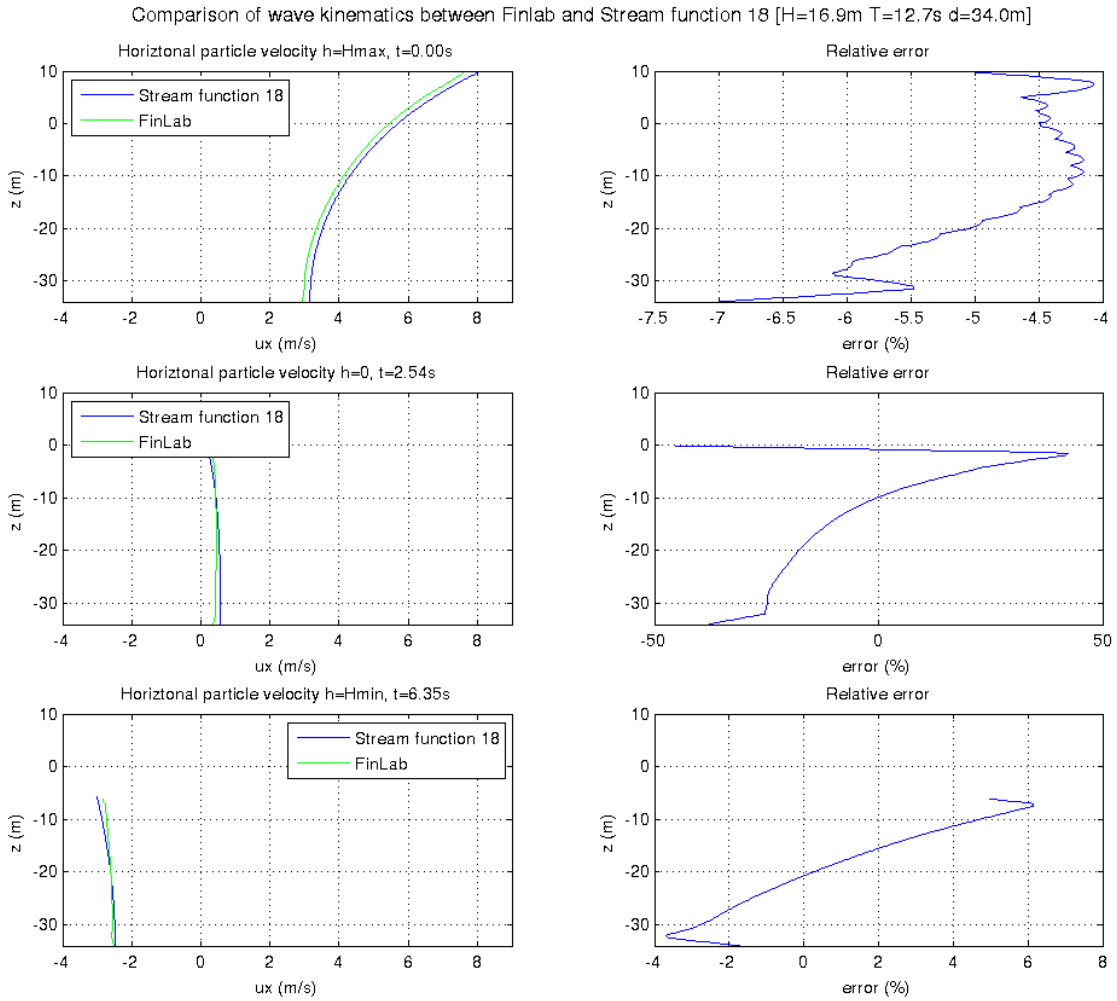

Figure 5.10 - Comparison of horizontal particle velocity profile between FinLab (extracted velocity profile at [-60;0;z]) and theory (Stream function 18) [Full monopile; H=16.9 T=12.7s d=34.0m]. Note that the relative error leads to relative high values for h≈0, because the velocity is relatively low, while the match is fairly good.

One could argue that the differences in wave kinematics by FinLab and theory (Figure 5.10) is the cause the high difference in forces. This is however not the case. The full argumentation can be found in Appendix C.3.3 but is summarized here. Around $t \approx 12s$ the force is maximal, and both drag and inertia force are of equal importance. Around this time differences in velocities and accelerations are in the order of 5% (see Figure 5.10 and Appendix C.3.3) where FinLab gives lower values than theory. Suppose the velocities and accelerations in FinLab were equal to theory (so an increase of about 5%), the maximum horizontal force found by FinLab would only increase. So, this wouldn't lead to lower, but even higher differences of the horizontal force found by FinLab and the Morison equation.

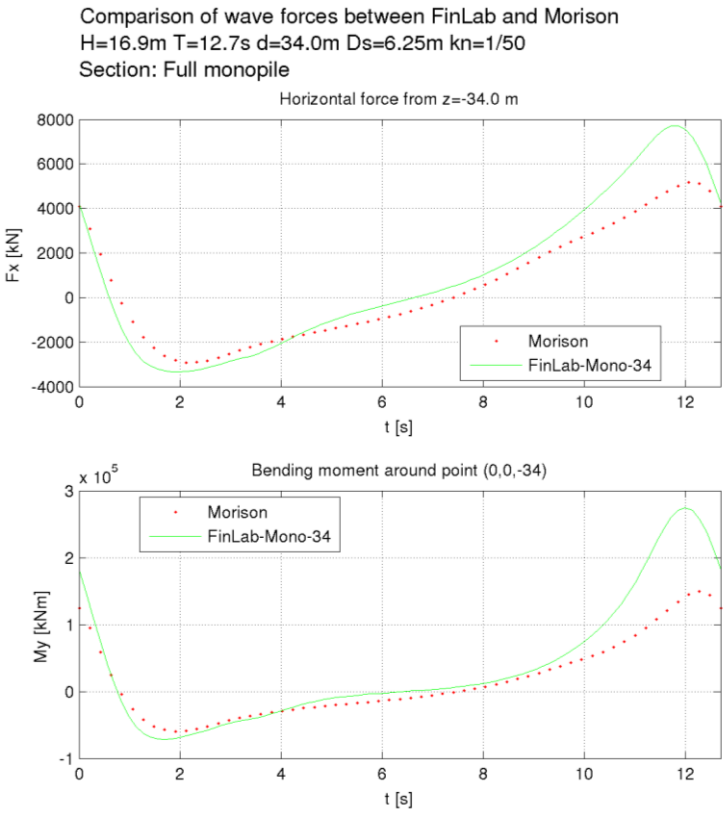

Parameter	Value	
$u_{z=WL;max}$	8.50	m/s
KC_{max}	17.3	-
Re_{max}	$5.3 \cdot 10^7$	-
k/D	0.0032	-
C_M	1.55	-
C_D	1.15	-

$F_{x;max}$ [MN]			$M_{y;\max\,\vert z-34}$ [MNm]		
Morison	FinLab	Diff [%]	Morison	FinLab	Diff [%]
5.17	7.72	49	149.7	274.6	84

Figure 5.11 - Comparison of forces between FinLab and theory. Forces from z=WL..-34m, bending moment around z=-34m. [Full monopile; D=6.25m; H=16.9m T=12.7 d=34.0m].

5.7 OVERVIEW OF PERFORMED TESTS WITH FINLAB

5.7.1 Influence of caisson

In order to investigate the influence of the caisson within FinLab two different structures with exactly the same environmental and numerical conditions were modelled:

- a monopile
- a GBS

By comparing the force on the shaft on the upper part of the monopile and the shaft of the GBS, the influence of the caisson becomes clear, see Figure 5.12.

Hypothetical influence of the caisson

The hypothesis is that blocking a part of the water depth by the caisson leads to an increase of the forces on the shaft. This is based on the following reasoning: when the caisson blocks a part of the water depth, this will lead to contraction of the stream lines just above the cone (the same amount of water has to pass a smaller area, the continuity equation requires an increase in velocity) . Due to this contraction the velocities at the bottom of the shaft will increase, leading to a higher friction force parallel to the wall (see section 5.3.1). Another effect is the increase in pressure in the stagnation point at the front of the cylinder, due to the increased velocities. This will lead to a higher pressure force at the bottom of the shaft. As a result a higher force is expected.

For relative short waves (deep water), the orbital motion near the bottom is practically zero (see Table 3.4). On the other hand, for relative long waves (shallow water), the orbital motion near the bottom is relative high. Therefore it is expected that for relative long waves the force increase due to the caisson will be highest.

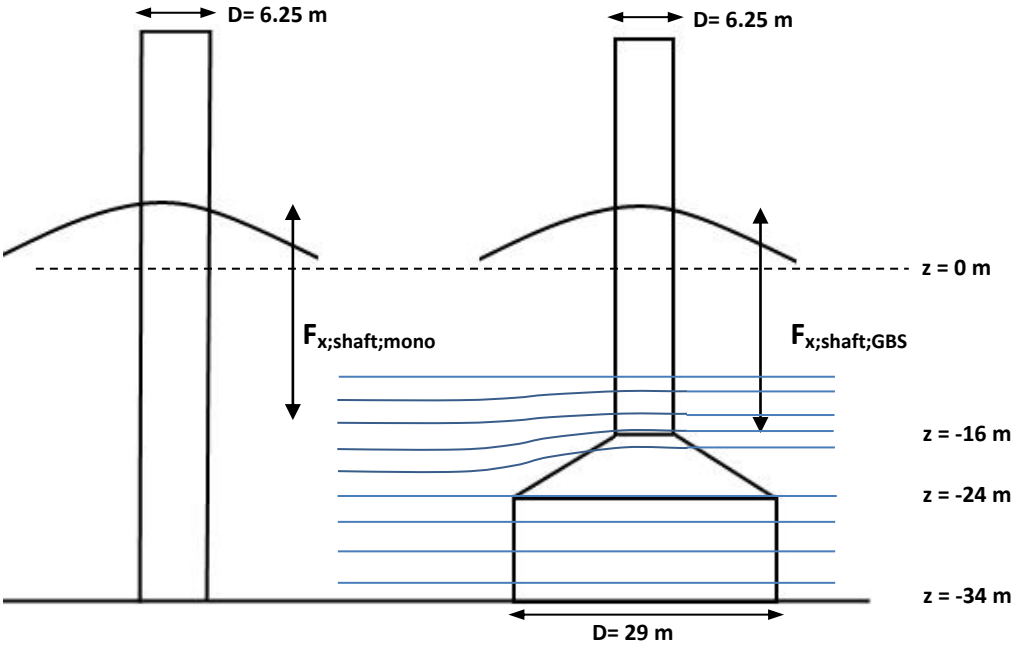

Figure 5.12 – Structures used to investigate the influence of the caisson, and flow lines around the caisson.

5.7.2 Performed simulations with FinLab

Both the Ultimate Limit State (ULS) as the Fatigue Limit State (FLS) influence the design of the shaft. For both cases the wave forces were determined with FinLab.

ULS wave

A water depth of 34m was chosen, because this is the smallest assumed water depth where the GBS will be installed. It is recalled from section 5.2 that the ULS wave is characterized by H=16.9m and T=12.7s. This wave is named “case 1” for the rest of this thesis, see Table 5.3. In order to investigate the influence of the water depth the same wave was implemented in a model with d=50m (“case 2”).

FLS waves

Because the FLS exists of multiple wave classes (see Table 5.1), a selection of the FLS sea-states was made. Ideally four classes would have been selected representing the whole range of waves, for example: class 1, 7, 13 and 18. For the intermediate classes the force in- or decrease due to the caisson could then be interpolated.
However, for the case with H=10.0m and T=9.7s (now called “class 17b”) in an earlier stage of this research simulations were performed, so this case was used as a ‘replacement’ for class 17.

Initially, for class 17b and 13 simulations within FinLab went well. But when the move to shorter waves (class 7) was made, based on visual observations the results obtained were not judged to be reliable. The wave running through the domain resulted in waves perpendicular to the wave direction (see Appendix C.4). This is a well-known problem for modelling relative short waves in finite element models. After an update of the code at 02/04/2014 the effect seemed to disappear. Due to limited time the results have however not been added to this thesis.
Note that for relative short waves like class 1, the Morison equation is not valid any more (D/L>0.2).

Lumped wave scatter diagram				
	Sign. wave height		Period	
Class	Range	Average	T02	L
(-)	[m]	[m]	(s)	(m)
1	0 - 1	0.5	3.8	23
2	0 - 1	0.5	5.1	41
3	0 - 1	0.5	7	76
4	1-2	1.5	4.8	37
5	1-2	1.5	5.9	55
6	1-2	1.5	7	76
7	2-3	2.5	5.4	47
8	2-3	2.5	7.2	81
9	3-4	3.5	5.9	56
10	3-4	3.5	7.2	82
11	4-5	4.5	5.9	58
12	4-5	4.5	7.3	85
13	5-6	5.5	7.4	88
14	6-7	6.5	7.5	91
15	7-8	7.5	7.9	100
16	8-9	8.5	7.9	102
17	9-10	9.5	8.5	116
17b	-	10	9.7	142
18	10-11	10.5	8.5	117

Figure 5.13 - Chosen wave states of the FLS analysis from the lumped wave scatter diagram in orange. Selected cases 13 and 17b are used for the hydrodynamic analysis with FinLab. Wavelengths are based on d=34m.

5.7.3 Overview of selected cases

All the cases used to investigate the influence of the caisson are listed in Table 5.3.
The radius of the grid, and corresponding maximum cell size dS_{max}, was chosen according to the indications of section 5.5.3. Also see Appendix C.2.1 for more information about the grid.
The number of periods is dependent of the start-up time. For near-linear waves this amount of periods is less than for highly non-linear waves.

		Wave			Geometry		Model		Grid	
	Case #	H [m]	T [s]	L [m]	d [m]	D_{shaft} [m]	dt [s]	Per [-]	r [m]	dS_{max} [m]
ULS	1	16.9	12.7	217	34	6.25	Tp/90	40	120	4.0
	2	16.9	12.7	236	50	6.25	Tp/90	40	120	4.0
FLS	3	10.0	9.7	142	34	6.25	Tp/90	30	80	2.6
	4	5.5	7.4	88	34	6.25	Tp/90	20	70	1.7

Table 5.3 - Load cases used to determine the influence of the caisson, H=wave height, T=wave period, L=wave length, d=water depth, D=diameter, dt=time stepping parameter, per=# of periods, r=grid radius, dS_{max}=maximum cell size of grid (L> dS_{max}·40)

A sensitivity check on several model parameters, and the diameter D, is performed in section 5.9.

5.8 RESULTS FOR THE FORCES ON THE SHAFT

5.8.1 Overview

In this section the wave forces on the shaft are calculated. A comparison is made between the force on the shaft of the GBS and the upper part of the monopile. In order to compare the results from FinLab with theory, for the upper section of the monopile the forces according to the Morison equation were determined. So, for every wave case three forces are given (Figure 5.14):

F1. Force on the upper part of the monopile – Morison equation
F2. Force on the upper part of the monopile – FinLab
F3. Force on the shaft of the GBS – FinLab

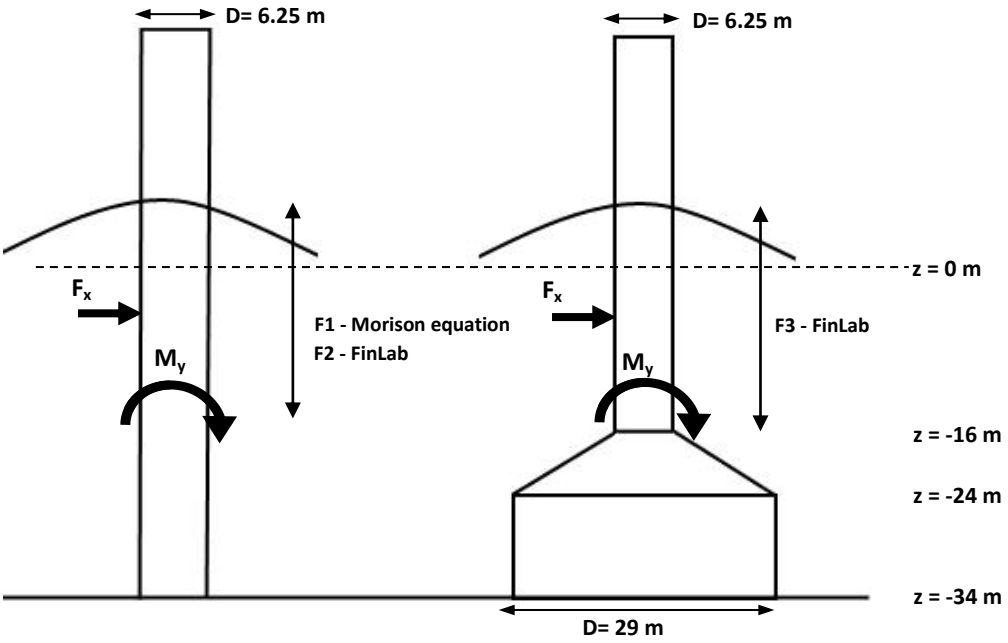

Figure 5.14 - Background of horizontal forces on the shaft

By comparing the results from F2 with F1 differences between FinLab and theory become clear. Comparing the results from F3 with F2 gives insight in the influence of the caisson. The results are interpreted in section 5.10.
Simulations with FinLab were performed for the wave cases of Table 5.3. The resulting maximum forces can be found in Table 5.5. For the FLS not the maximum value of the bending moment is important, but the bending moment cycle for a wave (see Figure 5.15). Therefore in Table 5.6 the bending moment cycles (absolute value of the maximum and minimum bending moment) are listed.

5.8.2 Calculated forces with the Morison equation

In order to calculate theoretical values of the forces on the upper part of the monopile (F1), the Morison equation was applied. The same approach as for the validation (see section 5.6.1) has been used, i.e. determining the wave kinematics with the aid of Stream function 18, determining the Morison coefficients based on the maximum KC number and relative roughness of k/D=0.02/6.25=0.0032, and using constant Morison coefficients as function of time and depth (design graphs can be found in Appendix C.1.7). The results for the four cases are listed in Table 5.4.

Parameter	Case 1	Case 2	Case 3	Case 4	
$u_{z=WL;max}$	8.5	5.4	4.6	2.9	m/s
KC_{max}	17.3	13.0	7.2	3.4	-
Re_{max}	$5.3 \cdot 10^7$	$3.4 \cdot 10^7$	$2.9 \cdot 10^7$	$1.8 \cdot 10^7$	-
C_M	1.55	1.55	1.75	1.93	-
C_D	1.15	1.30	1.50	1.50	-

Table 5.4 – Determined C_M and C_D coefficients for k/D=0.0032 as input for the Morison equation. See section 5.6.1 for a description how the coefficients were obtained.

5.8.3 Results of the simulations with FinLab

Below for the cases 1,3 and 4 the horizontal forces on the shaft are given. The results for case 2 (d=50m) showed about the same effect as case 1, and can be found in Appendix C.6.

5.8.3.1 Case 1 [H=16.9m T=12.7s d=34m]

The results for this case are given in Figure 5.15. Comparing F1 with F2 (FinLab vs. the Morison equation) shows a good match between t=1 and t=10 s. But around the wave crest (between t=10 and t=1 s), where the horizontal force has its maximum value, FinLab results in much higher forces. The difference in maximum horizontal force is 74%. The difference in maximum bending moment is with 120% even higher.

By comparing F2 with F3 (the upper part of the monopile vs. the GBS shaft) it becomes clear that both the minimum and maximum horizontal force are a little higher in magnitude. The maximum horizontal force increases with 8%. The lower figure shows that the influence on the bending moments is very limited, the maximum value of the bending moment increases with 2% only. The absolute value of the minimum bending moment becomes even smaller. As a result the bending moment cycle does not change due to the presence of the caisson.

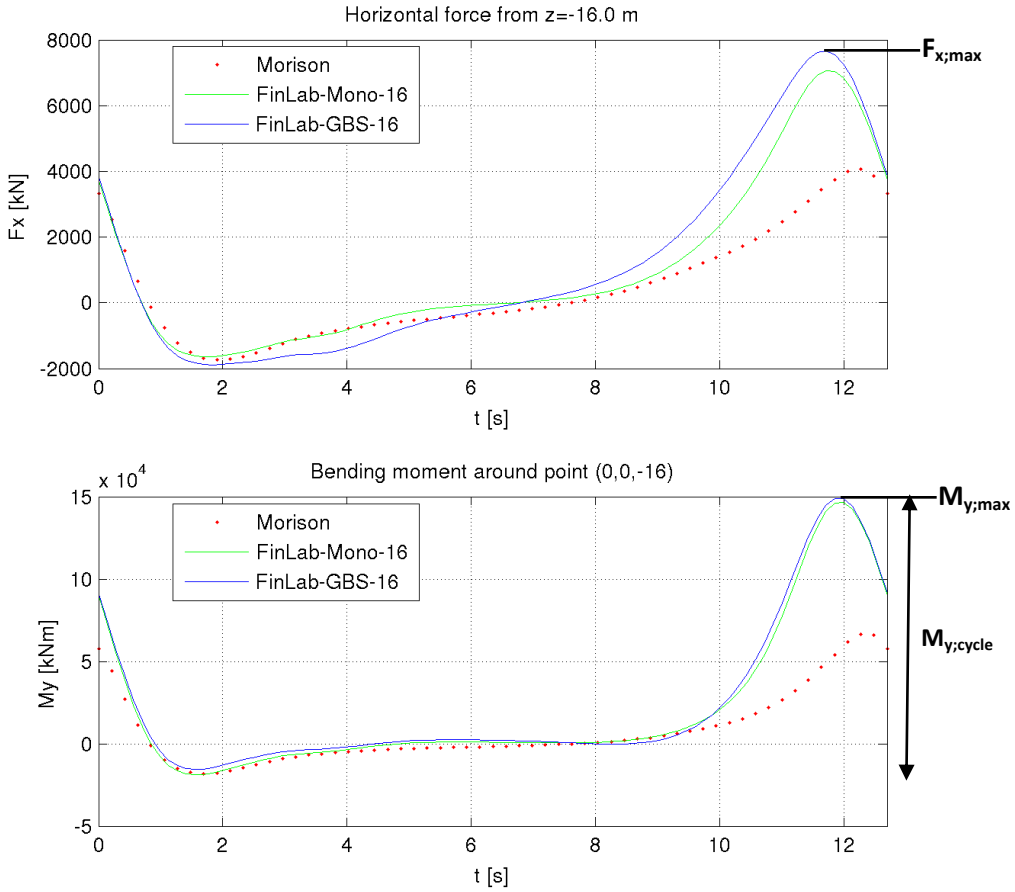

Figure 5.15 - Results for case 1

5.8.3.2 Case 3 [H=10.0m T=9.7s d=34m]

For this case the results are given in Figure 5.16. Comparing F1 with F2 shows about the same profile between t=0 and t=7s, although the minimum force and moment given by FinLab are slightly smaller (~15%). Also for this wave FinLab gives higher maximum values of the forces. The difference in maximum horizontal force is 28%. The difference in maximum bending moment is with 57% even higher. Both increases are less than for case 1.

By comparing F2 with F3 it becomes clear that both the minimum and maximum horizontal force are higher in magnitude. The maximum horizontal force increases with 23%, being more than for case 1. The lower figure shows that the influence on the bending moments is less, the maximum value of the bending moment increases with 9%. The absolute value of the minimum bending moment becomes smaller. As a result the bending moment cycle only increases with 2% due to the presence of the caisson.

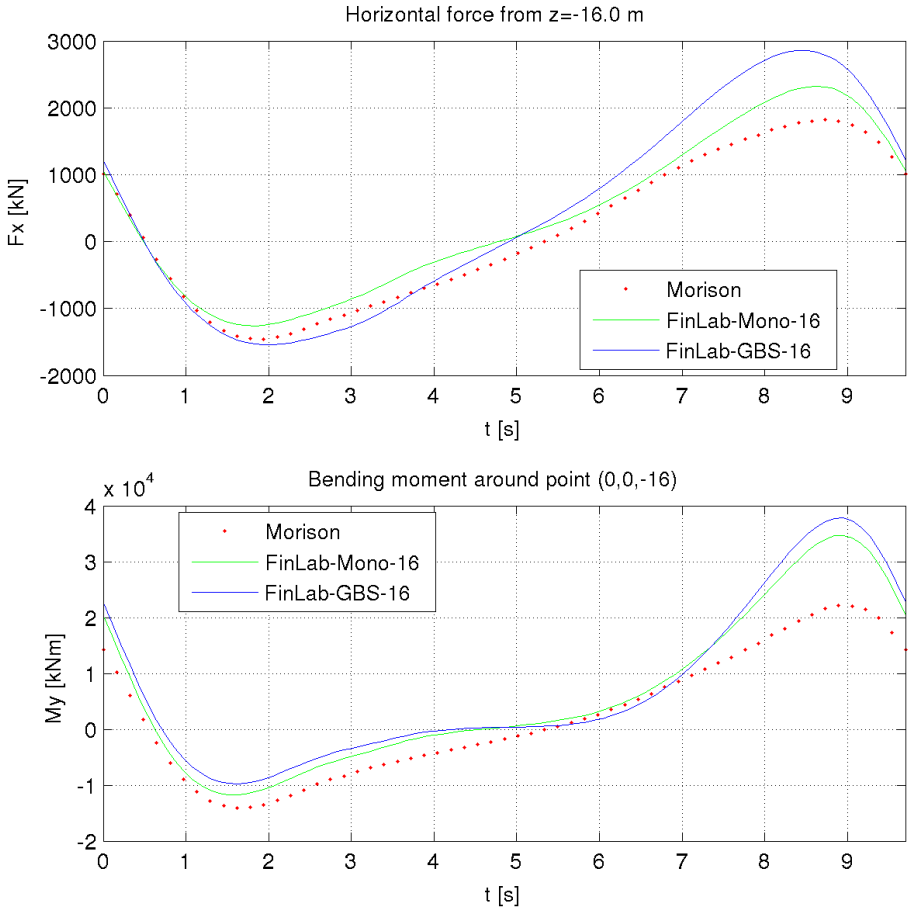

Figure 5.16 - Results for case 3

5.8.3.3 Case 4 [H=5.5m T=7.4s d=34m]

Results for this case are given in Figure 5.17. Comparing F1 with F2 gives lower magnitudes of the force by FinLab for both the minimum and maximum values (~10%). The difference in bending moment is only visible for the minimum bending moment (10%).

By comparing F2 with F3 it becomes clear that also here both the minimum and maximum horizontal force are higher in magnitude. The maximum horizontal force increases with 21%, being about the same as case 3. The lower figure shows that the influence on the bending moments is less, the maximum value of the bending moment increases with only 3%. The absolute value of the minimum bending moment becomes smaller. As a result the bending moment cycle decreases with 3% due to the presence of the caisson.

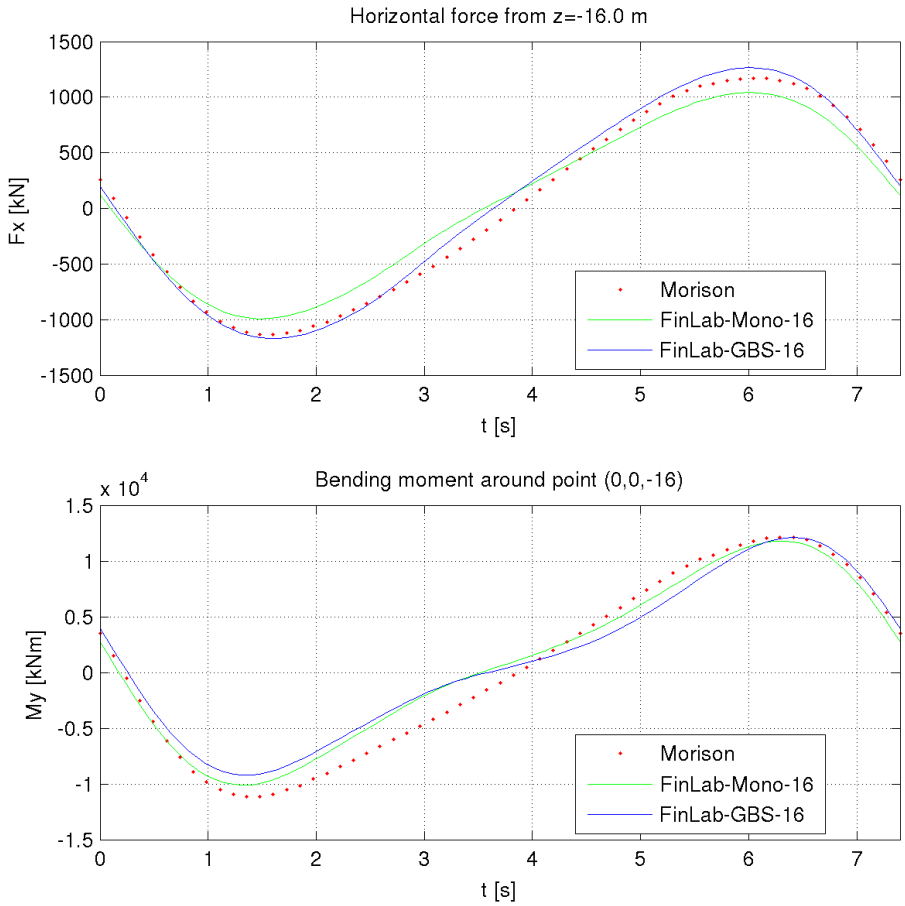

Figure 5.17 - Results for case 4

Case	Force	Morison [F1]	FinLab Mono [F2]	FinLab GBS [F3]	Difference Mono-Morison[%] [F1-F2]	Increase due to GBS [%] [F2-F3]
1	$F_{x;max}$ [MN]	4.06	7.07	7.66	74	8
	$M_{y;\max\|z-16}$ [MNm]	66.50	146.57	148.95	120	2
2	$F_{x;max}$ [MN]	3.87	5.68	6.19	47	9
	$M_{y;\max\|z-32}$ [MNm]	99.70	178.35	184.66	79	4
3	$F_{x;max}$ [MN]	1.82	2.33	2.86	28	23
	$M_{y;\max\|z-16}$ [MNm]	22.15	34.72	37.78	57	9
4	$F_{x;max}$ [MN]	1.17	1.04	1.26	-11	21
	$M_{y;\max\|z-16}$ [MNm]	12.14	11.80	12.13	-3	3

Table 5.5 – Values belonging to Figure 5.15 - Figure 5.17. Shaft only. See Figure 5.14 and Figure 5.15 for definitions.

	$M_{y;cycle\|TC}$ [MNm]				
Case	Morison [F1]	FinLab Mono [F2]	FinLab GBS [F3]	Difference Mono-Morison[%] [F1-F2]	Increase due to GBS [%] [F2-F3]
1	84.76	165.36	164.67	95	0
2	146.43	225.46	229.11	54	2
3	36.31	46.47	47.54	28	2
4	23.27	21.92	21.35	-6	-3

Table 5.6 – Bending moment cycles. See Figure 5.15 for definitions.

5.8.3.4 Velocities

With respect to the wave kinematics the comparison with theory, as for the validated waves, is less good. Validation was performed in section 5.6 for [H=2.5m T=10.0s] and for [H=16.9m T=12.7s], both for a full monopile (z=-34m..WL). For the first wave relative errors were very small (in the order of 2% only). The second wave resulted in little larger relative errors (in the order of 5%, see Figure 5.10).
For case 1 with only the upper section of the shaft (z=-16m..WL) the differences seemed to increase a bit. Instead of 5%, relative errors were in the order of 10% (see Appendix C.6.2). In section 5.6.3. it was argued that the 5% lower values found by FinLab are not responsible for the higher force compared to the Morison equation. The same holds true for the slightly higher differences of 10%.

5.8.3.5 Observations for case 1-4

Based on the results for case 1-4, as summarized in Table 5.5 and Table 5.6, the following observations can be done. The observations are analysed and discussed in section 5.10.

Forces from FinLab versus the Morison equation
By comparing F1 with F2:

- The Morison equation gives smaller forces than FinLab. Differences in maximum horizontal force are up to 74%. For the maximum bending moments the differences are up to 120%.
- For case 1 the minimum wave forces from Morison match very well with FinLab. For cases 3 and 4 FinLab gives 10-15% lower absolute values.
- For cases 3 and 4 between the extremes the match is not very good.

The influence of the caisson
By comparing F2 with F3:

- The caisson leads to an increase of the absolute value of both force peaks. The bending moment is only shifted upwards, leading to no significant differences in the bending moment cycles.
- For a larger absolute value of the minimum horizontal wave force the absolute value of the minimum bending moment decreases.
- The caisson leads to an increase of the maximum horizontal force in the order of 10-20%. The increase is strongest for case 3 and 4.
- The caisson leads to an increase of the maximum bending moment in the order of 2-10%. The increase is strongest for case 3.
- The increase in maximum bending moment is less than the increase in horizontal force, especially for case 4.
- The relative increase of the maximum horizontal force due to the caisson is strongest for the shorter waves.

5.9 SENSITIVITY CHECK

5.9.1 Selected cases

A sensitivity check was performed in order to investigate the influence of the numerical parameters chosen, see Table 5.7. For the following parameters the sensitivity check was performed:

- The grid radius r. The grid radius was increased with a factor 1.5.
- The grid size. The cell size of the grid was decreased with a factor 2.
- Damping. For the ULS wave the force for both high ($\Theta = 1$) and low ($\Theta = 0.5$) damping was compared.
- The time step dt. The time step was decreased with a factor 2.
- The amount of periods, in order to investigate the influence of a longer run. For case 1 the total simulation time was increased with a factor 1.5, for case 4 with a factor 2.5.

Further it was investigated whether a smaller diameter D also resulted in a difference between FinLab and the Morison equation. The structures chosen were all monopiles. No sensitivity checks for the GBS were performed. When the influence on a monopile is small, one can assume the influence on the shaft of the GBS to be small as well (flow patterns around both shafts don't show much differences).

	Case	Varied parameters	Value
Sensitivity	1	radius (r)	80 & 120m
	1	grid	2x as dense
	1	damping (Θ)	0.5 & 1.0
	3	time step (dt)	Tp/90 & Tp/180
	1	periods	40 & 60
	4	periods	20 & 50
Geometry	1	diameter	1.0 m

Table 5.7 - Cases for sensitivity check

5.9.2 Results

The sensitivity check can be found in Appendix C.7. Results are summarized in Table 5.2. Both the larger radius, denser grid and lower damping values don't seem to have much influence on the total forces. The influence of the smaller time step seems to be larger, and may lead to an increase of the maximum horizontal force. Because the variation is performed for case 3, the influence on case 1 is unknown. For case 1 increasing the number of periods doesn't have much influence. For case 4 the influence is larger, and leads to smaller forces.

Concluding, the influence of the different numerical parameters on the maximum forces seems to be relative small, although a small change in force may have a large influence on the fatigue load. Only the time stepping parameter may have some influence. For a full comparison the influence of this parameter on case 1 should be investigated.

Parameter	Difference $F_{x;max}$ [%]	Difference $M_{y;max}$ [%]	Difference M_{cycle} [%]
radius	-1	0	-1
grid	-1	-2	-1
damping	-2	1	1
time step	4	8	6
per case 1	-2	-1	-2
per case 4	-3	-5	-6

Table 5.8 – Influence of variation of numerical parameters

5.10 ANALYSIS OF THE RESULTS

In section 5.6 the result from FinLab (both velocities and forces) were validated for a relative long wave and a monopile. The results seemed to match very well with theory. In section 5.8 the forces on the shaft of the GBS were calculated. The observations ask for a discussion on the following topics:

1. The observed force difference between FinLab and the Morison equation.
2. The influence of the caisson on the forces on the shaft.

In this section the obtained results are analysed.

5.10.1 Differences between FinLab and the Morison equation

5.10.1.1 Observations

The main observation is that FinLab gives higher values for the maximum horizontal wave forces and bending moments. For case 1 the difference in maximum horizontal force is:

- about 50% for a full monopile (from -34m, see Appendix C.3)
- 75% for the upper section (from -16m)

The ratio at which the maximum bending moment increases is for all cases higher than the maximum horizontal forces. This indicates that the force increase with respect to the Morison equation is mainly caused at the top of the shaft. So, it seems that FinLab leads to higher wave forces near the surface than the Morison equation.

By plotting the differences between FinLab and Morison there seems to be a relation with the H/d ratio ('bottom feeling parameter'), see Figure 5.18. When instead of the H/d ratio the Ursell number U_r (a degree for the non-linearity, see Figure 5.20) is chosen, there also seems to be a relation, see Figure 5.19. The Ursell number is defined by:

$$U_r = \frac{HL_0^2}{d^3} \tag{5.8}$$

with:

U_r	Ursell number	[-]
H	wave height	[m]
L_0	deep water wave length	[m]
d	water depth	[m]

See Appendix C.8 for the values of the U_r and H/L ratio used here.
Within this section a closer look at the results, and the underlying physics, is performed in order to find an explanation for the differences.

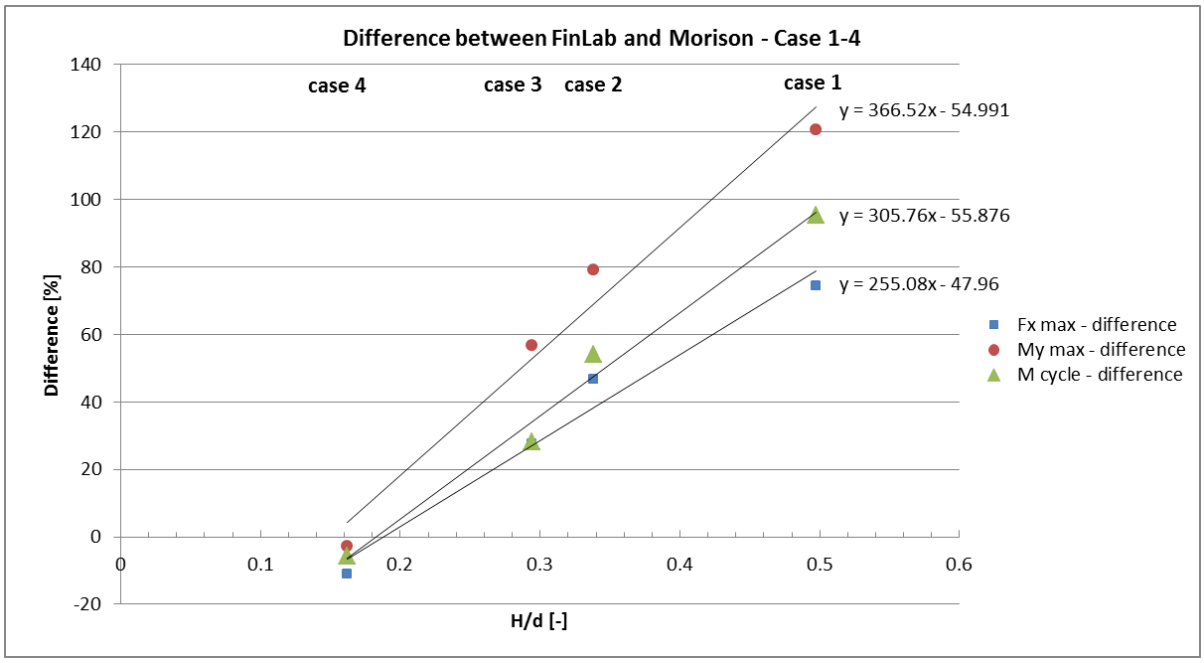

Figure 5.18 – Difference in maximum force and bending moment cycle between FinLab and Morison as a function of the H/d ratio (based on Table 5.5).

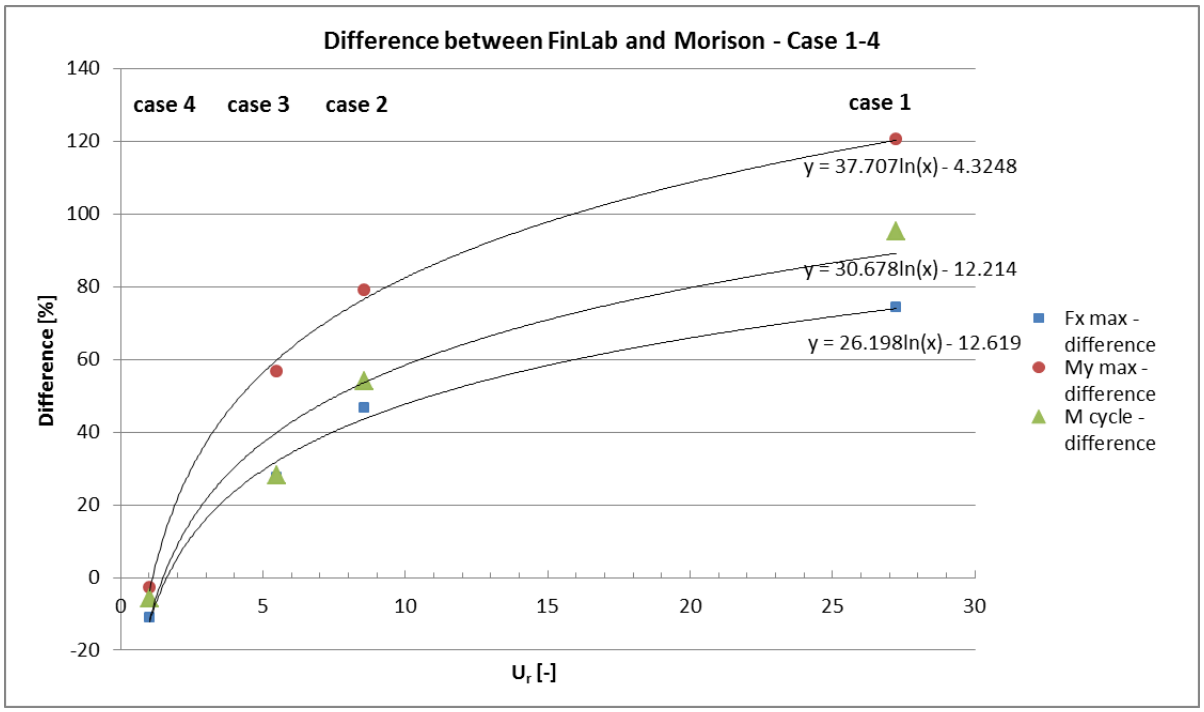

Figure 5.19 – Difference in maximum force and bending moment cycle between FinLab and Morison as a function of the Ursell number (based on Table 5.6).

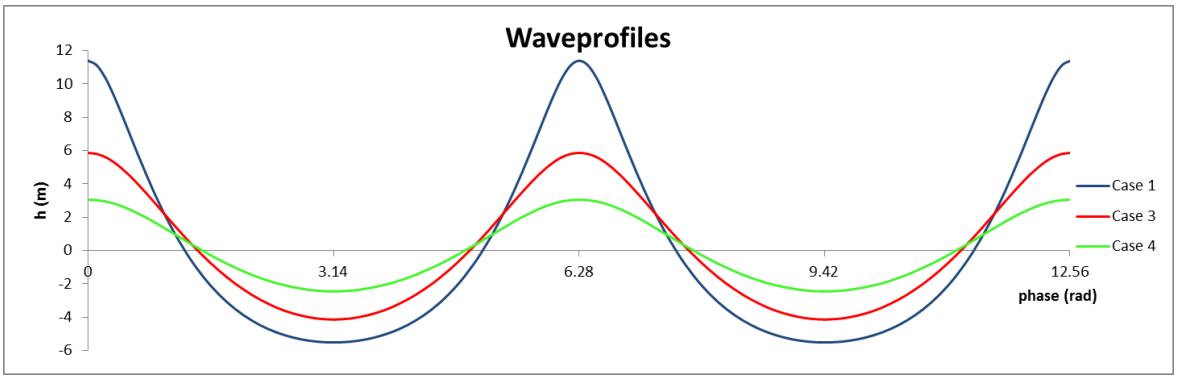

Figure 5.20 - Water elevation showing the (non)linearity for wave cases 1,3 and 4

5.10.1.2 Possible causes of the differences between FinLab and Morison

Both FinLab and the Morison equation have their limitations. The Morison equation is nothing but a model to describe the wave force, composed by a drag and inertia part. All physical processes are incorporated via the C_M and C_D coefficients. It is unclear which effects were present at the time the tests were performed (non-linearity, H/d ratio, wave run-up etc.). FinLab on the other hand simulates the real flow around a structure, but makes simplifications for the turbulence. Further it sensitive to numerical errors, like grid resolution or time stepping.

It is recalled that the differences between FinLab and the Morison equation, for case 1, are visible as:

- An increase in the maximum force on the upper part of the shaft (z=-16..WL) of 74%
- An increase in the maximum force on a whole monopile (z=-34..WL) of 49%

As a possible explanation is it possible that 1) an error is made in the application of the Morison equation 2) due to the fact that both the Morison equation and FinLab have another background the outcomes cannot be compared one-to-one 3) an error is made in FinLab. Especially the second cause is interesting, because it treats the difference between scale tests and the 'field' situation.

The differences between the maximum forces of FinLab and Morison may be attributed to the following possible causes:

1. Application of the Morison equation:
   1.1. The drag and inertia coefficients are determined incorrect from design graphs
   1.2. The Morison equation is not valid anymore due to diffraction
   1.3. Measuring and data processing errors that have occurred within the experiments being the basis of the Morison equation
2. Differences between the origin of the Morison equation and FinLab:
   2.1. Influence of non-uniform velocity pattern under a wave
   2.2. Influence of constant coefficients as function of time
   2.3. Influence of non-linear waves
   2.4. Presence of the free surface
   2.5. Wave slamming effect
3. Using FinLab:
   3.1. Numerical parameters within FinLab are chosen incorrect
   3.2. FinLab is giving incorrect values

When possible, for each of the aspects the influence on the difference is estimated. Note that the descriptions below aim to explain the differences for the ULS wave (case 1, see Figure 5.15).

Ad. 1.1: Variation in drag- and inertia coefficients
It may be that the drag and inertia coefficients used are not correct, due to a wrong interpretation from design graphs. For case 1 C_M=1.55 and C_D=1.15 were used (see Table 5.4). The sensitivity was checked by increasing the C_M and C_D coefficients to their maximum values found in literature for this case (roughness and Re number). As an upper limit: C_M=2.00 and C_D=1.50. The maximum force increased with about 30%, but by doing so the match at minimum force becomes rather poor, see Appendix C.8.

Ad 1.2: Diffraction
With respect to the validity of the Morison equation a lot of different statements can be found in literature. See Appendix C.1.6 for an overview.
Most of them can be brought back to the statement that the pile may not influence the flow field a short distance away from the pile. In Appendix C.5.3 for different wave cases figures resulting from FinLab are given, showing how the wave is moving along the structure. Based on case 1 (Figure 5.21) one may suggest that the original wave is distorted by the presence of the structure. For a near linear wave (see Appendix C.5.3) this is not the case. So, one could argue that the Morison equation is not valid anymore.

However, the influence of the pile on the flow field a short distance away from the pile has to be seen in another light: the Morison equation is nothing but a coupling between the wave kinematics at a distance far away from a cylinder and the forces on that cylinder, see Figure 5.22. When a wave interacts with a structure, always some reflection will occur. For slender structures this effect can be neglected. For these cases the Morison equation is valid.
In contrary, for compact structures the effects of reflection cannot be neglected anymore. The diffracted wave of Figure 5.22 will interact with the 'original' wave near the cylinder. When these effects start to play a role the force cannot be predicted with the aid of the Morison equation anymore, but diffraction theory should be applied.
Diffraction starts to play a role for D/L>0.2, where L is the (non)linear wavelength. This is definitely not the case for the ULS wave (D/L=0.03). So, diffraction plays a negligible effect and the Morison equation is just valid for this case.
This was also shown by decreasing the diameter of the shaft to D=1.0m. Here the D/L ratio is even smaller (D/L=0.005). Also in this case FinLab gave a higher maximum force than the Morison equation. The difference is again about 50%, see Appendix C.7.

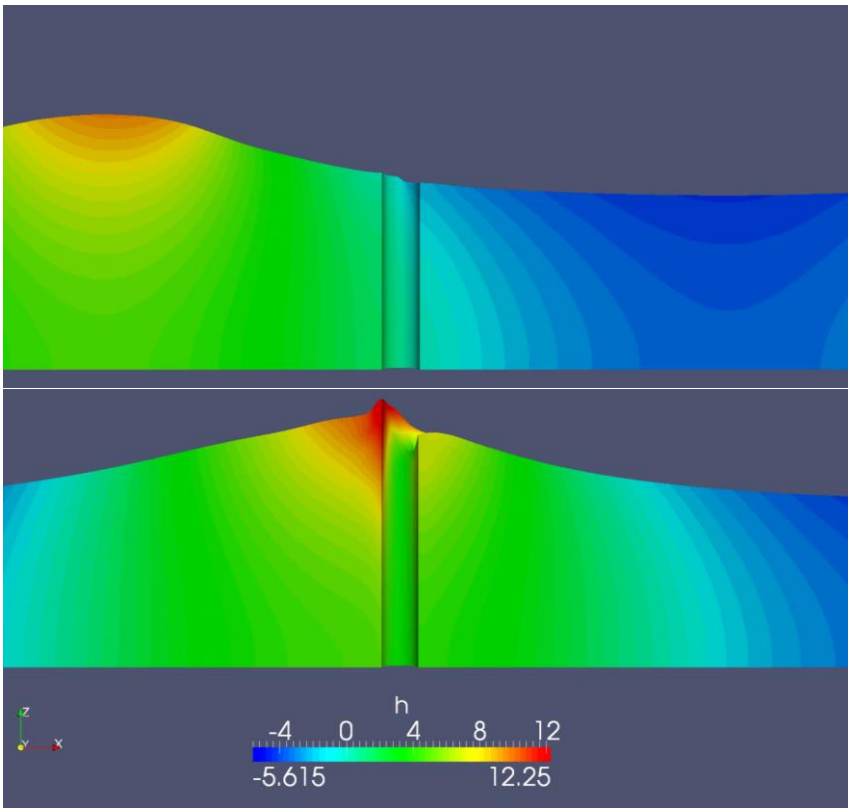

Figure 5.21 - Influence of the pile on the wave shape for different phases of case 1 (H=16.9m T=12.7s d=34m). h=piezometric level

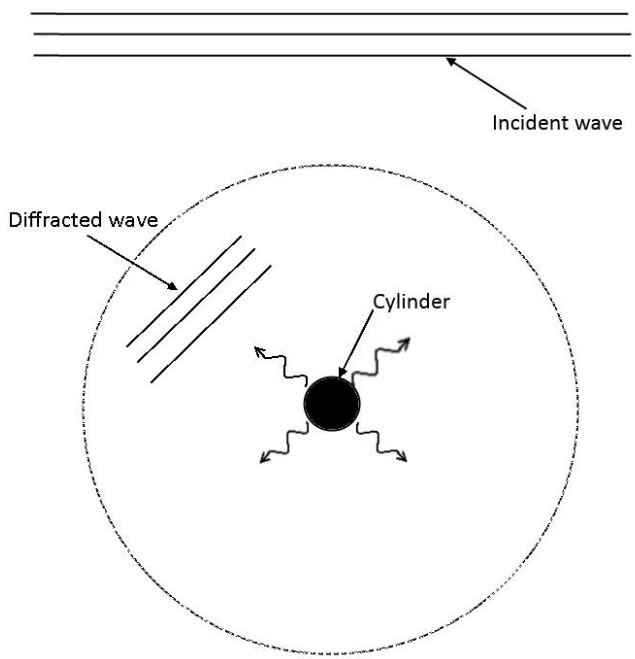

Figure 5.22 – Basic principle of the Morison equation (top view) and the presence of a diffracted wave.

Ad. 1.3: Measuring and data processing errors

From section 5.4.3 it is recalled that different data processing techniques like the Fourier analysis and (weighted) least square method give other force coefficients. For example, the weighted least square method is best in predicting the maximum force peaks. This effect is

causing an inaccuracy in the outcomes of the Morison equation in the order of at best several percent [27].
It is also recalled that the velocities under a wave for a certain test are possibly not measured but calculated based on a measured wave profile, which may be less accurate.

Ad 2.1: Influence of non-uniform velocity pattern under a wave
First it is repeated from section 5.4.2 that the C_M and C_D coefficients can experimentally have been deduced from:

1. Flow in an U-tube
2. Forced oscillations in still water
3. Fixed cylinder in regular waves

Coefficients based on the 3rd method can only be used correct if one exactly knows what the experimental conditions (wave height, wave period, water depth) were. This has to do with the fact that one often does not know what the KC number given represented: is it the maximum KC number, or has a coupling between a small section and the force on that small section been made? In the first case it should be kept in mind that a KC_{max} value only doesn't say anyting about the velocity profile under the wave. Two entirely different waves (long/short) can be described by the same KC_{max} value, but lead to a whole different force.

'Luckily', as known to the author, the design graphs from the DNV and Sarpkaya are mainly based on Sarpkaya's laboratory tests in a U-tube. Here, the process as described above doesn't play a role, due to the uniform velocity profile (and equal KC-numbers).
However, when applying this data to a cylinder in the field, one can wonder which approach to follow, due to the varying KC number as function of depth. In practise often the following approach is followed: the cylinder is divided in small sections. For every section the average velocity and corresponding KC number is determined. As a result, for every section a separate set of C_M and C_D coefficient is used. By doing so, one assumes that the water can be divided in small horizontal water layers, not influencing each other. In reality the layers will influence each other. Two effects play a role: the orbital motion and vertical velocities due to pressure differences between the top and bottom of a shaft.
For the ULS wave (case 1) the ellepticity of the orbital motion is small compared to a relative short wave for which the agreement between the Morison equation and FinLab seems better (case 4 for example). In [25] the effect of the orbital motion on the C_M and C_D values is investigated. For a KC number of about 17 the ellepticity seems to have negligible influence on the coefficients.

When instead of constant C_M and C_D coefficients as function of depth (as described in section 5.6.1) variable coefficients as function of depth, as described above, are used the force as found by the Morison equation increases a bit (~10%), see Appendix C.8.2.2.
It cannot be estimated what the effect of the assumption of horizontal layers not influencing each other is.

Summarized, the effects as described above are caused by differences between laboratory tests (2D) and the field/FinLab (3D). When exactly the same tests were performed in the laboratory as within FinLab (so with a fixed cylinder in regular waves with exactly the same velocity profile under a wave), one would expect the same outcome as from the Morison

equation. Using the results from tests with an U-tube by Sarpkaya may cause a possible difference between results from the Morison equation and FinLab. In the past several investigations based on field data partly confirmed the force coefficients found by Sarpkaya's tests. But it is unclear whether this has also been validated for a highly non-linear wave like the ULS wave. [27] Reports that the differences may be up to 40%, but this is also including data-processing techniques. Also for extreme waves differences are generally less. So this effect is roughly estimated at 20% (both higher and lower).

Ad 2.2: Influence of constant coefficients as function of time
The Morison equation is, in its original formulation, based on time averaged coefficients, but it can be questioned whether this is correct. The coefficients can in general be determined from two different data processing techniques:

- Fourier averaging technique/ (weighted) least squares method. Result: time independent coefficients
- Instantaneous values, as performed by Sarpkaya. Result: time dependent coefficients.

See for example Figure 5.23. Here the time dependent coefficients $C_M(\theta)$ and $C_D(\theta)$ as found by Sarpkaya are compared with the corresponding time averaged Fourrier coefficients C_M and C_D. The large peaks of the drag coefficient around 90 and 270° are possibly caused by measurement inaccuracies, due to the fact that the velocity is near to zero. The same is valid for the inertia coefficient around 0, 180 and 360°. But even when these large peaks are left out, the time depending aspect of the coefficients is clearly visible. The large variation is related to the vortex shedding process and occurs in the intermediate range of KC values (8<KC<25) [20]. This effect may lead to a mismatch between measured and predicted forces based on Fourier averaged coefficients like in Figure 5.24. Note that the difference between the measured and calculated force is about 25% at the peaks. This difference for drag-inertia dominated regions was also found in tests of Justesen [25].
Sarpkaya concludes that a) the Morison equation is not applicable in the so called drag-inertia dominated regime or that b) the Morison equation should be modified with the addition of a term. The latter gave rise to a lot of extensions of the Morison equation by different authors [20].

The fact that the magnitude of the time varying coefficients is related to the process of vortex shedding makes it difficult to apply to the case regarded in this thesis. Although the KC is about the same as for the ULS wave (case 1), the Re number is much lower here ($18 \cdot 10^4$ vs $5 \cdot 10^7$) leading to another flow regime (subcritical vs trans-critical). So, little can be said about the magnitude of increase.

It should be noted that case 1 is strongest inertia-and drag dominated, while case 4 is almost fully inertia dominated (see Appendix C.8 for the relative contribution of drag and inertia forces). The largest difference between FinLab and Morison occurs for case 1, which is in agreement with the statement that this effect is most noticeable for inertia- and drag dominated regimes.So, this effect may partly explain the differences between FinLab and the Morison equation. It may give rise to differences in the order of 25% (underestimation by the Morison equation).

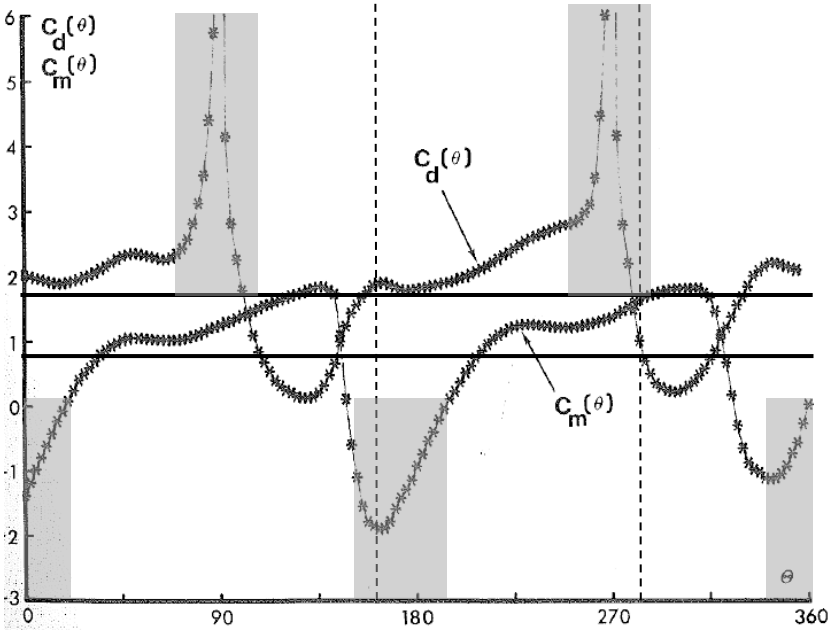

Figure 5.23 - Instantaneous values of C_M and C_D for K=15 and Re=18390 [20]. High peaks in shaded areas are probably caused by measuring inaccuracies.

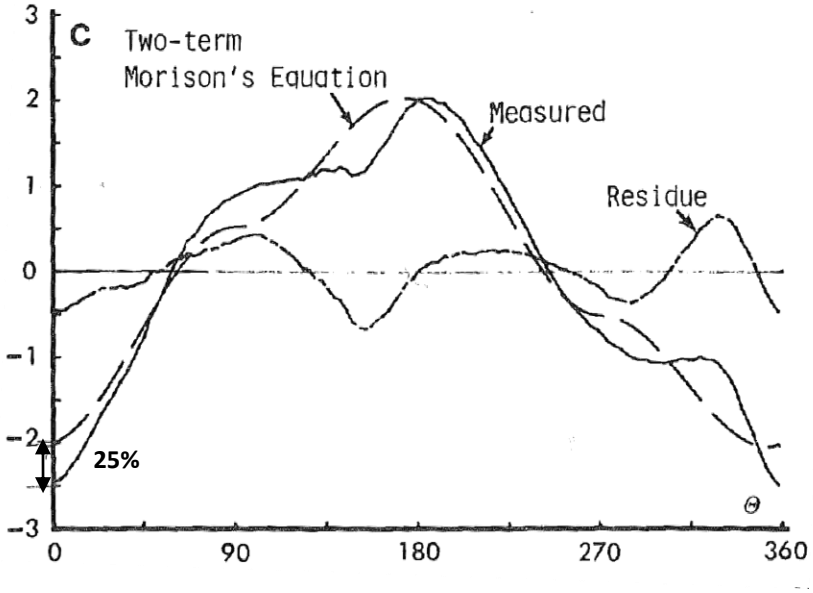

Figure 5.24 - Comparison between measured and calculated force, based on the 2 term Morison equation, KC=14 and Re=27800 [20]

Ad. 2.3: Influence of non-linear waves

Oscillatory flow tests in a U-tube by Sarpkaya were based on a sinusoidal flow. For this situation no orbital motion is present. 3D laboratory tests and field tests showed that the orbital motion doesn't lead to large changes of the coefficients for this case (see point 2.1). It is however unclear from literature what the background of these tested waves was. For a non-linear wave the orbital motion of the wave particles changes (no longer elliptical) which may lead to another flow field. However, as found by the author, in literature no references are made that the Morison equation may be less valid for non-linear waves.

Ad. 2.4: Presence of the free surface

The forces in the surface zone have an important contribution to the mud-line bending moment. In the surface zone there is a run-up at the upstream side. At the downstream side there is a drop in the water level, see Figure 5.25. One of the limitations of the Morison formula is that it does not take this free surface effect into account. This effect can be quite significant for highly non-linear waves.

The free surface effect approximately results in a hydrostatic pressure at the top of the structure, so the maximum pressure acts below the crest level. On the other hand, application of the Morison equation leads to the situation where the highest force acts at the level of the wave crest, where the horizontal particle velocity is maximal (see Figure 5.27).

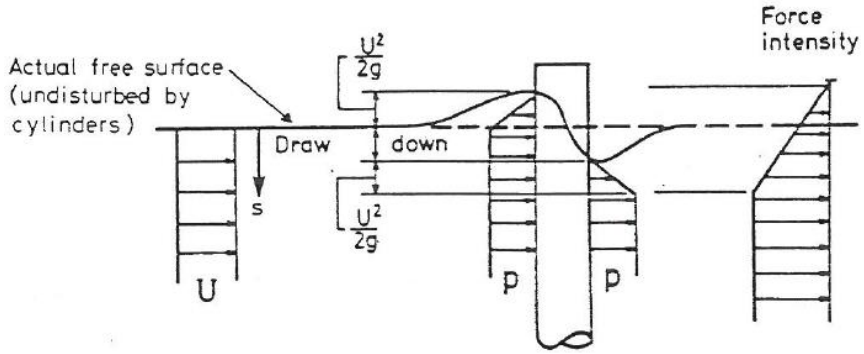

Figure 5.25 – Free surface effect and resulting force intensity [34]

The exact influence of this effect remains unclear. In literature different investigations show both higher and lower forces with respect to the Morison equation. Based on model tests Frigaard [34] shows that the measured force in the surface zone is higher than calculated with the Morison equation. On the other hand, according to [35], field measurements during a hurricane lead to a lower force than calculated with the Morison equation (see Appendix C.8). Tϕrum recommended the use of modified force coefficients, see Figure 5.26.

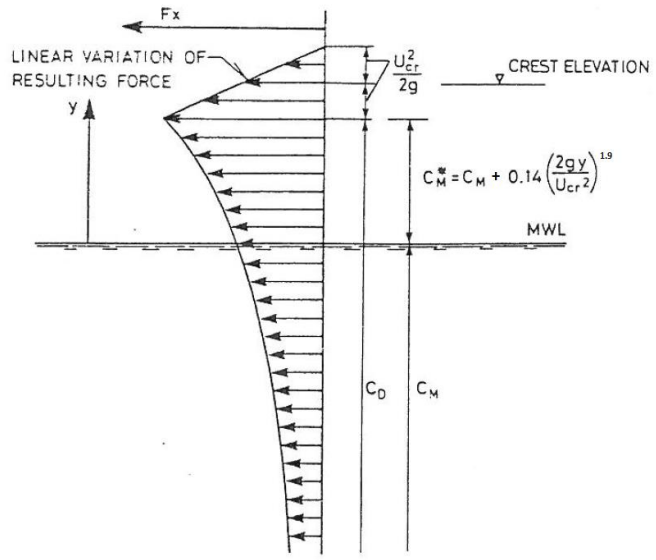

Figure 5.26 - Recommended force coefficients in the free surface zone [34]

For the ULS wave (case 1) both the original and adapted force distribution according to Tϕrum have been compared, see Figure 5.27 and Appendix C.8. Due to the free surface effect the horizontal force on the upper section of the shaft (from z=-16m), increases from 4.0 to 4.4 MN, leading to an increase of 10%.

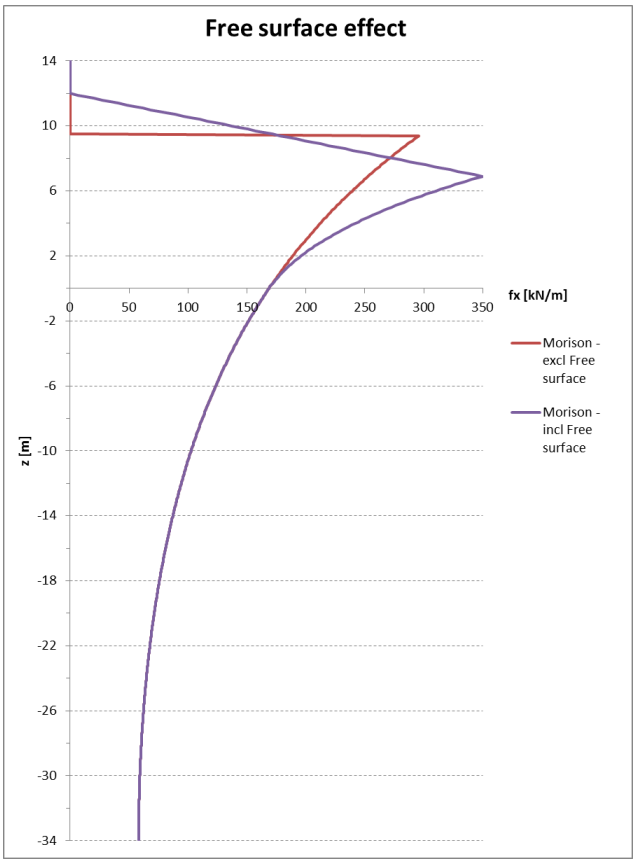

Figure 5.27 – Force distribution as calculated with the original Morison equation and due to inclusion of the free surface effect. Forces calculated for case 1 (H=16.9m, T=12.7s, d=34m) at time of maximum force.

Ad. 2.5: Wave slamming

Wave slamming occurs when a volume of water suddenly hits a body. This leads to high pressure peaks. According to the DNV and other literature for a vertical cylinder slamming is related to wave breaking. In that case the slamming force can be calculated based on the breaker type. This force can be quite high, see for example the case study in Appendix B.4.5 where the force in the surface zone doubles due to wave breaking.

For the cases regarded with FinLab, the maximum wave breaking limit is $H/H_b \approx 0.7$ for case 1. This is not near the breaking wave limit. Breaking may occur when the bottom slope suddenly changes, but due to the flat bottom this is not the case either. So, wave breaking is not expected to occur.

One could argue that wave slamming also may occur for a very steep wave. Although for case 1 the wave is highly non-linear, the maximum wave steepness is not that high (<45°, see Figure 5.28). Wave slamming only occurs when there is an air gap between the volume of water and the structure. So, when a particle that hasn't been influenced by other particles in front of him, hits the structure. This is definitely not the case here, so wave slamming as a possible explanation for the differences between Morison and FinLab is rejected.

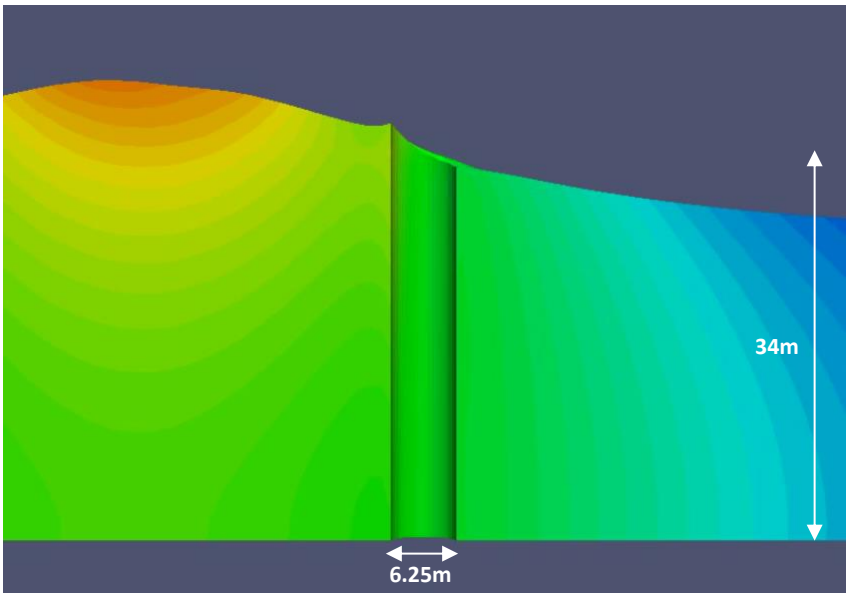

Figure 5.28 – The ULS wave of case 1 (H=16.9m T=12.7s d=34m). Horizontal and vertical scale the same.

Ad. 3.1: Numerical paramters

The influence of the numerical parameters within FinLab was already investigated by a sensitivity check (see section 5.9). Differences were small (~10%), although the influence on the fatigue load may be significant.

Ad. 3.2: Incorrect output FinLab

A possible cause that should be mentioned as well is that FinLab also may give inaccurate forces. The newly developed force module has never been validated before. The validation of section 5.6 gives good confidence in the outcomes for linear waves. But based on this validation it cannot be stated that the same is valid for (higly) non-linear waves as well. The main differences in physical effects between the validated wave and the ULS wave (case 1) are: the larger influence of the free surface and the larger influence of drag. It may be that one of these effect is not correctly modelled within FinLab yet. However, expert advice by R.J. Labeur confirmed the reliability of the outcomes of FinLab for the ULS wave. See the next section for a final discussion.

5.10.1.3 Summary of the possible causes

The difference in the maximum force peak between FinLab and the Morison equation seems to be related to the magnitude of the non-linearity. For near linear waves (around U_r=1.5) both methods give the same about output, although this is based on one simulated case only (case 4). But for increasing non-linearity the differences increase, up to a 49% higher horizontal force found by FinLab for case 1.

Possible causes and their influence

In the previous section different possible causes were investigated. The most promising are summarized in Table 5.9. If possible the effect on the total difference is estimated.

Possible cause	Effect on difference
1.3a Data processing technique used	unknown (may be large)
1.3b Inaccurate velocity determination	unknown (probably small)
2.1a Force coefficients as function of depth	- 10%
2.1b From U-tube to the field	±20%
2.2 Constant coefficients as function of time	-25%
2.3 Free surface effect	-10%
3.1 Numerical parameters	±10%

Table 5.9 – Most promising causes for the difference between Morison and FinLab and their effects for case 1. N.b. magnitude of effects are based on rough estimates.

None of the mentioned effects can completely explain what causes the difference between FinLab and Morison. But when combined the difference of about 50% found may be explained. Similar results as in this thesis have been found with the CFD packages ComFlow and OpenFoam. A difference in maximal horizontal wave force between a CFD package and the Morison equation for highly non-linear waves was also found in literature. In [36] for high waves in shallow water the maximum difference in horizontal force was about 25%.

It may however still be the case that an effect is overlooked which would lead to an increase of the force found by the Morison equation, or that the influence of one of the effects mentioned is higher and dominates. But it may as well be that the outcome of FinLab is not correct for these waves.

Validation of results

The only way to get this clear is by calibrating the FinLab model with experimental data. This experimental data should be based on a highly non-linear wave in preferably not too deep water. During the last few years an increasing number of investigations on the forces of (near)breaking waves on monopile foundations in relative shallow water were performed. So, this data is expected to be available within literature. Due to time restrictions this calibration step was not performed.

Another way to partially validate FinLab is by performing oscillatory flow tests within FinLab without the free surface effect. Instead of a free surface, one should use a closed boundary at the water surface. When for this case the force from FinLab corresponds with theory, it can be concluded that the difference is caused by the presence of the free surface or the orbital motion.

5.10.2 Influence of the caisson

Velocity increase around the shaft

From the observations of section 5.8.3.5 follows that the maximum bending moment increases less than the maximum horizontal force. This means that the force increases mainly at the bottom of the shaft. This effect was expected to occur, see the hypothesis of section 5.7.1. This statement is confirmed by a comparison of flow velocities just above the cone. For case 1 both flow velocities and hydrostatic pressures at the lowest part of the shaft increase due to the presence of the caisson, see Figure 5.30 - and Appendix C.5.

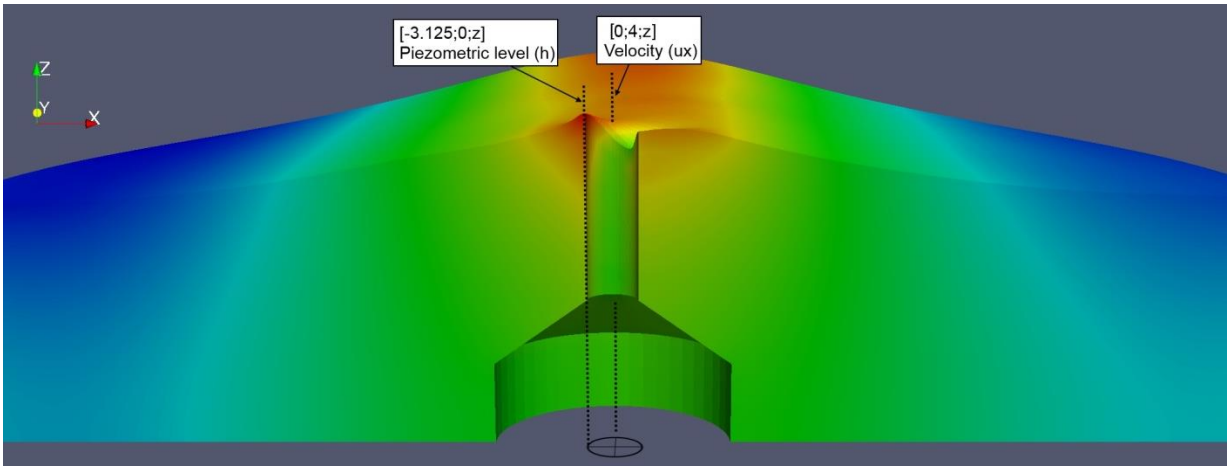

Figure 5.29 – Locations used to extract the profiles of Figure 5.30 from FinLab.

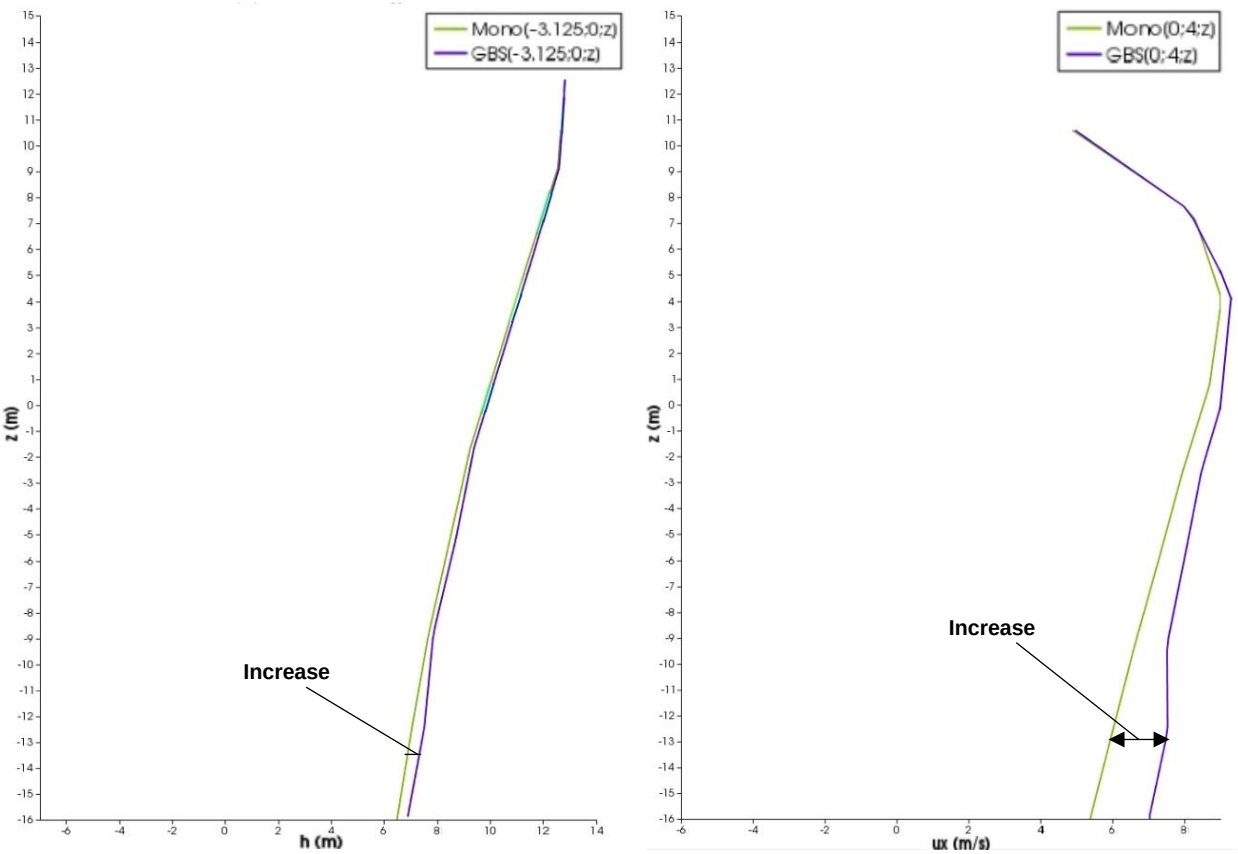

Figure 5.30 - Increase in hydrostatic pressure and velocity due to the caisson. A) Piezometric level at the front of the cylinder as function of depth B) Horizontal particle velocity at 1 meter next to the cylinder. Comparison of results by FinLab for the upper part of the Monopile (green) and the GBS shaft (blue).

Discussion of observed force differences due to the caisson

With respect to the caisson, one of the observations is that a larger absolute value of the minimum force leads to a smaller bending moment, see for example Figure 5.17.
If the irreversible reasoning as described above for the wave crest is applied, then one would indeed expect a higher magnitude of the minimum horizontal force on the shaft due to the caisson. The increase is expected to occur just above the cone, but due to the submerged part of the shaft (about 8 m only) the increase will probably be uniform. Based on this reasoning one would expect a higher magnitude of the minimum bending moment (instead of a lower as observed). No explanation for this effect could be found.

Another observation is that the increase of the maximum horizontal force on the shaft (due to the caisson) is largest for the relative short waves. The hypothesis was that the increase would be highest for the relative long waves (see Table 5.5). This hypothesis was based on the relative high orbital motion for relative long waves (shallow water) near the caisson, see section 5.7.1. So, this finding is opposite to the hypothesis. No explanation for this effect could be found either. It may be that the hypothesis is wrong, or that another effect causing the higher force due to the presence of the caisson is overlooked.

5.11 CONCLUDING REMARKS

FinLab was used to determine the hydrodynamic load on the shaft of the GBS. For this purpose a force module was developed within the model. Validation gave very good results for a nearly linear wave.

Within FinLab simulations were performed for the ULS wave and two FLS waves (from the lumped wave scatter diagram). The model initially seemed not to be able to model relative short waves. An update of the FinLab code gave better results, but due to limited time the results for these relative short waves (2 out of 6 wave-cases) have been left out of the discussion of this chapter.

From the results followed that FinLab often resulted in a higher force than the Morison equation (up to 74% for the shaft). The difference was found to be related to the degree of non-linearity of a wave. By comparing the Morsion equation (and its background) with FinLab different possible causes for the difference found were presented. The combined effect may (partially) explain the differences. But, in order to be sure about the outcome of FinLab, the model should be calibrated with experimental data.
The influence of the caisson on the maximum bending moment was found to be small (max 10%). The influence on the bending moment cycles even smaller (max 2%), although it should be kept in mind that a small difference in force may have a large influence on the fatigue load.

Although the outcome of FinLab may be too conservative, it is used as an input for the following chapter. Here the influence of the higher forces found by FinLab is investigated. Based on the observations of the hydrodynamic analysis with FinLab and the Morison equation recommendations for the design of the steel shaft are given. The recommendations summarize the results of this chapter and are mainly based on Figure 5.19:

ULS wave (case 1)[Table 5.5]

- For the maximum horizontal force: use the results from FinLab (+74%). The influence of the caisson is small (10%).
- For the maximum bending moment: use the results from FinLab (+120%). The influence of the caisson is negligible.

FLS waves (case 3,4) [Table 5.6]

- For Ur<1.5 (class 14 and lower): use the bending moment cycle from Morison. The Morison equation can be applied on the upper part of the monopile, because the caisson doesn't seem to influence the bending moment cycle. Also, compared to the evaluation with Morison, FinLab doesn't result in higher values.
- For Ur>1.5 (class 15 and higher): increase the bending moment cycle with the ratio of Figure 5.19, as found by simulations with FinLab. The influence of the caisson doesn't have to be taken into account.

6

6 INFLUENCE OF A DETAILED HYDRODYNAMIC LOADING ANALYSIS ON THE DESIGN OF THE STEEL SHAFT

6.1 INTRODUCTION

Hydrodynamic forces can have a significant influence on the dimensions of the steel shaft. In this chapter it is investigated what the influence of the results obtained with FinLab is. The focus is the design of the steel shaft of the GBS. This is done by applying the results from FinLab to the case study as introduced in Chapter 5.2.

In the previous chapter it was concluded that the caisson, with respect to the bending moment cycle, does not influence the magnitude of the hydrodynamic loads significantly. For both the ULS and the FLS wind and wave loads have to be used. The wind loads follow from the wind turbine manufacturer, wave loads from the previous chapter, see the recommendations of Chapter 5.11.

For the ULS the maximum design values were used. The FLS is based on the wave scatter table introduced in Chapter 5.2. In order to determine the fatigue load the quadratic superposition method, as described in Chapter 4, is used.

For both the ULS and the FSL a unity check was performed. By keeping the diameter constant, the required wall thickness was determined in order to have both unity checks smaller than one. Finally, for both cases (the Morison equation and the results from FinLab) the amount of required steel could be compared, see section 6.2.4. This comparison gives insight in the impact and utility of the detailed hydrodynamic calculation with FinLab.

Section 6.3 summarizes the effects of the detailed hydrodynamic loading analysis with FinLab. It also discusses the influence for another location or water depth.

6.2 DETERMINING THE DIMENSIONS OF THE STEEL SHAFT

6.2.1 Overview of the performed steps

Within this chapter the offshore wind turbine is schematised as described in Chapter 5.2, also see Figure 6.1. Please note that the wall thickness at tower top is a characteristic of the wind turbine ($t_1 = 0.02$m). Within this chapter the required wall thickness at TC level is calculated (t_2). The wall thickness is assumed to vary linear between TC and TT level, and is assumed to be constant below TC level.

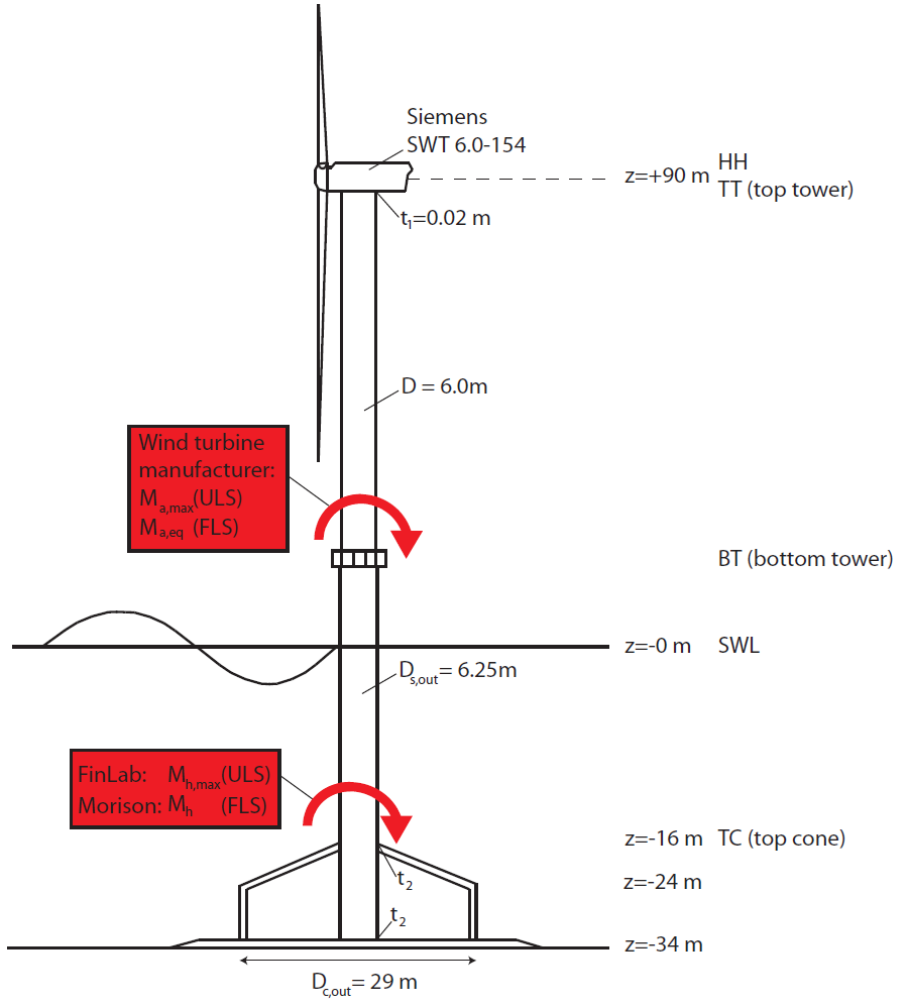

Figure 6.1 – Schematisation of the offshore wind turbine as in Figure 5.1. In red boxes an overview of the obtained forces. D=diameter, t=wall thickness, HH=Hub Height, SWL=Still Water Level

The wall thickness is calculated by performing:

- An ULS analysis: The maximum wind load is provided by the wind turbine manufacturer as a maximum bending moment at BT level ($M_{a,max}$). The maximum wave load at TC level ($M_{h,\max}$) follows from the hydrodynamic analysis with FinLab, see section 5.11. Both loads are combined. By applying safety factors the design bending moment at TC level ($M_{d,tot}$) can be calculated. Next, the unity check can be performed by dividing the load by the resistance.
- An FLS analysis: The wind loads during lifetime are provide by the wind turbine manufacturer as a damage equivalent bending moment at BT level ($M_{a,eq}$) which is transferred to a damage equivalent stress ($\Delta\sigma_{a,eq}$). For the fatigue load due to waves, for each case of the lumped wave scatter diagram the fatigue load is calculated. For

the magnitude of the wave loads the recommendations of section 5.11 are used (which is: use the Morison equation in most cases). Now, the damage equivalent bending stress due to waves ($\Delta\sigma_{h,eq}$) can be calculated. Both damage equivalent stresses can be combined according to the quadratic superposition method, leading to ($\Delta\sigma_{ah,eq}$). Next, the unity check can be performed by dividing the combined damage equivalent stress by the maximum allowable value ($\Delta\sigma_{eq,max}$).

6.2.2 Performing an ULS analysis

An overview of the ULS analysis was already given in section 3.4.3. In this section the ULS analysis is applied to the offshore wind turbine as schematised in Figure 6.1. The full ULS analysis is described in Appendix D.2.

Wind and wave loads

Both the extreme wind and wave load are required. By comparing different load cases, the extreme wind load was found by the wind turbine manufacturer. The bending moment is converted to the top of the cone (TC level). With a safety factor of 1.35 this leads to the design value of the bending moment found $(M_{d,a})$ in Table 6.1. Off course, this value is independent of the method used to determine the wave loads.

According to the wind turbine manufacturer, the wind load provided should be combined with the 50 year extreme wave. The resulting wave forces on the shaft are according to the recommendations of section 5.11 and follow from case 1 of Chapter 5 (see Table 5.5). Two cases are distinguished: the hydrodynamic force resulting from the Morison equation (S1, 'lower bound') and from FinLab (S2, 'upper bound'). The resulting force from the Morison equation was multiplied with a safety factor of 1.25. The force from FinLab is multiplied with a safety factor of 1.10, due to the higher accuracy of the method and the more conservative results obtained. The design values of the bending moments at TC level $(M_{d,h})$ can be found in Table 6.1.

Combined load

The total load is the combination of the wind and wave load.
When the Morison equation (S1) is used to calculate the wave forces, the influence of the waves on the total bending moment is quite small (about 25%). When FinLab is used (S2) this influence is larger (about 40%). When the results from FinLab are used, resulting in 120% (!) higher wave loads, the total bending moment increases with only 26%.
So, for the ULS FinLab leads to a 26% higher total bending moment compared to application of the Morison equation.

d=34 m Case	$M_{d;a}$ [MNm]	$M_{d;h}$ [MNm]	$M_{d;tot}$ [kNm]	Increase [%]
S1. Morison equation	220.8	83.1	303.9	-
S2. FinLab shaft mono	220.8	161.2	382.0	26%

Table 6.1 – Design values of bending moments at TC level for the ULS. a=aerodynamic, h=hydrodynamic loads. $M_{d;h}$ following from Table 5.5 (case 1). For S1 the safety factor is 1.25, for S2 a value of 1.10 has been used.

Finally, a unity check for the ULS was performed, by dividing the design value of the load by the design value of the strength (yielding and buckling moment). The buckling moment was assumed to be governing. The value of the buckling moment changes per case, due to the

fact that the wall thickness is adapted in order to find the minimum wall thickness required (see section 6.2.4 for the resulting unity checks).

6.2.3 Performing a FLS analysis

The FLS analysis was introduced in section 3.4.2 and Chapter 4. In this section the FLS analysis is applied to the offshore wind turbine as schematised in Figure 6.1. The full FLS analysis is described in Appendix D.3. The approach applied here is based on the quadratic superposition method (see section 4.3.2)

Fatigue load due to wind

The fatigue load due to wind is provided by the wind turbine manufacturer. All individual stress cycles for the entire lifetime are transferred to a damage equivalent load ($M_{a,eq}$).). This bending moment at BT level is converted to TC level by simple mechanical laws. This damage equivalent load in combination with a number of cycles *n* leads to a fatigue load D_{fat}. The resulting damage equivalent stress due to wind can be found in Table 6.2.

Fatigue load due to waves

A lumped wave scatter diagram (see Table 5.1) forms the input for the fatigue load analysis of waves. For these FLS waves the magnitude of the wave force can be determined with the Morison equation for classes 1-14, according to the recommendations of section 5.11. For the classes 15-18 a scale factor was applied according to Figure 5.19.
The structure is schematised as a mass-spring system with one degree of freedom (see Appendix A.4.5). For this system the dynamic amplification factor (DAF) was deduced. This was done under the assumption of 5% total critical damping always present and a natural frequency of the system of 0.25 Hz. The static bending moments were multiplied with the DAF in order to obtain the dynamic results, see Figure 6.2.
Especially for wave classes 1,4 and 7 the bending moment due to a dynamic analysis is significantly higher than for a static analysis. This has to do with the excitation frequency of the waves being close to the natural frequency of the system.

The fatigue load per wave class (Figure 6.3) is calculated by taking the lumped wave scatter diagram and wave directionality into account. Due to their high DAF and probability of occurrence wave classes 1,4 and 7 play a dominant role in the total fatigue load due to waves. The total fatigue load can be found in Table 6.2. The fatigue load of the waves is only a few percent of the fatigue load due to the wind. The fatigue load seems to be strongly wind-dominated for this case.

	D_{fat}	%	$\Delta\sigma_{eq}$ [N/mm^2]
Wind	0.1748	96.2	55.2
Waves	0.0069	3.8	29.0
Combined			62.4

Table 6.2 - Combination of wind and wave loads for the FLS.

Combined fatigue load

The damage equivalent stress due to wind and waves is calculated according to equation (4.3). Finally a unity check for the FLS was performed, by dividing the combined damage

equivalent stress by the maximum allowable damage equivalent stress ($\Delta\sigma_{eq,max}$, see section 4.3.3). The allowable damage equivalent stress is calculated from the S-N curve and the corresponding equation (4.1). Input for the formula is $N = 3 \cdot 10^7$ cycles (including a safety factor 3), $D_{fat} = 1$ and $t = t_{ref}$. The latter is incorrect as will be discussed in Chapter 7.1. Luckily the effect is small. The equation leads to $\Delta\sigma_{eq;max} = 62.8$ N/mm^2.

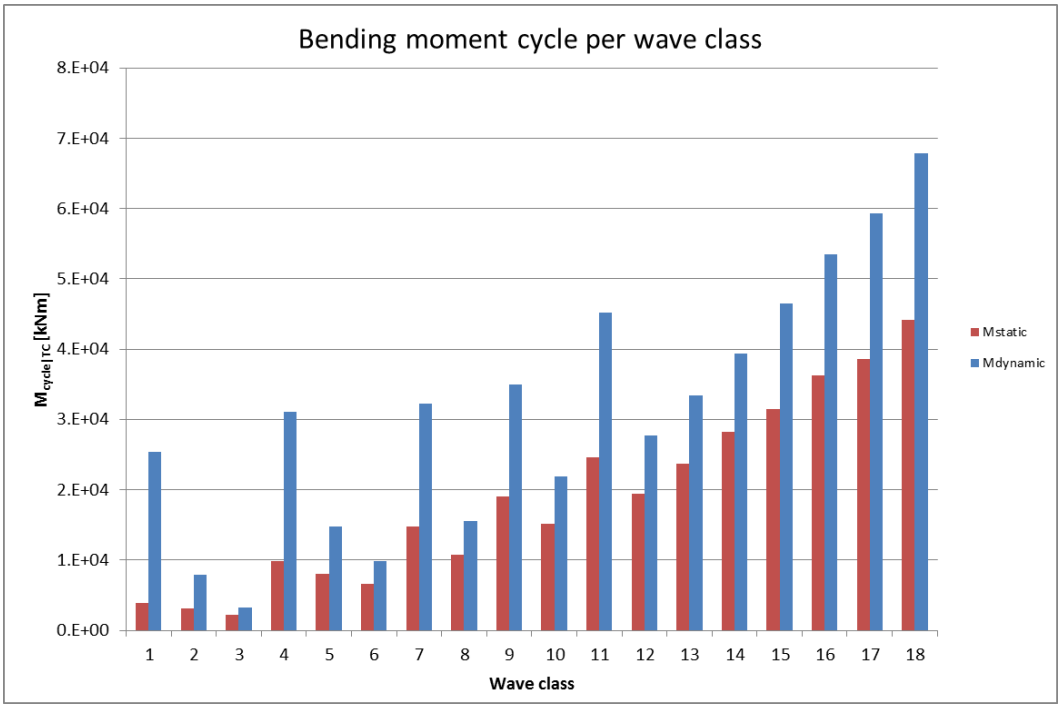

Figure 6.2 – Static and dynamic bending moment at TC level per wave class. $M_{dynamic} = M_{static} \cdot DAF$

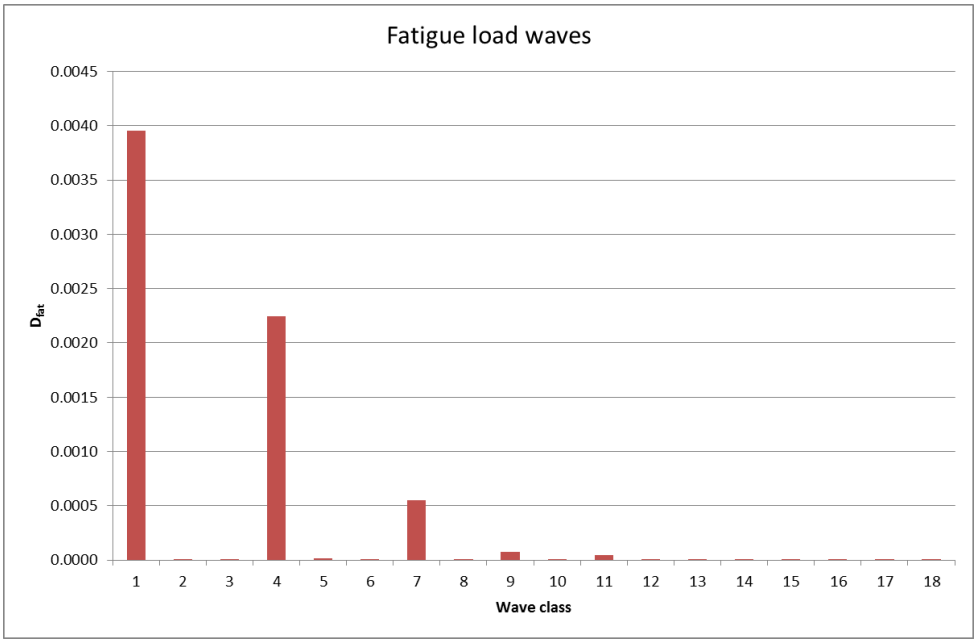

Figure 6.3 - Fatigue load per wave class

6.2.4 Resulting dimensions of the shaft

In the previous sections the unity check for the ULS and FLS was explained. The wall thickness was adapted until one of the unity checks became governing (≈1).

The required wall thicknesses and values of the unity checks can be found in Table 6.3. From the wall thickness the mass of the shaft is calculated.
For both cases the required wall thickness of the shaft is 0.045 m. This has to do with the fact that the bending moment cycles for the FLS do not change significantly when instead of the Morison equation FinLab is used to determine the hydrodynamic load. Therefore the $U.C._{FLS}$ doesn't change significantly for both methods. When the Morison equation is used (S1) the unity check for the ULS has some capacity left. When the higher ULS wave load from FinLab is applied (S2) this leads to about the same unity check as for the FLS. Due to the capacity still being present the wall thickness doesn't have to be increased.

Case	$t_{2;required}$ [m]	U.C. ULS	U.C. FLS	m_{shaft} [t]
S1. Morison equation	0.045	0.76	0.99	318
S2. FinLab shaft mono	0.045	0.96	0.99	318

Table 6.3 – Required wall thickness of the lowest part of the shaft calculated for two situations of hydrodynamic loading. U.C. is Unity Check. Shaft from z=-34m..BT

6.3 INFLUENCE OF THE DETAILED HYDRODYNAMIC LOADING ANALYSIS

6.3.1 Influence for this specific case

The detailed hydrodynamic loading analysis with FinLab resulted in recommendations for the wave loads. In general these were, with respect to the Morison equation, a higher bending moment for the ULS and an increase of the wave loads for the highest wave classes of the FLS.
In the previous section it was found that for the FLS the detailed hydrodynamic loading with FinLab didn't lead to any significant changes. This was mainly caused by the low probability of occurrence of the highest wave classes.

For the ULS the higher wave loads found by FinLab resulted in a higher value of the unity check. But due the fact that there was still some capacity with respect to the ULS, this didn't result in a larger wall thickness.

Although a simplified model was used to determine the fatigue load, this finding is still expected to be valid when for example a time domain analysis is performed. The probability of occurrence of those highly non-linear waves will also be small there.
What may change due to a more sophisticated fatigue load calculation method is the wind or wave dominance. Also the simplified method of quadratic superposition and structural schematisation used here may have resulted in relative high inaccuracies in the magnitude of the fatigue load.

When a more sophisticated fatigue load calculation is performed, this may result in a higher fatigue load. In that case a detailed hydrodynamic analysis won't change the outcome for the wall thickness. But when the fatigue load becomes smaller the ULS will start to 'govern' the design of the steel shaft. Now, the detailed hydrodynamic analysis will result in a larger wall thickness.

6.3.2 Influence for other cases

When instead of this specific case the shift to another location or water depth (up to 60m) is made, the findings may change.

For other locations and larger water depths the fatigue load due to the detailed hydrodynamic analysis isn't expected to increase either. Most waves are near linear waves, which can be described by the Morison equation quite well. For those few upper wave classes where the Morison equation gives lower values the influence on the fatigue load is probably not so large. Off course this statement is only valid when the probability of occurrence of those wave classes is low.

For a larger water depth the magnitude of the fatigue load is however expected to increase, due to the higher arm of the wind force and higher bending moment due to waves.
Also the contribution due to waves will probably increase, due to the relative higher bending moment expected.
For the ULS wave the load due to the detailed hydrodynamic analysis will be higher as well, due to the highly non-linear character of these kind of waves. For larger water depths both the wind and wave load at the bottom of the shaft will increase, due to the higher arm and

larger submerged part of the shaft (see case 2 of Table 5.5). This will for sure lead to a larger wall thickness as calculated for a water depth of 34 m.

It is hard to say what the influence of the detailed hydrodynamic analysis is. This will be strongly dependent on the unity check for fatigue. Suppose the unity check for the ULS is governing for this water depth. Then performing a simulation with FinLab will result in a higher wall thickness compared to application of the Morison equation.

7

7 CONCLUSIONS AND RECOMMENDATIONS

In this final chapter the results are summarized. In section 7.1 the limitations of the methods applied, and their influence on the outcome, are mentioned. Also an interpretation of the outcome by the author is given. This discussion on the results leads to the conclusions and recommendations given in section 7.2 and 7.3.

7.1 DISCUSSION OF RESULTS

7.1.1 Limitations and their influence

In this section the obtained results of Chapter 5 and 6 are discussed. The limitations mentioned in Chapter 3.3 and 5.2 are recalled, and their influence on the outcome is discussed.

Hydrodynamic analysis

- Rigid structure: within FinLab the structure was schematised as a rigid structure. In reality the shaft of the offshore wind turbine will oscillate due to the time varying load. The magnitude of the oscillations will be strongly influenced by the structural and foundational stiffness. Due to these motions, the wave-structure interaction may change. Instead of the 'normal' Morison equation, the relative Morison equation has to be applied. When the oscillations of the structure are relatively large, also structure-wave interaction (the influence of the structural motions on the wave shape) have to be taken into account. As a first estimate of the structural motions the maximum tower top deflection is estimated to be 1 m [37]. The deflection around water level is, with an increase due to foundation stiffness, estimated to be about 10% of that, so 0.1m. Suppose the maximum tower to deflection occurs due to resonance, so at a loading frequency of 0.25 Hz (=4.0s). When a sinusoidal load is assumed, the maximum velocity at the water level is 0.16 m/s ($x = \int_0^{T/4} \hat{u} \sin(\omega t) = \frac{\hat{u}}{\omega} = \frac{2\hat{u}}{\pi} = 0.1 \rightarrow \hat{u} = 0.16$m/s). This is relatively small compared to the maximum horizontal wave particle velocities (~1.0-8.5 m/s at water level). Therefore this influence is expected to be small.

Concluding: the assumption of having a rigid structure has probably little influence on the wave loads found.

Shaft design

- Wave breaking: wave breaking is not taken into account for the design of the steel shaft. This may hold true for the hypothetical situation in this thesis. The probability

of occurrence of wave breaking is very small on an entire flat bottom. In the field this may however not be the case. Also the risk of wave breaking may be too high, so that is has to be taken into account. If wave breaking is taken into account this will most likely lead to an increase of the wave loads for the ULS and an increase of the dimensions of the steel shaft.

- Lift forces: lift forces were neglected, but may be significant for the design of the steel shaft. For the ULS wave, the vortex shedding frequency is far above the natural frequency of the offshore wind turbine (f_s ≈0.4, f_n ≈0.25, see Appendix A.4.2.3). This will lead to relatively low lift forces in cross-wave direction compared to the horizontal wave load in wave direction.
  For a certain range of the FLS waves the vortex shedding frequency will be equal to or smaller than the natural frequency, leading to resonant behaviour. This may lead to high lift forces. These forces may even be higher than the wave forces in wave direction. Therefore the fatigue load should not only be calculated in wave direction, but also in cross-wave direction. The combined effect of drag, inertia and lift forces may even lead to a governing fatigue point along the circumference that is not parallel or perpendicular to the wave direction, but somewhere in between.
- Current loads: the effect of currents on the wave load was not taken into account. The current velocity (~0.5-2 m/s) is small compared to the maximum horizontal particle velocity (~8.5 m/s). But due to the quadratic drag force, an increase in the horizontal particle velocity of about 20% already leads to an increase in drag force of about 50%. For the FLS waves, which are characterized by a smaller horizontal particle velocity, the current velocity may even have the same order of magnitude as the horizontal particle velocities under a wave. This may lead to a 4x as high wave force. So the effect of currents on the fatigue load may be quite significant. Please note that for combined wave and current interaction other drag and inertia coefficients have to be used than for waves only.
- Accidental loads: Accidental loads (ship impact, breaking ice) were assumed to be negligible. Compared to the ULS wave load this probably is the case, but this should be verified.
- Additional effects: effects like marine growth and corrosion have not been taken into account. But marine growth will lead to an increasing wave load (due to a higher roughness), while corrosion leads to a decrease of the strength. Both effects should be taken into account and will probably lead to an increase of the shaft dimensions.

Concluding: be aware that several effects are not taken into account that probably lead to higher hydrodynamic loads. For the ULS this is wave breaking and the effect of current. For the FLS these are the lift forces.

Fatigue load analysis

- Quadratic superposition: the quadratic superposition method is based on the assumption that the period of the aerodynamic load is equal to the hydrodynamic load ($T_{z,a} \approx T_{z,h}$), see equation (4.3). Generally the zero crossing period of wave response is higher than for wind response [21]. Also the response due to wind and wave loads is assumed to be independent. This can be questioned, because the responses due to wind and waves on the long term are to some extent correlated. Application of the method in [21] did lead to relative low errors (~10% compared to

a full time domain analysis), but the critical note is placed that this may be strongly dependent on the wind and wave conditions used within this research.

- Wave directionality: the most occurring wave direction is not necessarily the direction where the fatigue load is highest. This is because the wind direction may be different from the wave direction. The analysis applied in this thesis is however based on this approach. Probably this is a conservative assumption, because two loads in the same direction lead to a higher load than when this is not the case (the effect of aerodynamic damping excluded).
- Lumped wave scatter diagram: For the description of a sea state some simplifications are made, where one should be aware of. First, a measured wave signal is described by a wave scatter diagram. This in general goes without large errors. For fatigue calculations the wave scatter diagram is transformed to a lumped wave scatter diagram. Errors of this step are in the order of several percent, but one should be aware that critical cases can be missed [38]. Each class of a lumped wave scatter diagram represents a wave spectrum. In the analysis of this thesis the underlying spectrum is replaced by a regular wave. By doing so, the full range of wave periods in the original measured signal is reduced to 18 periods only. One should be aware that waves near the natural frequency of the system, resulting in a high contribution to the fatigue load, may easily be missed.
- Regular only: In reality the environmental wave state consists of irregular waves.
  In this thesis only regular waves are looked at. The ULS wave can be approached by a regular wave, but this is not the case for the FLS waves.
  When the lumped wave scatter diagram is used as input for a time domain analysis, irregular waves will be created again. But in this thesis the full irregular wave state is replaced by a series of regular waves. Wave kinematics may change significantly in an irregular wave. It is however hard to say what the exact influence on the fatigue load is (higher/lower). But one should be aware of this simplification.

Concluding: be aware that the quadratic superposition method, as used here, is a relative simple approach. Also replacing an irregular wave state by a series of regular waves may have a large influence.

7.1.2 Incorrect approaches as noticed during performance of this thesis

During the research some incorrect approaches were noticed by the author.
Due to time restrictions, they could not be 'repaired'. Instead, they are mentioned here:

- Turbulence model in FinLab: In section 5.5.2 was described that within FinLab the $\kappa - \epsilon$ model was chosen as turbulence model, due to the presumed predominant inertia force. For increasing non-linearity the drag force starts to play a significant role, leading to an increasing importance of turbulence. Although the $\kappa - \epsilon$ model is assumed to model the turbulence as well, it is advised to also perform a simulation with the LES model.
- Constant drag and inertia coefficients as function of height: In section 5.6.1 was mentioned that one set of C_M and C_D coefficients was used for the full height of the structure. When variation of the velocity over the depth is high, this is, looking at the original experimental test, probably not correct. The effect of applying variable coefficients as function of depth was investigated in Appendix C.8.2, but found to be small (differences in force the order of 10%).

- Maximum damage equivalent stress: In chapter 6 (and Appendix D) the maximum damage equivalent stress $\Delta\sigma_{eq;max}$ was calculated independent of the wall thickness. This is not correct, because the wall thickness has an influence, see equation (4.1). The influence is however relatively small: with a wall thickness of 0.045 m $\left(\frac{t}{t_{ref}}\right)^k$ becomes 1.07 instead of 1.0. For the waves the fatigue load D_{fat} now becomes 0.0098 instead of 0.0069, which is still small compared to the wind load. The unity check for fatigue UC_{FLS} now becomes 1.06 instead of 0.99.
- Small influence of caisson on fatigue: it was often mentioned that a few percent difference in the outcome of FinLab was small (for example: the influence of the caisson on the bending moment cycle, ~2%). But for the fatigue load a small difference in load, may results in a large difference in outcome. This has to do with the fact that $D_{fat} \sim \Delta\sigma^m$. For m=5, a difference in bending moment cycle of 2% leads to a difference in fatigue load of 10%.

7.1.3 Interpretation of results

In this section an interpretation of the results by the author is given.

Hydrodynamic analysis

Although the results from FinLab are different from the Morison equation for non-linear waves, the author has confidence in the outcome of FinLab. This is based on the fact that there are enough possible causes explaining the differences in outcome. Also other investigations with Open Foam and ComFlow show the same effect as observed within this thesis. In literature little was found on differences between field data and the Morison equation, but due to time restrictions no full literature study on this effect could be performed. This is recommended as a starting point for further research.
With respect to the observed relation for the difference between FinLab and the Morison equation the critical note is placed that this is only based on four wave cases. Based on this data nothing can be said about waves with a lower Ursell number, although the expectation is that differences are small.

Shaft design

With respect to the fatigue analysis of Chapter 6 the author has some doubts about the outcomes. The fatigue load due to waves seems to be very small (4% only). This may have to do with the simplified method used for pre-design. Also the mass-spring system used to determine the dynamic amplification factor is a very basic schematisation of the dynamic behaviour. A full time domain analysis (taking the turbine behaviour, wind an wave states and directionality and structural behaviour into account) is therefore highly recommended for a final design.
Also the resulting wall thickness found seems to be rather small (D/t>100). For a 5MW turbine in a water depth of 30 m a wall thickness of 0.01 m is no exception. The relative low wall thickness found here may partially be contributed to the fact that the steel shaft is clamped at a higher level due to the caisson. Hereby the maximum bending moment in the shaft reduces. But it is also good possible that the relative simple fatigue analysis results in too low values.

7.2 CONCLUSIONS

In chapter 1 both research questions were introduced. In this section, as an answer to the research questions, the conclusions are summarized.

7.2.1 Hydrodynamic analysis with FinLab

The main of this research was performing a detailed hydrodynamic analysis with FinLab. This analysis was performed in order to investigate the influence of the caisson on the hydrodynamic load on the shaft of the GBS (the first research question). This analysis led to the following conclusions:

- The outcome of FinLab matches very well with theory for a nearly linear wave. This is so for both the undisturbed wave kinematics found by FinLab and the horizontal wave force on a monopile.
- For increasing wave non-linearity FinLab gives higher maximum horizontal wave forces than the Morison equation. This effect has nothing to do with the presence of the caisson, because it also occurs for a monopile. For a water depth of 34 m and the ULS wave used within this thesis, FinLab gives a 50% higher wave force. The bending moment at sea bottom level is 75% higher.
- For the shaft of the GBS the differences between FinLab and the Morison equation are even higher. Differences in maximum horizontal force are up to 75%. Differences in maximum bending moment at the top of the caisson are up to 120%.
- The difference between FinLab and the Morison equation was found to be related to the H/d ratio or the Ursell number. Differences occur for U_r>1.5. Based on these observations it is concluded that the Morison equation should be treated with care for non-linear waves an may be less accurate in predicting the wave forces.
- Compared to the difference in forces between FinLab and the Morison equation, the influence of the caisson is relatively small. The highest increase of the maximum horizontal load on the shaft of the GBS due to the caisson is 20%. The increase is highest for the relative short waves, and lowest for the relative long ULS wave.
- For the cases investigated in this thesis, the influence of the caisson on the bending moment cycles is very small (about 3%).

7.2.2 Design of the steel shaft of the GBS

The results of the hydrodynamic analysis with FinLab have been used in a case study in order to investigate their influence on the design (cross-sectional dimensions) of the steel shaft. This step gave answer to the second research question and led to the following conclusions:

- Material costs of the steel shaft of the GBS are about 3% of the total construction costs.
- The detailed hydrodynamic analysis with FinLab does not have a noticeable influence on the fatigue load due to waves. Two effects are responsible: 1) Non-linear waves with U_r>1.5 have a very small probability of occurrence 2) The presence of the caisson doesn't influence the bending moment cycles.
- For the ULS the increase in bending moment of 120% due to waves leads to an increase of the total combined bending moment, due to wind and waves, of 26% only.
- For this specific water depth (34m) and fatigue analysis method used (quadratic superposition) the higher ULS wave loads, as found by FinLab, don't lead to increasing shaft dimensions. This is because the FLS is governing the dimensions of the steel shaft.

- When looking at larger water depths (>34m), or while performing a more advanced fatigue analysis, the increase in ULS wave loads, as found by FinLab, may have an influence on the design of the steel shaft.
- Instead of optimizing the dimensions of the shaft so that it can do with less material, the detailed hydrodynamic analysis with FinLab resulted in higher loads found. This will rather lead to more material required.

7.3 RECOMMENDATIONS

Based on the discussion of the results in section 7.1 the following recommendations are given. The recommendations can be seen as a starting point for further research.

7.3.1 Hydrodynamic analysis

- Calibrate the resulting forces from FinLab for a highly non-linear wave with data from the field. Another option is to perform a model test, or to use experimental data from model tests.
- Perform an oscillatory flow test within FinLab in order to eliminate the presence of the free surface. Next, investigate the differences between the wave force found by FinLab and the Morison equation.
- Investigate whether there is more literature reporting that the Morison equation leads to lower horizontal wave forces than measured/simulated for highly non-linear waves.
- Investigate why the increase in horizontal force on the shaft due to the caisson is highest for the relatively short waves.
- Perform simulations for the relatively short waves of the wave scatter diagram. Investigate the differences between FinLab and the Morsion equation and the influence of the caisson, and see if there are really no differences.
- Investigate the influence of using the LES model within FinLab, to model the turbulence, for a highly non-linear wave.
- Determine the influence of wave breaking and currents on the ULS loads.
- Use FinLab to calculate the hydrodynamic force on the total GBS and check whether stability is still achieved.

7.3.2 Shaft design

- Use a more sophisticated fatigue analysis method to calculate the fatigue load. For example the method based on superposition of response spectra could be used (but for pre-design only). Use a full TD analysis for detailed design.
- Use a more sophisticated structural model to calculate the fatigue load due to waves. The model should represent the dynamic behaviour more accurate.
- Take the contribution of lift forces into account within the fatigue analysis.

7.3.3 Detailed design of GBS shaft by BAM

- For the FLS analysis: an analysis with FinLab will result in about the same fatigue load as application of the Morison equation for the shaft of the GBS. Therefore, just use the Morison equation in combination with the upper section of a monopile for the FLS waves.
- For the ULS analysis: the Morison equation probably leads to too low wave forces on the shaft. Therefore, use a numerical CFD package like FinLab, perform scale tests, or increase the force found by the Morison equation. The caisson does not have to be a part of the structure used.

7.3.4 Development of FinLab

- Make the force module post-processing. Instead of calculating the force during the simulation, develop a module that is able to calculate the force afterwards. By doing so one could deduce the distributed force. This has been tried by the author, but the distributed force found was not equal to the total force found by FinLab. Due to time considerations this module was not further developed.
- Improve the user friendliness of FinLab by developing an user-interface instead of using raw code as input.

7.3.5 Using FinLab

- Optionally, construct the 3D grid in a separate mesh generator like SEPRAN. By doing so, one has more freedom in choosing the height of structural elements and the vertical layer distance.
- Make sure the values of theta and zeta in the input file are equal to each other. If not, this will probably lead to incorrect velocity profiles.

REFERENCES

[1] GWEC, "Global Wind Report Annual Market Update 2012," Global Wind Energy Council, Brussels, 2012.

[2] J. Twidell, Offshore Wind Power, Essex: Multi-Science Publishing Co. Ltd, 2009.

[3] M. Sanz, *Wind Energy Systems,* CRC, 2012.

[4] Roland Berger Strategy Consultants GmbH, *Offshore wind toward 2020,* 2013.

[5] ISE Fraunhofer, "Levelized cost of electricity renewable energies," Fraunhofer Institute for Solar Engergy Systems ISE, Freiburg, 2012.

[6] Navigant Consulting, *US Offshore wind supply chain and manufacturing development,* Burlington: Navigant, 2013.

[7] W. d. Vries, "Final report WP 4.2 Support structure concepts for deep water sites," Delft University of Technology, Delft, 2011.

[8] BAM Infraconsult/ Van Oord, *General presentation Offshore Wind,* Gouda: BAM Infraconsult, 04-2013.

[9] BAM Infraconsult/ Van Oord, *Beatrice presentation,* Gouda, 02-05-2013.

[10] BAM Infraconsult, "Beatrice Perliminary Design Study," Gouda, 20-3-2012.

[11] DNV, "Design of offshore wind turbine structures - DNV-OS-J101," Det Norske Veritas, 2011.

[12] T. Burton, N. Jenkins, D. Sharpe and E. Bossanyi, Wind Energy Handbood, 2nd ed., Wiley, 2011.

[13] W. Byrne and G. Houlsby, "Foundations for offshore wind turbines," University of Oxford, Oxford, 2003.

[14] J. v. d. Tempel, "Design of support structures for offshore wind turbines," DUWIND, Delft, 2006.

[15] G. v. Kuik and W. Bierbooms, "Introduction to wind energy design," DUWIND, Delft, 2002.

[16] J. v. Ginhoven, "Het effect van erosie en de grondeigenschappen op het dynamische gedrag van offshore windturbines," Delft University of Technology, Delft, 2006.

[17] W. d. Vries, "Implementing a frequency domain approach for the fatigue analysis of offshore wind turbine support structures," Delft University of Technology, Delft, 2006.

[18] T. Sarpkaya, Wave forces on offshore structures, New York: Cambridge University Press, 2010.

[19] M. Zaaijer, "Comparison of monopile, tripod, suction bucket and gravity base design for a 6 MW turbine," Delft University of Technology, Delft, 2003.

[20] T. Sarpkaya, Mechanics of wave forces on offshore structures, New York: Litton Educational Publishing, Inc., 1981.

[21] M. Kuhn, "Dynamics and Design optimisation of offshore wind energy conversion systems," DUWIND Delft University Wind Energy Research Institute, Delft, 2001.

[22] M. Kuhn, W. Bierbooms, G. van Bussel, M. Ferguson, B. Goranson, T. Cockerill, R. Harisson, L. Harland, J. Vugts and R. Wiecherink, "Opti-OWECS Final Report Vol. 0," Delft University of Technology, Delft, 1997.

[23] L. Hofland, "Fatigue of the support structure of an OWEC due to the combined loading of wind and waves," Delft University of Technology, Delft, 1999.

[24] M. Kuhn, "Design optimisation of an offshore wind energy converter by means of

tailored dynamics," Institue for Wind Energy, Delft University of Technology, Delft, 1999.

[25] B. Sumer and J. Fredsoe, Hydrodynamics around cylindrical structures, Singapore: World Scientific Publishing Co., 1997.

[26] C. United States Army, Coastal Engineering Manual, U.S. Army Corps of Engineers, 2006.

[27] J. Journee and W. Massie, Offshore Hydromechanics, Delft: Delft University of Technology, 2001.

[28] T. Sarpkaya, "Vortex shedding and resistance in harmonic flow about smooth and rough circular cylinders at high Reynolds numbers," Naval Postgraduate School, Monterey, 1976.

[29] T. Sarpkaya, "A critical assessement of Morison's equation," in *International symposium on Hydrodynamics in Ocean Engineering* , Trondheim, The Norwegian Institute of Technology , 1981, pp. 447-467.

[30] R. Labeur, "Finite element modelling of transport and non-hydrostatic flow in environmental fluid," TU Delft, Delft, 2009.

[31] R. Labeur and J. Pietrzak, "A fully three dimensional unstructured grid non-hydrostatic finite element coastal model," TU Delft, Delft, 2005.

[32] C. v. d. Boon, "Numerical modelling of internal waves in the Browse Basin," TU Delft, Delft, 2011.

[33] J. Wierenga, "Dichtheidsstroming en bodemligging achter de extra spuisluis in de Afsluitdijk," TU Delft, Delft, 2007.

[34] P. Frigaard and H. Burcharth, "Wave loads on cylinders," University of Aalborg, Aalborg, 1989.

[35] S. Chakrabarti, Hydrodynamics of offshore structures, Plainfield, USA: CBI Industries, 1987.

[36] E. Christensen, L. Yde, H. Gravesen, E. Hansen, N. Tarp-Johansen and M. Damsgaard, "Wave Loads on offshore wind turbine foundations in shallow water. Engineering models vs. refined flow modelling," DHI, Denmark, 2007.

[37] T. Fisscher, "Load Mitigation of an Offshore Wind Turbine by optimization of Aerodynamic Damping and vibration control," Danmarks Tekniske Universitet, Stuttgart, 2006.

[38] F. Savenije and J. Peeringa, "Aero-elastic simulation of offshore wind turbines in the frequency domain," ECN, 2004.

[39] IER, "Levelized costs of new electricity generating technologies," Institute for Energy Research, Washington, 2013.

[40] USG Energy, "De Monopile," [Online]. Available: http://www.usgenergy.com/doelpagina/2743893/2743879/De-monopile.html. [Accessed 03 07 2013].

[41] K. Lesny, Foundations for offshore wind turbines, VGE, 2010.

[42] S. Malhotra, Selection, design and construction of offshore wind turbine foundations, InTech, 2011.

[43] K. Abdel-Rahman and M. Achmus, "Behaviour of monopile and suction bucket foundation systems," University of Hannover, Hannover, 2006.

[44] A. Laguna, *Course Offshore Wind Farm Design,* Delft: Delft University of Technology, 2013.

[45] LORC, “Lindoe Offshore Renewables Center,” 2013. [Online]. Available: http://www.lorc.dk/offshore-wind-farms-map. [Accessed 22 05 2013].

[46] Inhabitat, “Inhabitat,” 02 07 2007. [Online]. Available: http://inhabitat.com/floating-wind-turbines-in-the-north-sea/. [Accessed 03 07 2013].

[47] K. Peire, H. Nonneman and E. Bosschem, “Gravity base foundations for the Thornton bank offshore wind farm,” *Terra et Aqua,* pp. 19-29, 2009.

[48] Dredging International, *Presentation gravity based foundations for the thornton bank offshore wind farm,* DEME, 2008.

[49] G. Dewaele, *Presentation Thorntonbank Belgium - 325MW Offshore Windfarm - Successes, hurdles, experiences,* C Power, 2013.

[50] N. Diepeveen, A. Jarquin Laguna and A. Kempenaar, “Water-hydraulic power transmission for offshore wind farms,” Delft University of Technology, Delft, 2012.

[51] Nabtesco Corporation, “pddnet,” Product Design and Development, [Online]. Available: http://www.pddnet.com/articles/2012/10/powering-wind-turbine-gear-performance-realistic-simulation. [Accessed 11 10 2013].

[52] Holthuijsen, Waves in Oceanic and Coastal Waters, Cambridge: Cambridge University Press, 2007.

[53] M. v. d. Meulen, *Presentation Hydrodynamic Loading on offshore wind turbines,* 2013.

[54] M. v. d. Meulen, “Influence of nonlinear irregular waves on the fatigue loads of an offshore wind turbine,” Siemens, The Hague, 2012.

[55] J. Vrijling, H. Kuijper, S. v. Baars, K. Bezuyen, W. Molenaar, C. v. d. Hoog, B. Hofschreuder and M. Voorendt, “Collegedictaat CT3330 - Manual Hydraulic Structures - Technische Universiteit Delft,” Delft University of Technology, Delft, 2011.

[56] J. Vugts, J. v. d. Tempel and E. Schrama, Hydrodynamic loading on monotower support structures for preliminary design, Delft: Delft University of Technology, 2001.

[57] API, “Recommended Practise for Planning, Design and Constructing Fixed Offshore Platforms-Working Stress Design,” American Petroleum Institute, Washington D.C., 2007.

[58] ABPmer Ltd et al, “A further Review of Sediment Monitoring Data,” COWRIE Ltd, 2010.

[59] J. Wilson, Dynamics of offshore structures, New Jersey: Wiley, 2003.

[60] A. Metrikine, *Dynamics, Slender Structures and an Introduction to Continuum Mechanics; Lecture Notes CT4145,* Delft: Delft University of Technology.

[61] J. Blaauwendraad, *Dynamica van Systemen; Lecture Notes CT2022,* Delft: Delft University of Technology.

[62] D. Salzmann and J. v. d. Tempel, “Aerodynamic damping in the design of support structures for offshore wind turbines,” Duwind, Delft, 2005.

[63] DONG Energy, “Comparing Sources of Damping of Cross-Wind Motion,” DONG Energy, Kopenagen, 2010.

[64] P. Kolkman and T. Jongeling, “Dynamisch gedrag van waterbouwkundige constructies - Deel B Constructies in golven,” Rijkswaterstaat, Delft, 1996.

[65] T. Jager, “Golftheorieën en golfkrachten,” Delft Universitiy of Technology, Delft, 2013.